uOttawa

L'Université canadienne
Canada's university

FACULTÉ DES ÉTUDES SUPÉRIEURES ET POSTOCTORALES

uOttawa

L'Université canadienne
Canada's university

FACULTY OF GRADUATE AND POSDOCTORAL STUDIES

Abdulrahman Alhazmi

AUTEUR DE LA THÈSE / AUTHOR OF THESIS

Ph.D. (Chemistry)

GRADE / DEGREE

Department of Chemistry

FACULTÉ, ÉCOLE, DÉPARTEMENT / FACULTY, SCHOOL, DEPARTMENT

Mass Spectrometry of Polymers: From Synthesis to Sequence

TITRE DE LA THÈSE / TITLE OF THESIS

Paul Mayer

DIRECTEUR (DIRECTRICE) DE LA THÈSE / THESIS SUPERVISOR

CO-DIRECTEUR (CO-DIRECTRICE) DE LA THÈSE / THESIS CO-SUPERVISOR

EXAMINATEURS (EXAMINATRICES) DE LA THÈSE / THESIS EXAMINERS

Maria De Rosa

Alain St-Amant

Darrin Richeson

Chrys Wesdemiotis

Gary W. Slater

Le Doyen de la Faculté des études supérieures et postdoctorales / Dean of the Faculty of Graduate and Postdoctoral Studies

MASS SPECTROMETRY OF POLYMERS: FROM SYNTHESIS TO SEQUENCE

Abdulrahman M. Alhazmi

Thesis submitted to the
Faculty of Graduate & Postdoctoral Studies

In partial fulfillment of the requirements for
the degree of Doctor of Philosophy

In the Ottawa-Carleton Chemistry Institute
Department of Chemistry, University of Ottawa
Ottawa, Ontario, Canada

May 2008

Candidate

Abdulrahman M. Alhazmi

Supervisor

Dr. Paul M. Mayer

Your file Votre référence
ISBN: 978-0-494-48381-7
Our file Notre référence
ISBN: 978-0-494-48381-7

Abstract

Electrospray ionization (ESI) and matrix assisted laser desorption-ionization (MALDI) mass spectrometry were used to determine the composition (monomer ratios) and structure (end group analysis), relative to ^{1}H NMR spectroscopy and theoretical predictions, for three different copolymers: poly(butyl acrylate/vinyl acetate) (PBA/PVAc), poly(methyl methacrylate/vinyl acetate) (PMMA/PVAc) and poly(butyl acrylate/methyl methacrylate) (PBA/PMMA). The ESI results were found to be in excellent agreement with ^{1}H NMR spectroscopy for PBA/PVAc and PBA/PMMA copolymers whereas there was more divergence in the case of PMMA/PVAc. In the case of PBA/PMMA copolymers similar distributions of products were observed by ESI-MS and MALDI-MS; two major product classes were observed differing by their end-groups. One class has hydrogen and dodecylthio end groups while in the other the dodecylthio has been replaced by α-cyanoisopropyl from the initiator. The relative abundance of these distributions as a function of copolymer conversion for a series of reaction conditions was investigated by both ESI and MALDI.

The collision-induced dissociation (CID) mass spectra for a variety of chain lengths of four ionized polymer samples have been quantified according to their observed total relative fragment ion abundances. The CID mass spectra of oligomers of ionized PMMA with three different types of end groups and polystyrene, PS, were obtained at fixed centre-of-mass collision energies and collision numbers. For the PMMA polymers, the total fragment ion abundance increases with increasing chain length, consistent with an increase in internal energy deposition with size of the ion. A discontinuity in the increase in total fragment ion abundance appears to correspond to a change in conformation of the polymer

ions from linear (at short chain lengths) to cyclic (at long chain lengths). Ionized PS does not exhibit this change in conformation as all chain lengths show compact structures and accordingly the total fragment ion abundance does not change with increasing chain length.

Protonation of polymers in the gas-phase was achieved by the dissociation of proton-bound complexes of the oligomers with small peptides and amino acids. Protonated PMMA and PBA oligomers were shown to fragment in unique pathways that involved losses of neutral molecules from their side chains, until all that is left is a hydrocarbon backbone. For PMMA the neutrals were primarily CO and methanol, while for PBA butyl ether is lost. We also explored the threshold fragmentation of the proton-bound complexes as a function of the amino acid used (and its proton affinity) which allowed a kinetic bracketing of the oligomer PA as a function of chain length. The results were consistent with a change from bidentate to tridentate binding of the proton with increasing length of the PMMA oligomers.

Acknowledgments

I would like to express my thanks and appreciation to my supervisor Dr. Paul Mayer. His guidance, support and encouragement enable me to pursue successfully my Ph.D. studies.

Special thanks go to Dr. Clement Kazakoff for his help and valuable discussions on analytical instruments. Also my thanks go to Dr. John Holmes and Dr. Sander Mommers for their support. During my five years in the mass spectrometry center I met and worked with many colleagues and friends who either I learned from, help me, or made my journey more enjoyable. I would like to take this opportunity to thank (in no particular order) Dr. Juile Garbowy, Dr. Clement Poon, Anne-Marie Boulanger, Dr. Annick St-Amand, Dr. Xian Wang, Dr. Emma Rennie, Mohammed Qadura, Madlena Rabaev, Yawei Lin, Marie-Soleil Giguère, Andre Stewart and all other past colleagues.

Last but not least, I would like to thank my family for their support, patient and understanding. I would like also to thank Saudi Arabia Basic Industries Corporation (SABIC) for financially supporting me.

Table of Contents

List of Figures

List of Tables

List of Abbreviations

AIBN	Azodiisobutyronitrile
CE	Collision Energy
CID	Collision-Induced Dissociation
CTA	Chain Transfer Agent
D	Polydispersity
Da	Dalton
DC	Direct Current
DHB	2,5-dihydroxy benzoic acid
DiGly	Diglycine
DP-MS	Direct Pyrolysis Mass Spectrometry
ESI-MS	Electrospray Ionization
FAB	Fast Atom Bombardment
FD	Field Desorption
FTMS	Fourier Transform Mass Spectrometry
Gly	Glycine
GPC	Gel Permeation Chromatography
HPLC	High Performance Liquid Chromatography
IR	Infrared
LC	Liquid Chromatography
LDI	Laser Desorption Ionization
LS	Light Scattering
LSIMS	Liquid Secondary Ion Mass Spectrometry

MALDI-MS	Matrix Assisted Laser Desorption-Ionization
mer	monomer unit
MM/MD	Molecular mechanics/molecular dynamics
$\overline{M_n}$	Average molecular weight by number
MS	Mass Spectrometry
$\overline{M_w}$	Average molecular weight by weight
m/z	mass-to-charge ratio
NIST	National Institute of Standards and Technology
NMR	Nuclear Magnetic Resonance
PA	Proton Affinity
PBA/PMMA	Poly(butyl acrylate/methyl methacrylate)
PBA/PVAc	Poly(butyl acrylate/vinyl acetate)
PDMS	poly(dimethylsiloxane)
PEG	Polyethylene glycol
PMMA/PVAc	Poly(methyl methacrylate/vinyl acetate)
PS	Polystyrene
Py-GC/MS	Pyrolysis Gas Chromatography Mass Spectrometry
RF	Radio Frequency
SEC	Size Exclusion Chromatography
TOF	Time-of-Flight
TQMS	Triple-Quadrupole Mass Spectrometers
TriGly	Triglycine

1

Introduction

1.1 Scope and Goals

The goal of this thesis was to explore the utility of mass spectrometry in the analysis of polymers. More specifically, it was to directly compare electrospray ionization (ESI) and matrix assisted laser desorption-ionization (MALDI) mass spectrometry with the more established method of ^{1}H NMR in the study of polymer composition (monomer ratios) and structure (end group analysis). Mass spectral analysis of polymers is usually carried out by forming metal ion adducts of the oligomers. I wished to explore the impact this has on the mass spectral analysis. To this end I examined both how the conformation of such ionized polymer oligomers, and how changing the mode of ionization to protonation, affect the way they dissociate.

1.2 Polymer

The word Polymer[1-3] [derived from the Greek] means "many parts" and is a large molecule consisting of smaller repeating units called monomers. The term was introduced by Hermann Staudinger (Noble Prize 1953) in 1920. The term macromolecule is used interchangeably with polymer, mostly in biological science. For example, a protein or a

peptide is not made of one (two or three) monomer(s), but rather up to 20 different amino acids. Polymers can be obtained naturally, such as cellulose or rubber, or made synthetically. Polymers play a big role in our life since they are used in a wide range of consumer goods. Applications range from household materials (cloth, shoes, fiber, cookware, toys, etc.) to industrial goods (cars, aircraft, adhesive, pipes, paints, tires, etc.) and medical applications (artificial hip joints, contact lenses, drug delivery, etc).

If the repeating unit of the polymer is a single monomer, it is called a homopolymer and when two or more different monomers make up the repeating units it is called a copolymer. For example, poly(methyl methacrylate) (PMMA) and poly(butyl acrylate) homopolymers are made from methyl methacrylate (MMA) and butyl acrylate (BA) monomers respectively, while poly(butyl acrylate/methyl methacrylate) (PBA/PMMA) copolymer is made from both MMA and BA monomers (Figure 1.1).

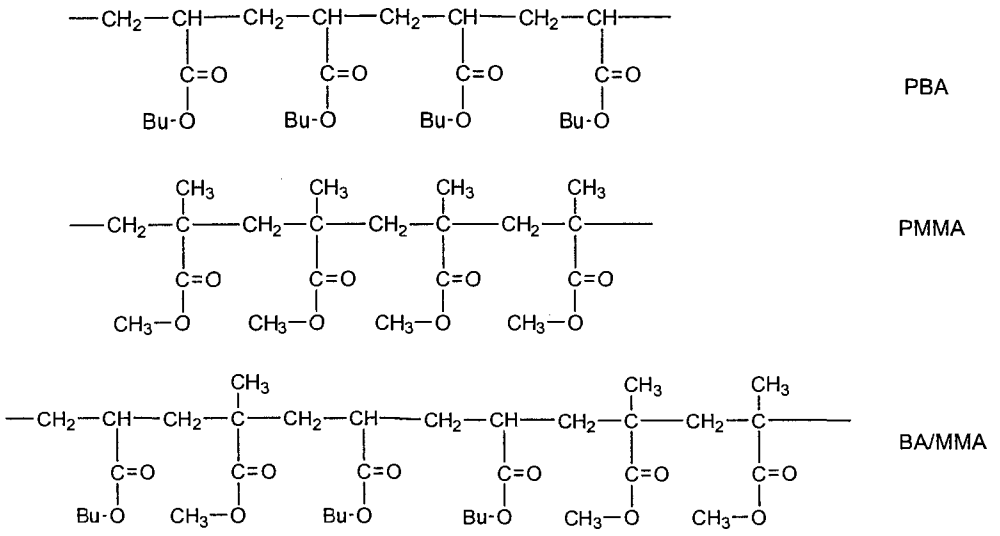

Figure 1.1: Homopolymers and copolymers

Normally a polymer sample consists of oligomers that have different chemical structures and compositions. The difference in the chemical structures could lie in the backbone of the oligomers and/or end-groups which are the chemical groups that terminate the oligomer chains. Polymers may have similar chemical structure but may differ in their composition, chain length and molecular weight distribution. Usually plastic is the end use of polymers, and after adding the appropriate additives and going through industrial processes, plastics are made for different purposes. Determining the chemical structures and composition of the polymers is important since it will affect the chemical and physical properties of the final products. Therefore the more that is known about the polymers, the more control one can have over the quality of the final product.

There are many ways to classify polymers: based on the source (natural or synthetic), application (rubber, plastic, adhesive, etc.), chemical structure (polyester, polystyrene, etc.) and others.[1-6] Polymers can be also classified based on the way they are made: condensation or addition polymers. Condensation reactions involve combining two molecules to form a single molecule with the elimination of a small molecule. Therefore, the repeating units of a condensation polymer, also known as a step-growth polymer, lack one or more atoms compared to the monomers used in the synthesis. Polyester is a good example of a condensation polymer where two bifunctional monomers combine and water is eliminated (equation 1.1).

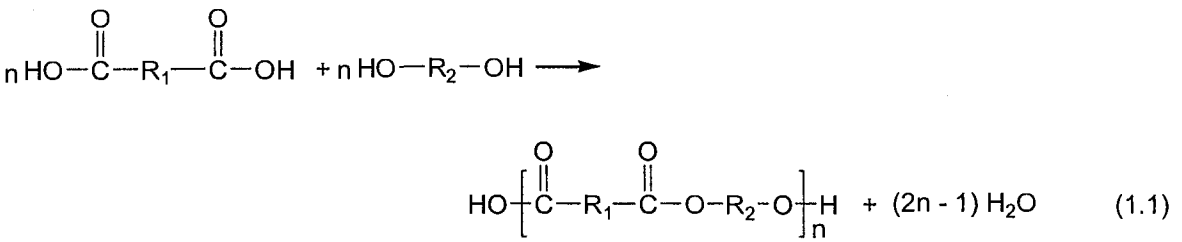

$$n\,HO{-}\overset{O}{\overset{\|}{C}}{-}R_1{-}\overset{O}{\overset{\|}{C}}{-}OH + n\,HO{-}R_2{-}OH \longrightarrow HO{-}\left[\overset{O}{\overset{\|}{C}}{-}R_1{-}\overset{O}{\overset{\|}{C}}{-}O{-}R_2{-}O\right]_n{-}H + (2n-1)\,H_2O \qquad (1.1)$$

The repeating units of addition (or chain growth) polymers have the same structure as the reacting monomers. Many addition polymers are formed from unsaturated vinyl monomers (equation 1.2).

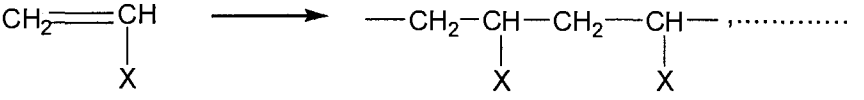

(1.2)

Addition (chain-growth) polymerization occurs by different mechanisms: free radical, anionic or cationic, coordination addition and ring-opening processes.

Free radical polymerization is divided in three steps: initiation, propagation, and termination. In the initiation step, a radical has to be generated to set off the polymerization reaction. Different compounds are used to produce a radical through various processes such as heat and UV and visible light absorption. Azodiisobutyronitrile (AIBN) is a popular initiator used to form a radical in different poly(alkyl acrylate) polymerization reactions.[7,8] When heated the two C-N bonds break and two isobutyronitrile radicals are formed along with N_2 (Figure 1.2). Propagation occurs when the formed radical attacks (for example) the double bond of an unsaturated vinyl monomer to form a saturated radical oligomer (Figure 1.2). The latter formed radical will attack other monomer and so on.

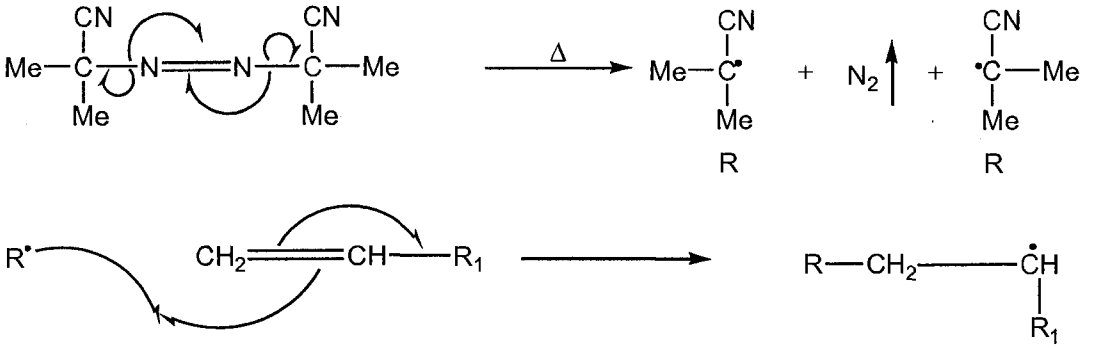

Figure 1.2: The initiation and propagation steps in free radical polymerization

The polymerization will be terminated when: a) two growing radicals combine together to form single bond (radical combination), b) disproportionation occurs in which two radicals react together to form saturated and unsaturated polymers (Figure 1.3), or c) a chain transfer agent (CTA) such as butanethiol and dodecanethiol terminate the polymerization reaction by hydrogen atom transfer.

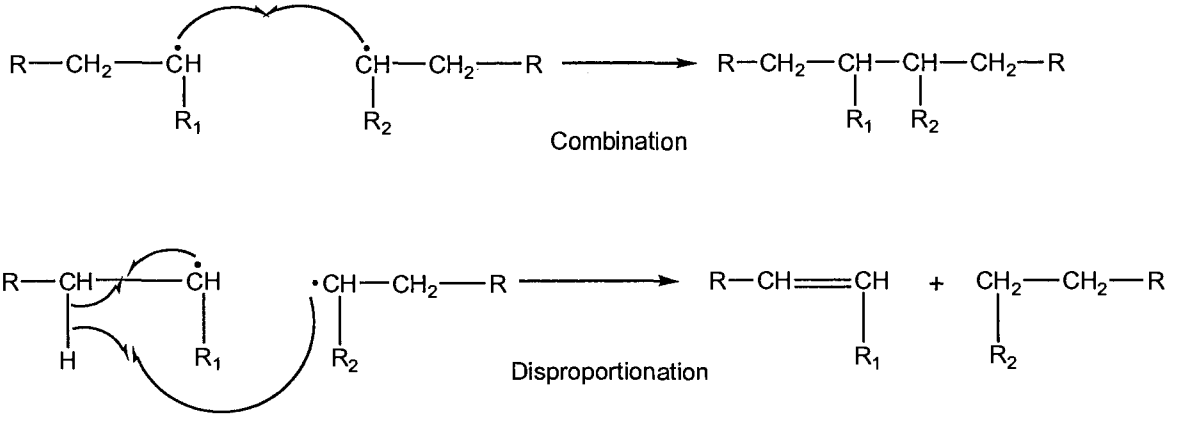

Figure 1.3: Termination in free radical polymerization.

In general the ionic mechanisms follow the three steps that occur in free radical polymerization but the initiator is different. Anionic and cationic polymerizations are

initiated by forming either a negative charge on the monomers (carbanions) or positive charge (carbenium ions). In anionic polymerization, basic compounds are used as initiators whereas compounds such as BF_3 , $AlCl_3$ and $TiCl_4$ in water or alcohols are good cationic initiators. For example, butyl lithium is used to generate the anion (Figure 1.4) which reacts with unsaturated vinyl to start anionic polymerization. Ionic polymerization is affected by the conditions such as solvent and temperature. Highly polar solvents lead to solvated ions but may also react with the initiator ions. Therefore, moderately polar solvents are usually used in this type of polymerization.[5]

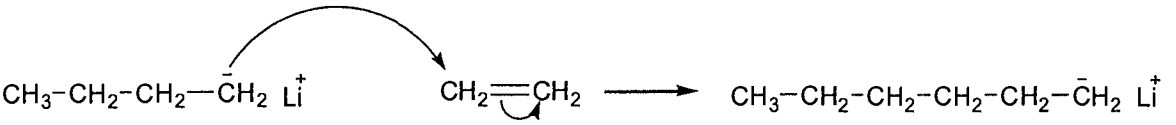

Figure 1.4: Initiator step in anionic polymerization.

In coordination addition, monomers are inserted between the catalyst and polymer. Early in 1950s, Ziegler in Germany and Natta in Italy first introduced a catalyst system to polymerize ethylene and 1-alkenes, which is now known as Zieglar-Natta catalysis. It is a combination of transition metals from groups IVB-VIIIB and organometallic compounds with group IA-IIIA metals. The most widely used combination is alkyl aluminum with titanium, vanadium, chromium or zirconium salts.[5] Zieglar-Natta catalysts produce a well-controlled polymer reaction leading to linear structures and specific stereoregularity (isotactic and syndiotactic). Most of the olefin polymers are made by various Zieglar-Natta catalysts.

Cyclic compounds (3-8 atoms) can be polymerized by ring-opening reactions.[1] One bond in the ring will break so one side can then react with the initiator. The other side will react with another monomer ring and so on. For example, hexamethylcyclotrisiloxane monomers polymerize to form polydimethylsiloxane by using potassium alkoxide as an initiator (Figure 1.5).

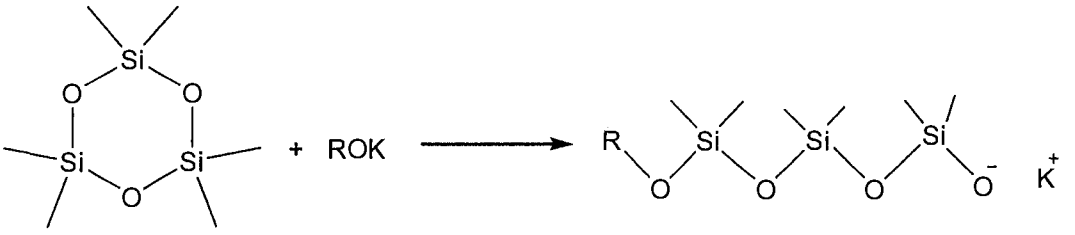

Figure 1.5: Ring-opening polymerization.

1.3 Polymer Characterization

There are many proprieties one can look for in the polymer as shown in table 1.1.[2,3] Typically, the first property determined is the molecular weight. Since the polymer is a mixture of different compounds (oligomers) its molecular weight always yields an average. This average can be expressed in two ways: the average molecular weight by number ($\overline{M_n}$) and average molecular weight by weight ($\overline{M_w}$) and they are given by equations 1.3.

$$\overline{M_n} = \left(\sum m_i N_i\right)/\left(\sum N_i\right) \qquad \overline{M_w} = \left(\sum m_i^2 N_i\right)/\left(\sum m_i N_i\right) \qquad (1.3)$$

where N_i the number of chains with mass m_i.

The polydispersity, D, of a polymer sample is given by:

$$D = \overline{M_w}/\overline{M_n} \tag{1.4}$$

The value of D will determine if the polymer sample is composed of a narrow (close to 1) or broad distribution (2 or more) of oligomer sizes. Typically, light scattering (LS) or gel permeation chromatography (GPC) (also know as size exclusion chromatography (SEC)) are used to measure the average molecular weight of polymers. In LS, the scattered intensity of light passed through a sample is related to particle size in the solution. GPC is liquid-solid chromatography used to fractionate the polymer oligomers based on their hydrodynamic volume. The polymer solution is injected onto a column that is packed with gel having different pore sizes. Detectors used with GPC include ultraviolet, refractive index and light scattering all of which provide no information about polymer structure and composition.

Table 1.1: Different properties used to characterize polymers

Property	Information gained
Molecular weight distribution	Weight and number molecular weight and polydispersity
Configuration and conformation	cis or trans, isotactic,syndiotactic or atactic repeating units
Identification of end-group	chemical compounds that terminated oligomer chains
Topology	Chain branching: linear, branched.
Mole fraction of each monomer	In the case of copolymer
Copolymer composition drift	Identification of the variation of the polymer composition as function of chain grows

Techniques like infrared (IR) and nuclear magnetic resonance (NMR) spectrscopies have been extensively used to determine the composition and chemical structure of polymers. In a typical case, a unique peak or signal for each constituent monomer will be resolved and quantified, yielding the chemical composition of the polymer. Although the end-groups exist in small amounts compared to the monomers they are important indicators of the synthetic process and can play a major role in further chemical reactions of the polymer. NMR has been used to some extent to determine the end-groups but only for low molecular weight polymers because the end-group signal from high molecular weight polymers is lost in the large signals due to the polymer backbone.[9]

1.4 Polymer Mass Spectrometry

Mass spectrometry (MS) is one of the most powerful analytical techniques and most analytical laboratories have one or several MS instruments. In mass spectrometry, ions are studied in the gas phase, so samples have to be transferred from their original state to the gas phase. Prior to the 1990`s the largest molecules that mass spectrometry was able to analyze successfully were in the range of 1000 Da.[10] Mass spectrometry techniques like fast atom bombardment (FAB) and liquid secondary ion mass spectrometry (LSIMS) were used to analyze peptides, small proteins and polymers. Field desorption (FD) [9] showed promise for compounds up to 15,000 Da, but several drawbacks related to FD operation and sensitivity restricted its popularity. Pyrolysis[9] has been successfully used to study the structure and composition of polymers. Direct

pyrolysis mass spectrometry (DP-MS) is based on the thermal degradation of a sample and usually detects ions based on the constituent monomers of a polymer. However, depending on the analyte reactivity, an analyte may react before reaching the mass analyzer. Pyrolysis gas chromatography mass spectrometry (Py-GC/MS) has the advantage of separating the pyrolysis products before they enter the mass analyzer. Catalysis may be used to improve the efficiency of the degradation under the flow of N_2 and He gas.

Mass spectrometry has recently (the last two decades) become an important technique to analyze and study synthetic polymers (Figure 1.6). This was made possible by the development of two new ionization methods: electrospray ionization (ESI)[11,12] and matrix assisted laser desorption/ionization (MALDI).[13-15] The value and impact of inventing both ionization techniques on science led to John B. Fenn and Koichi Tanaka being awarded the 2002 Nobel Prize. ESI and MALDI are soft ionization methods allowing large compounds such as protein, peptide and synthetic polymers to be transferred to the gas phase. More details about how both ionization techniques work will be discussed in chapter two. In ESI and MALDI, ionization is typically achieved by the generation of protonated $[M+H]^+$ or deprotonated $[M-H]^-$ ions. Synthetic polymers are not usually basic enough in solution to acquire a proton from an added acid, so a metal such as Na^+, K^+, Ag^+ or NH_4^+ are added to form adduct ions.

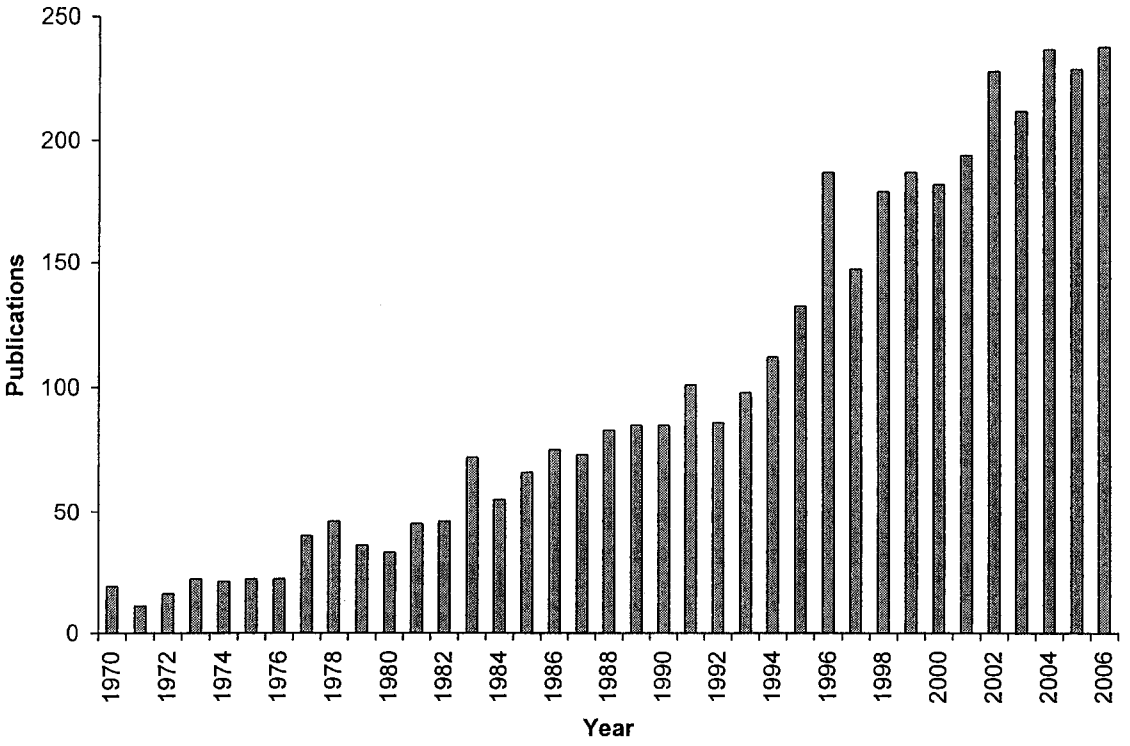

Figure 1.6: Polymer mass spectrometry publications (produced from SciFinder Scholar^{TM}, American Chemical Society (ACS)).

MALDI coupled to time-of-flight mass spectrometry has been widely exploited in polymer characterization due to the high molecular weight polymers that can be desorbed. ESI has been used in a more limited manner since polymer samples have to be soluble, thus limiting the molecular weight range accessible for study. It is advantageous to use mass spectrometry for polymer analysis since it is provides molecular level information in complex mixtures of oligomers. To illustrate how the different oligomers are identified in MS, we will take the mass-to-charge ratio (m/z) 588 oligomer of polybutyl acrylate (PBA) ionized with Li^+ as an example (Figure 1.7)

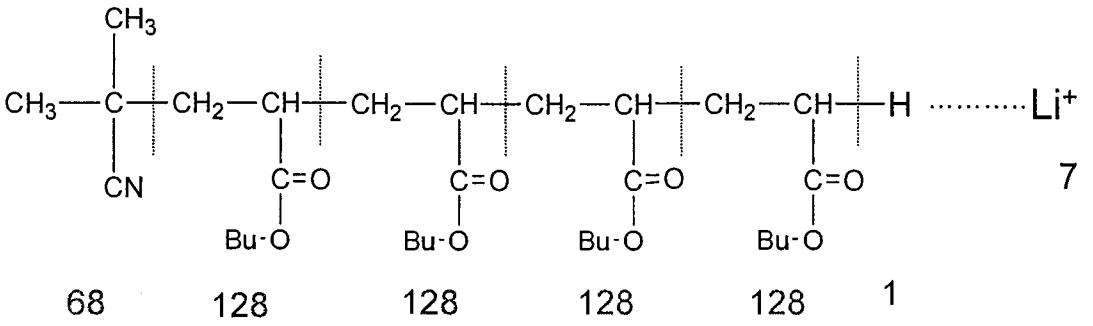

Figure 1.7: M/z 588 Oligomer of poly(butyl acrylate).

What does the m/z 588 mean? First, let's subtract the mass of the lithium cation Li^+ (7 Da) and then as many units of BA (128 Da) as possible until we are left with the sum of both end-groups, which in this case is 69 Da (corresponding to isobutyronitrile and the hydrogen atom). In principle, the sum of the end-group masses could be 69 plus one or more units of 128 Da, but this can be resolved by having some knowledge of the procedure used to synthesize the polymer.[9] In the case of PBA, the polymer was synthesized by free radical polymerization and isobutyronitrile came from the AIBN initiator. Each peak in the mass spectrum can be identified in the same manner to provide information on the sample at the molecular level, in contrast with IR and NMR which give only a bulk picture of the polymer. While both ESI-MS and MALDI-MS have been shown to give molecular weight distributions for polymer samples that differ from GPC,[9,16-18] they have been used for molecular composition (chemical structure and end-group identification), conformation and for copolymer sequencing.[9]

1.4.1 Composition

One polymer property that has been explored extensively by MALDI is the molecular weight distribution (MWD). Polymer MWDs are measured directly from oligomer ion intensities in the mass spectrum. Several homopolymer and copolymer MWDs have been obtained by MALDI: PMMA, polystyrene (PS), nylon, polyethylene glycol (PEG), polyesters, t-butyl acrylate/methyl acrylate and PS/PMMA.[9,19-21] Only narrow polydispersity polymers (D < 1.4) tend to yield correct MWD values compared to conventional GPC. Several reasons ranging from sample preparation to detector design were suggested for unsuccessful measurements of MWD of broad polydispersity polymers by MALDI,[22] and so a method was proposed to overcome this problem by fractionating a polymer by GPC prior to analyzing the resulting fractions by MALDI.[23,24]

Mass spectrometry is also used to analyze polymer structure and end groups. Distinguishing between two polymers that have different repeating units is straightforward in mass spectrometry. Each polymer will generate a mass spectrum that has different mass spacing between its constituent oligomers: for example, PMMA and PBA polymers produce mass spectra in which the oligomers are separated by 100 and 128 m/z, respectively. Different polymer structures such as cyclic, branched and star have been characterized by MALDI and ESI MS provided the end groups are chemically distinct from the structure of the oligomer backbone. Otherwise, determining polymer structures will be impossible, as in the case of most polyolefins.[19] As was discussed earlier, a variety of initiators may be employed to start a polymerization reaction.

Likewise, several termination processes can take place. Therefore, determining the oligomer end groups will provide insight into how these polymers are made (the polymerization mechanism). In addition, identifying polymer end groups is very important if further reactions need to be carried out such as derivatization. An example is the use of MALDI-TOF mass spectrometry (MS) to determine the polymer end groups for four Nylon 6 samples.[25] Each sample was synthesized separately with different procedures. Four end groups were identified: diamino, amino-methyl, dicarboxyl and amino-carboxyl moieties. Several distributions were generated for each sample due to ionization with different metal cations and H^+. Kuhn and Weidner used MALDI-TOF MS to study the mechanisms and kinetics of the reactions of derivatized PEG.[26] Three alkylhalogenides (ethyliodide, methyliodide and triphenylmethylchloride) were used to derivatize the hydroxyl PEG end groups. The decrease of hydroxyl PEG and the formation of mono- and disubstituted PEG were monitored as function of reaction time by mass spectrometry. MALDI-TOF MS was utilized to investigate PMMA polymerization photoinitiated by 2,2-dimethoxy-2-phenylacetophenone (DMPA) and benzoin.[27] Both initiators produce benzoyl radicals upon exposure to UV light together with either acetal or benzyl alcohol radicals (Figure 1.8).

Identifying oligomer end groups by MALDI led them to conclude that benzoyl radicals are responsible for PMMA free radical polymerization when DMPA and benzoin were use as photoinitiators. Also, initiation by DMPA was found to be cleaner than with benzoin since the MALDI mass spectrum of the latter showed several distributions of PMMA products. Wood et. al. studied poly(dimethylsiloxane) (PDMS) by ESI- Fourier Transform Mass Spectrometry (FTMS).[28] Four different aminopropyl end groups were

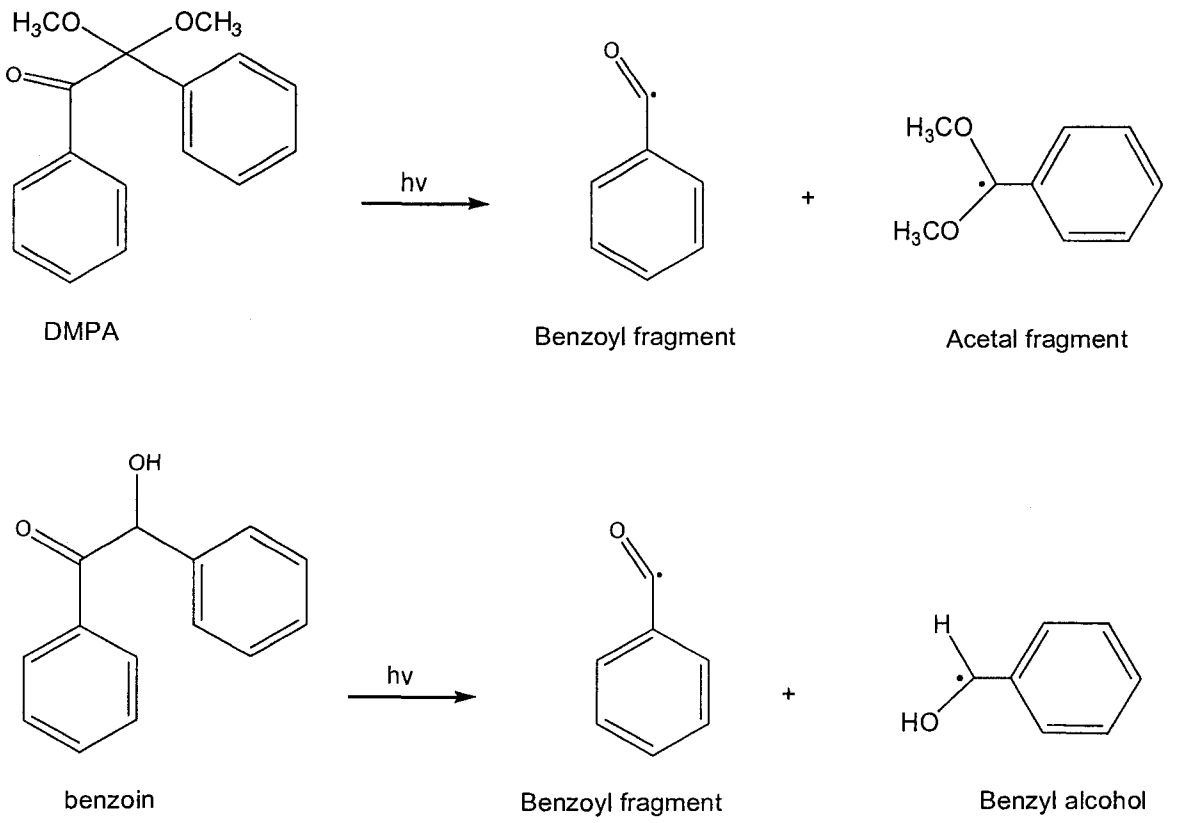

Figure 1.8: DPMA and benzoin UV light decomposition.

determined by comparing experimental masses with theoretical masses of expected structures. The major distribution corresponded to PDMS terminated by aminopropyl at each end. A proposed mechanism for the other three distributions revealed that they were formed from the initial PDMS major distribution. For example, PDMS terminated by aminopropyl and a hydrogen atom was generated from a hydrogen transfer reaction from an aminopropyl methyl group to an adjacent oxygen atom. PMMA free radical polymerization using four different peroxypivalate initiator compounds was studied by ESI-MS.[29] Decomposition of peroxypivalate produces different radicals that may start the radical polymerization. These radicals will incorporate into the growing polymer as end

groups. Therefore, determining the end groups of the different PMMA oligomer distributions gave information on which radical actually participates in the polymerization process at both the initiator and termination stages. Chen et. al. used ESI-MS/MS and gas-phase ion reactions to study various aspects of polymerization catalysts.[30-36] For instance, they developed screening methods for olefin polymerization catalyst libraries and determined rate constants of active species in polymerization reactions.

1.4.2 Copolymer Sequencing and Polymer Conformation

Before attempting to sequence a copolymer one should determine the fragmentation pattern of homopolymers that make up the copolymer under study. Collision induced dissociation (CID), which is MS/MS, has been used to determine the fragmentations pathway of several polymers. Jackson and Scrivens investigated a whole range of poly(alkyl methacrylate)s by different mass spectrometry techniques including MALDI and ESI CID and found that, for the most part, they have similar fragmentation patterns.[37-43] In each case the CID mass spectrum was dominated by low m/z fragment ions. Low intensity peaks at high m/z were assumed to be formed by neutral losses and from fragmentation along the polymer backbone. The end result was a variety of fragment ion progressions, each differing by one monomer unit. In the case of PMMA two major fragments were observed generated by homolytic cleavage for each end of oligomer backbone (Figure 1.9). Also PMMA shows minor fragments formed by 1,5-

hydrogen rearrangement. The authors proposed mechanisms for these homolytic cleavage and 1,5-rearrangment reactions as shown in Figures 1.10 and 1.11.

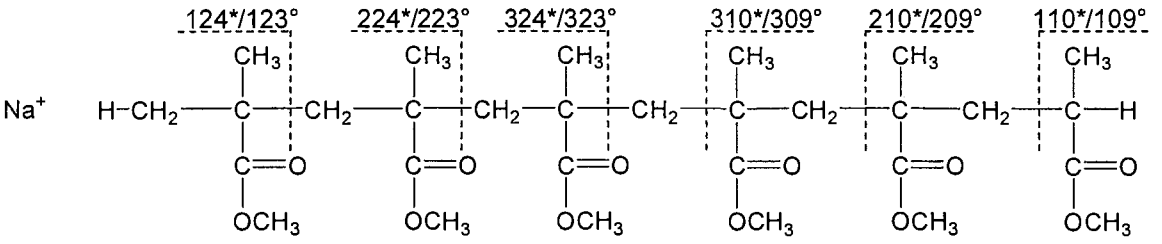

Figure 1.9: CID fragmentation pattern of poly(methyl methacrylate) ionized by Na^+ : (*) generated by homolytic cleavage and (°) generated by 1,5- hydrogen rearrangement.

Bowers et. al. proposed two possible mechanisms for the loss of the metal ion and backbone fragmentation.[42] Molecular mechanics/molecular dynamics (MM/MD) simulations demonstrated that the oligomer/metal ion adduct of PMMA takes on a quasicyclic structure. Upon collisional activation this ring opens leaving the metal ion attached to either end of the oligomer. The metal ion focuses dissociation near the end of the chain producing low m/z fragment ions. In the second mechanism, the ring opens by dissociation of the cyclic oligomer chain (Figure 1.12). The second mechanism should produce fragment ions with higher m/z ratio, in contrast to the observed experimental result. Recently, an alternative mechanism has been proposed by Wesdemiotis et al. in which the metal ion acts as a spectator while the oligomer undergoes what is essentially a free-radical decomposition pathway similar to that which occurs during pyrolysis.[44] When the oligomer backbone undergoes homolysis, the resulting radical can loss

sequentially monomers or back-bite the remaining chain, a process that can continue until only low mass fragments remain

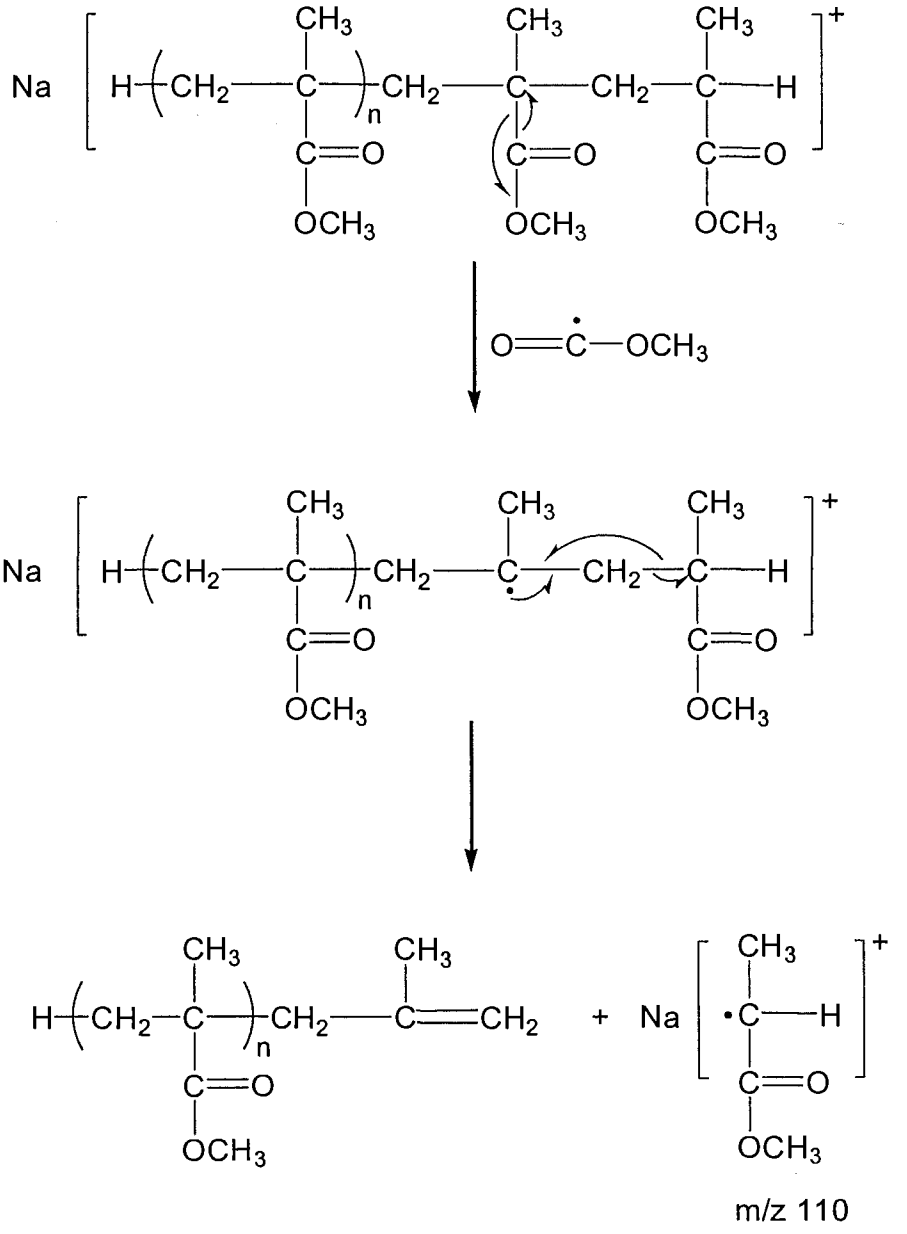

Figure 1.10: PMMA proposed homolytic cleavage mechanism.[41]

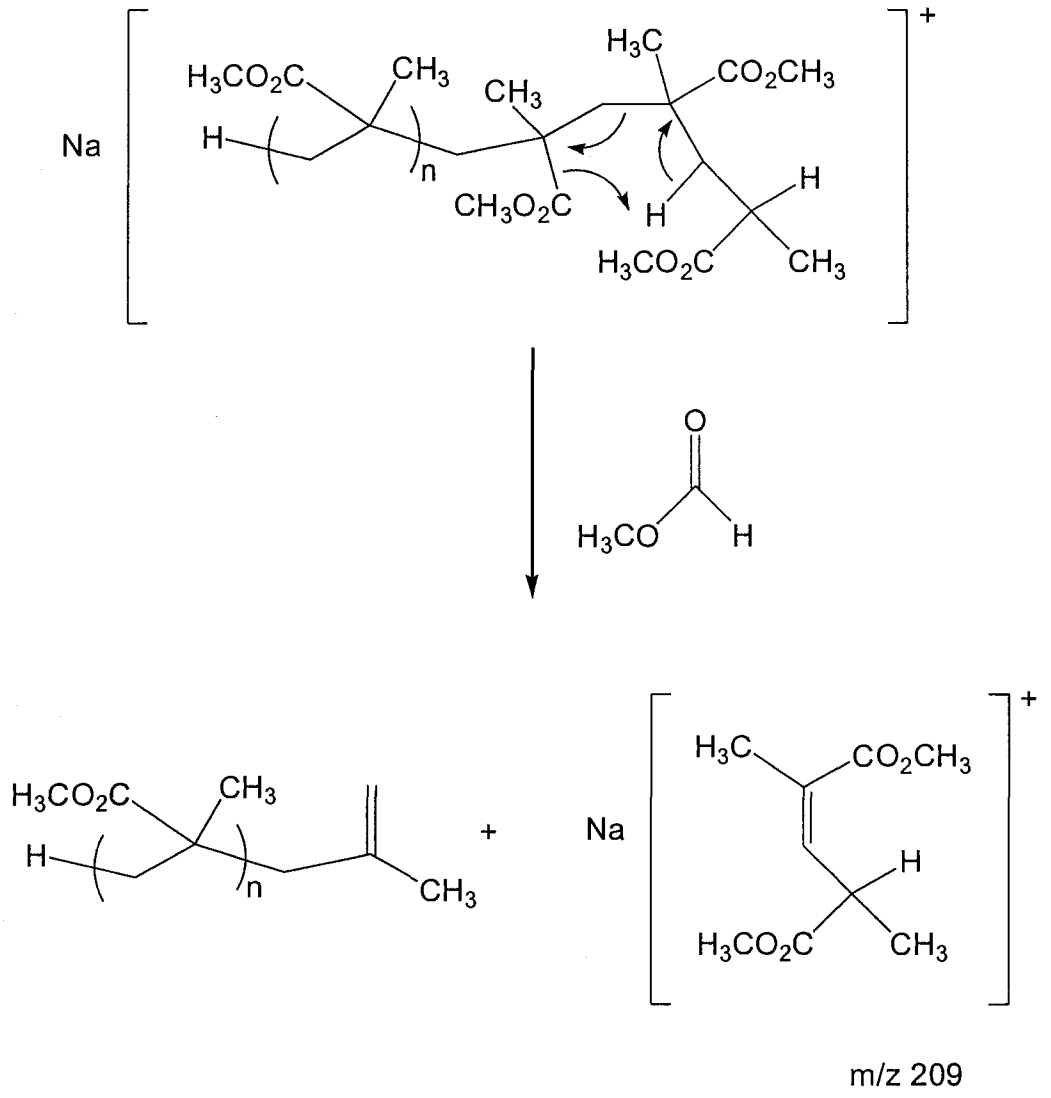

Figure 1.11: PMMA proposed 1,5- hydrogen rearrangement mechanism.[40]

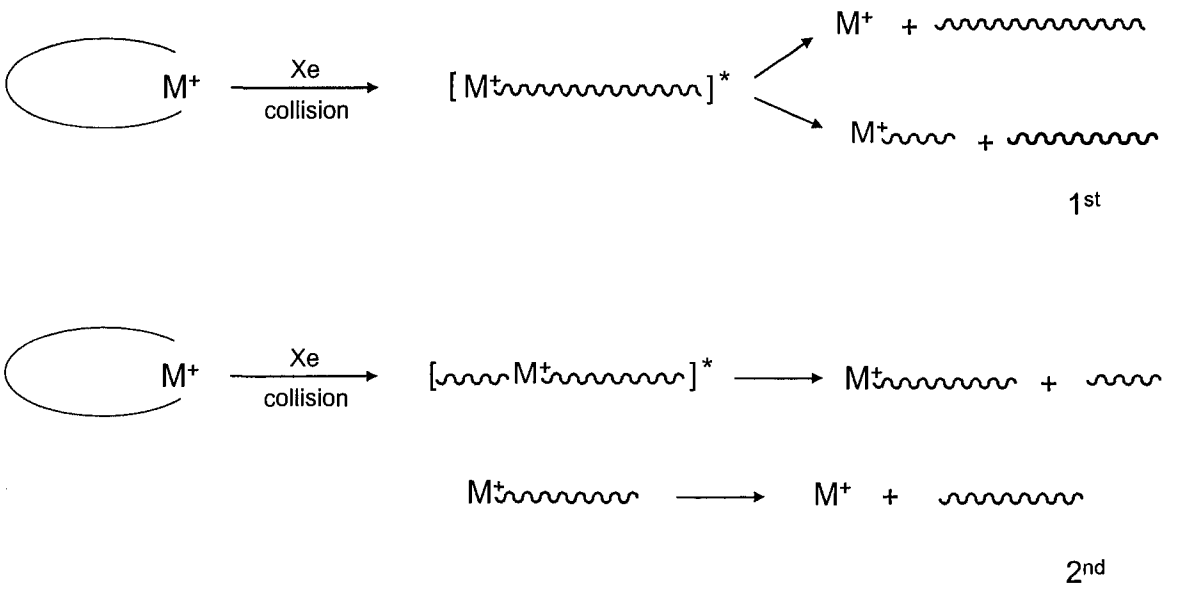

Figure 1.12: The two proposed mechanisms for the loss of metal ion and backbone fragmentation.

that are too short to undergo the radical back-bite. Several polymers undergo this fragmentation along the backbone such as polystyrene, poly(3-hydroxybutanoic acid), poly(ethylene oxide) and poly(propylene oxide).[45-48]

Usually gas phase polymer ion conformation is established by molecular modeling. Knowing the conformation of an ionized polymer can provide information that aids the interpretation of how ionized polymers behave in mass spectrometry, as we just saw for the case of polyacrylates. The cyclic PMMA structure forms because the ester side chains of the oligomer complex the metal cation.[42] In contrast, MM/MD simulations of ionized polystyrene predicted quasilinear structures with the metal cation associated between two adjacent benzene rings near the middle of polymer backbone.[49]

Coordination of the metal ion by oxygen atoms of oligomer side chains was also observed in the cases of PEG and poly(propylene glycol).[50]

1.5 Synopsis and Outline of Thesis

This thesis employs ESI and MALDI to explore the composition (monomer ratios) and structure (end group analysis) relative to ^{1}H NMR spectroscopy and theoretical predictions for three different copolymers: poly(butyl acrylate/vinyl acetate) (PBA/PVAc), poly(methyl methacrylate/vinyl acetate) (PMMA/PVAc) and PBA/PMMA. During this work it became necessary to investigate the effects of sample preparation on the MALDI mass spectra of these oligomers (Chapter 4). The effects of polymer conformation on the gas-phase collisional activation of ionized oligomers is explored in Chapter 5 by measuring their total relative fragment ion abundances. Observed trends were interpreated with the aid of MM/MD simulations of oligomer conformation as a function of chain length. In Chapter 6 a way to change the ionization of oligomers is discussed. As mentioned earlier, the use of metal ions tends to yield CID mass spectra dominated by low m/z fragment ions. This behaviour was changed by generating protonated oligomers in the gas phase by first forming proton-bound complexes of the oligomers with amino acids or peptides by electrospray ionization. These complexes dissociate first by loss of the amino acid/peptide to form protonated oligomers, which then undergo a unique fragmentation chemistry. In this chapter the results for PMMA and PBA will be discussed. A variety of methods have been developed to determine accurate proton affinity (PA) values. By and large, these methods have been applied to small

molecules due to the need for reference bases of similar structure and PA. But what of larger, poly-functional species, such as polymers? Can one define the PA for an oligomeric compound with many of the same functional groups? Chapter 7 tries to answer these questions.

2

Experimental and Computational Techniques

2.1 Electrospray Ionization (ESI)/Triple-Quadrupole Mass Spectrometers (TQMS)

The electrospray ion source was developed by John Fenn et. al. at Yale's department of engineering and applied science in 1984.[11,51,52] ESI mass spectrometry (ESI-MS) has resolved two long lasting challenges of mass spectrometry: ionizing high molecular weight compounds and coupling MS with liquid chromatography (LC). ESI-MS is capable of analyzing a protein with a molecular weight in access of 130,000 as well as low molecular weight compounds.[53] Today the coupling of ESI-MS to high performance liquid chromatography (HPLC) is a standard, commercially available option. ESI-MS has been applied to a wide range of compounds such as peptides, proteins, drugs, organic, inorganic and organometallic compounds and polymers.[10]

ESI transfers ions formed in solution to the gas phase through a process that can be broken down to three stages: formation of charged droplets, solvent evaporation and producing the gas phase ions. Usually the ions will form in solution by mixing the analyte

with an acid, base or salt (organic or inorganic). Apparent from this condition is that the analyte must be polar, and indeed ESI is used preferentially for polar compounds. The sample solution is carried into a metal tube capillary (Figure 2.1) with a flow of 1 μl/min to 1 ml/min (this flow rate is further reduced in a related technique called nanospray).[54] A high electric potential (2-5 kV) is applied to the tip of the capillary (relative to the counter electrode, which sits 2-3 cm away), Figure 2.1. Spraying under this strong field will lead to the separation of positive and negative charges in the solution. In positive ion mode, a high positive potential is applied to the tip so that negative ions will be attracted to the capillary and positive ions will travel toward the liquid surface. The positive charges will accumulate at the capillary tip on the liquid surface. These charges will repel each other and then expand away from the tip. This liquid expansion leads to the formation of a "Taylor cone", which is a cone-shaped liquid surface that forms when the electrostatic force from the accumulated charge equals the surface tension of the mobile phase (Figure 2.1).[10,55] Under the high field the Taylor cone liquid surface will breakdown and highly positively-charge droplets will spray from the capillary tip.

The size of these positively-charge droplets will get smaller and smaller as the solvent evaporates. This process occurs in the atomospheric pressure region between the capillary and the inlet cone of the mass spectrometer. A heated desolvation gas (N_2, 220°C) and a heated inlet (80°C) expedite solvent evaporation of the charged droplets. As the charge droplets shrink the ratio of their surface charge to surface area increases until Coulomb repulsion exceeds the surface tension of the droplet, at which point the droplet

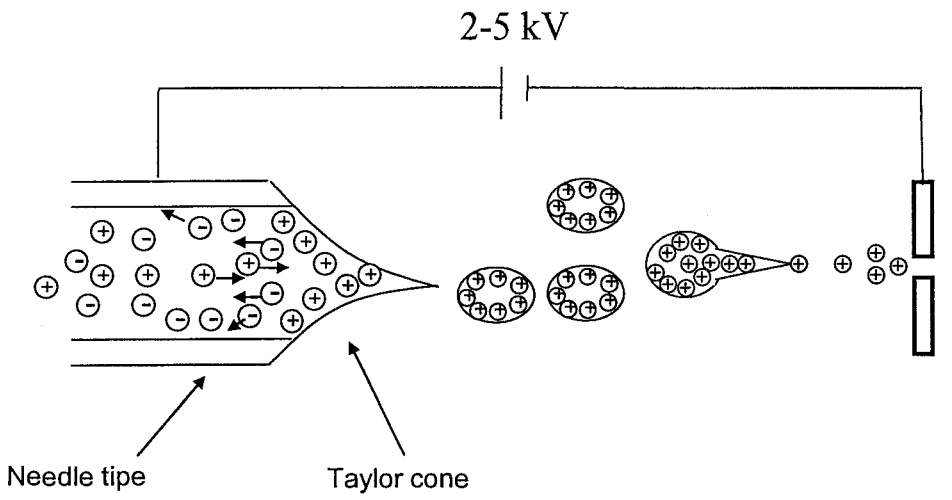

Figure 2.1: The process of ion formation in ESI (positive mode)

dissociates into smaller droplets (Coulomb explosion).[10,12] The Rayleigh stability limit[10] (2.1) is used to predict the point where the Coulomb repulsion equals the surface tension.

$$q_{Ry} = 8\pi(\varepsilon_o \gamma R^3)^{1/2} \qquad (2.1)$$

Where, q = droplet charge, R = droplet radius, ε_o = permittivity of vacuum and γ = surface tension

This process of solvent evaporation, shrinking and breakdown of droplets occurs many times until eventually solvent-free gas phase ions are produced. Also ions can be produced by direct evaporation from solvent droplets.[56] One of ESI-MS characteristics is the formation of multiply charged ions which can facilitate analyzing high molecular weigh compounds such as peptides and proteins. Since the mass spectrometer measures mass-to-charge ratio, multiple charges can reduce the m/z ratio of high molecular species so that they can be detected with instruments that typically have limited m/z ranges, such as quadrupole mass analyzers.

Quadrupole mass filters are commonly used in conjunction with ESI sources.[9,10,57,58] They produce low resolution mass spectra and are relatively inexpensive compared to other mass analyzers. Paul and Steinwegen demonstrated the principles of the quadrupole filter operation in 1953 at Bonn University.[59] The quadrupole mass filter consists of four parallel rods in a square configuration (Figure 2.2).[60,61] Ideally, the rods have a hyperbolic shape but in practice can be made cylindrical to simplify their manufacture. Opposite rod pairs are connected and supplied two voltages: direct current (DC) and radio frequency (RF), as shown in Figure 2.2. The total potential for each rod pair is similar but with different alternating polarity:

$$\text{Total potential} = \pm (U + V\cos \omega t) \qquad (2.2)$$

Where,

U = direct potential

V = amplitude of RF voltage

ω = angular frequency ($\omega = 2\pi\nu$), and ν = radio frequency

t = time

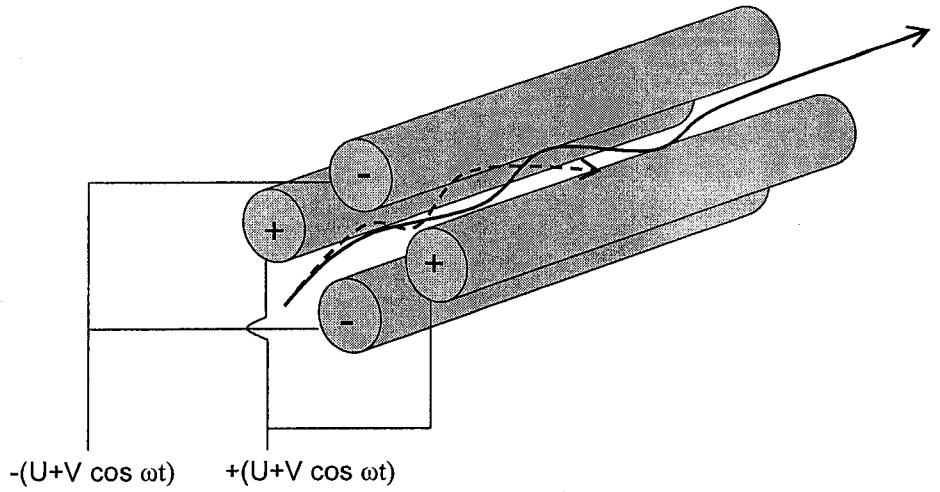

Figure 2.2: A quadrupole mass analyzer. The solid arrow represents the tragectory of a transmitted ion whereas the dashed arrow is an ion with an unstable trajectory (and thus is not transmitted).

As the ion travels along the z-axis through the rods it will be influenced by the total potential. For example, a positive ion will be attracted to the negative rod set. Prior to colliding with the negative rods, the polarity of the rods is switched, changing the trajectory of the positive ion. Rapid switching of the rod polarity effectively traps the ion motion in the x-y plane. So, a quadrupole mass filter is a 2-dimensional ion trap. The motion of the ion in the quadrupole filter is described by the Mathieu equation which has been studied in detail by McLachlan.[58,60] The solutions of the Mathieu equation produce two variables a and q:

$$a = \frac{8zU}{mr^2\omega^2} \tag{2.3}$$

$$q = \frac{4zV}{mr^2\omega^2} \tag{2.4}$$

The radius of the inner surface of the quadrupole rods (r) is a constant based on their manufacture. Therefore, keeping the radio frequency constant the a/q ratio yields 2U/V. Changing the values of U and V but keeping the ratio constant leads to the separation of different m/z ions. The plot of different U vs. V values in Figure 2.3 demonstrates the ion stability condition and the line of constant U/V ratio is often referred to as the operating line.[57] For example, three ions with different m/z each will have many U/V values that give stable trajectories and these conditions may overlap. By keeping the U/V constant along the operating line, m_1 can be successfully transmitted in the absence of m_2 and m_3, which will be discharged on the rods (unstable trajectory). In the same manner m_2 and m_3 will be separated by increasing the values of U and V.

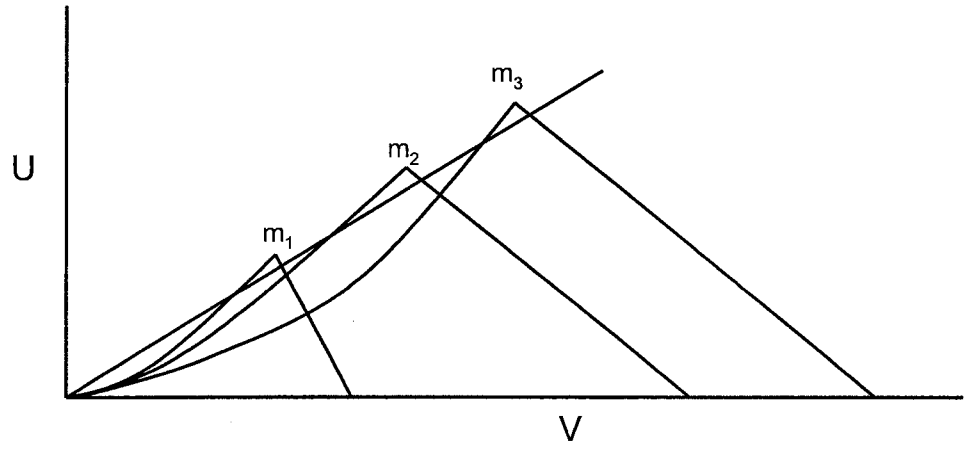

Figure 2.3: Ions stability condition in U vs. V plot. m_1, m_2 and m_3 are three different m/z ions.

In triple-quadrupole mass spectrometers three quadrupole analyzers are placed in series as is seen in Figure 2.4. While referred to as a triple-quadrupole mass spectrometer, the central quadrupole is usually replaced with a hexapole or octapole to improve 2-D

trapping in the experiments that will be discussed below. The first quadrupole (Q1) is used to select the precursor ion from all ions produced by the source (Figure 2.5). The second quadrupole (or hexapole) (Q2) is operated in RF-only mode as a collision cell where a gas can be introduced to collide with the selected ion to give collision-induced dissociation (CID). Then the fragment ions produced in this processes can be analyzed by the third quadrupole (Q3).

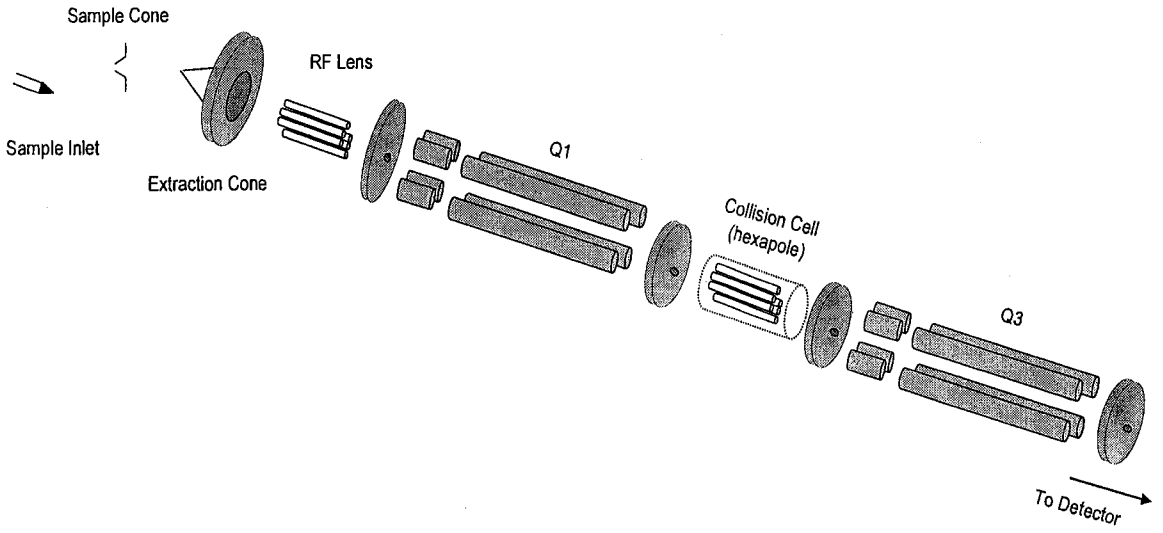

Figure 2.4: Schematic diagram of a triple-quadrupole mass spectrometer

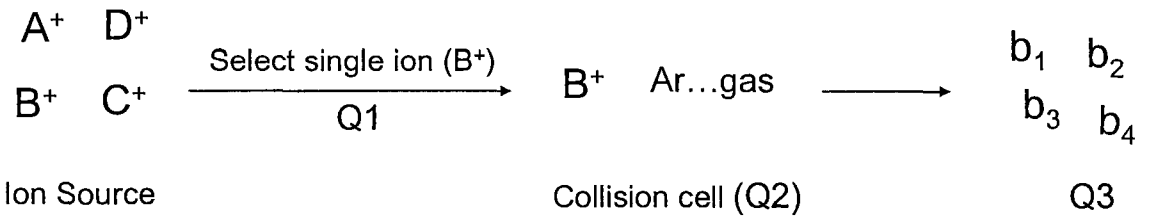

Figure 2.5: Presentation of CID process

2.2 Matrix-Assisted Laser Desorption Ionization (MALDI)/Time-of-Flight (TOF)

From the name of this technique its similarity and relationship to Laser Desorption Ionization (LDI) is clear.[9,57,61,62] When a molecule is exposed to a photon, it can absorb the photon provided it has a chromophore with the correct energy level spacing (i.e., an absorption spectrum that matches the wavelength of the laser).[61] If enough energy is delivered, the molecule can be desorbed from the surface and even ionized. Thus, the wavelength of the laser has to be adjusted to analyze different samples in LDI. This problem is overcome by the use of a matrix in which the analyte is mixed. Now, only the matrix needs to have an absorption spectrum matching that of the laser pulse, and is the same for all compounds to be analyzed.[13-15]

Typically in MALDI the ratio of matrix to analyte is quite large, and other additives such as metal salts may be added to help ionization (as is the case for most polymer analyses by MALDI). About 1μL of the resulting mixture is deposited onto a sample target and is allowed to dry and form a solid solution. During solid solution

formation, a competition occurs between crystallization (which is favourable) and precipitation followed by separation of the matrix and analyte.[63] The latter does not allow molecule to molecule contact which is needed to facilitate energy transfer. The sample is then irradiated by a pulsed laser, typical examples of which are N_2 lasers (337nm) and CO_2 IR lasers(10.6 μm).[9] The matrix absorbs the photon energy and can ionize (Figure 2.6). Some of this absorbed energy will be transfered to the analyte and lead to its ionization. Ion formation in MALDI is not well understood, however detailed studies of the process show that ionization occurs at the surface of the analyte/matrix solid solution.[9,62,64,65] Upon laser irradiation, a supercompressed gas "plume" of matrix and analyte is formed in which a charge transfer between them can take place. As the MALDI 'plume" expands, it carries the analyte along with it to the mass analyzer.

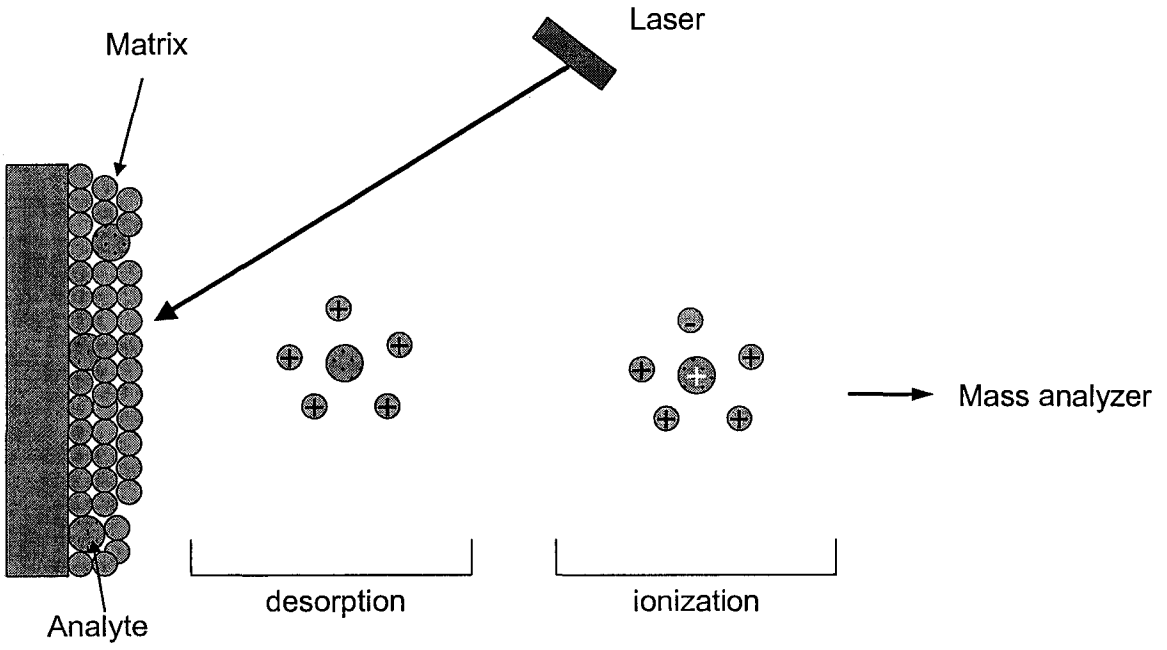

Figure 2.6: The ionization process in the MALDI

MALDI matrices used in the analysis of synthetic polymers tend to be aromatic organic compounds and some of the most frequently used are: 2,5-dihydroxy benzoic acid (DHB), 2-(4-hydroxyphenylazo)benzoic acid (HABA), 1,8-dihydroxy-9(10H)-anthracenone (Dithranol), 3,β-indolacrylic acid (IAA), and α-cyano-4-hydroxycinnamic acid (CHCA) (Figure 2.7). Some textbooks give a preferred analyte:matrix molar ratio in the range of 1:100-1:1000, while others suggest up to 1:50,000. The ratio will vary depending on the polymer and one should try different ratios before deciding on the optimal one. The selection of the right matrix is still a trial –and-error method. One can look at lists or libraries prepared by National Institute of Standards and Technology (NIST) as start [http://polymers.msel.nist.gov/maldirecipes/].

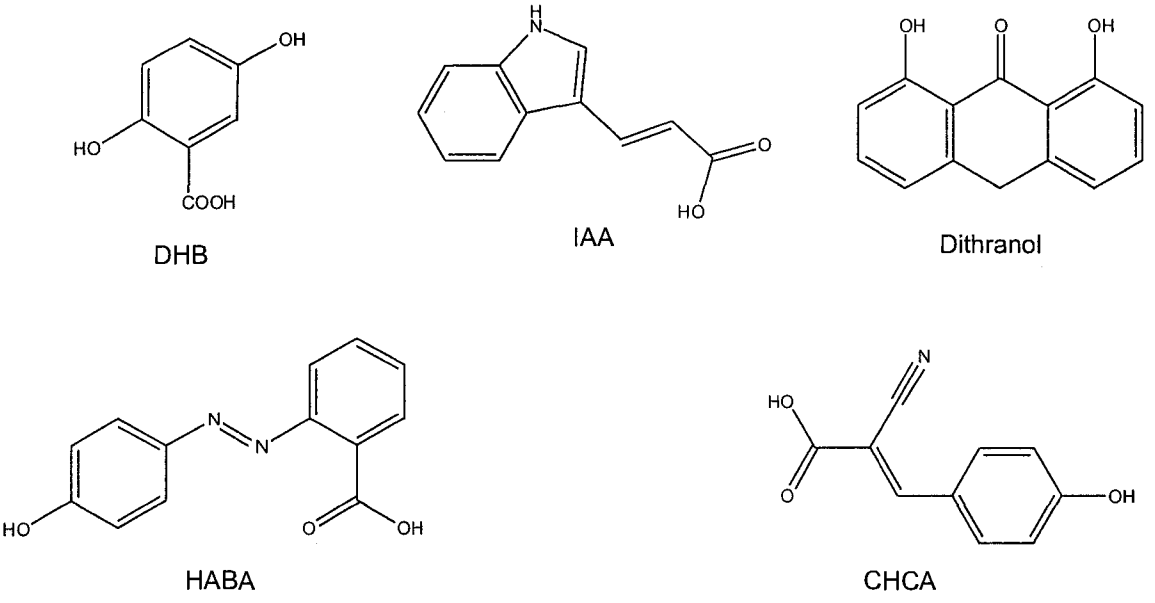

Figure 2.7: Common matrices used in the analysis of synthetic polymers by MALDI.

The quality of MALDI spectra is sensitive to sample preparation, ionization efficiency issues related to oligomer structure and end-groups (in the case of polymers), and instrumentation.[66-73] Sample preparation consists of different components:

preparation procedure, type of matrix, solvent, salt and the ratio between them. Changing or altering one of these factors may have a significant impact on the resulting mass spectrum. Intensive work has been carried out on method development for mixing of the polymer with a matrix and loading it on the MALDI target.[9,19,20,62,74,75] MALDI is considered a soft ionization process in that it tends to generate intact molecular ions (usually protonated, deprotonated or as adducts). It is also a sensitive method that can analyze samples in the low femtomole range. MALDI is capable of analyzing high molecular weight synthetic polymer (1,500,000 Da) and proteins (300,000 Da) when coupled with time-of-flight (TOF) mass spectrometry.[76,77]

Time-of-flight (TOF) mass spectrometry is based on the simple idea that when ions are given the same kinetic energy, ions with larger mass will have lower velocities and thus take a longer time to travel an evacuated distance (d) than lower mass ions.[9,57,58,61] It is important that the ions be formed at the same time in the ion source and so the use of a laser pulse on the ns timescale in MALDI is an obvious reason why these two techniques are commonly found together. After the formation of the ions in the MALDI source they will be accelerated by a potential (V). The kinetic energy of the ion is given by equation (2.5).

$$zeV = \frac{1}{2}mv^2 \qquad (2.5)$$

Where,

z = number of the charges

e = the charge on the ion

m = mass

v = velocity of the ion

Ions having equal velocity will travel the distance in the same time as given by equation 2.6.

$$t = d/v \tag{2.6}$$

Substituting 2.6 into 2.5 yields 2.7:

$$zeV = \frac{1}{2}m\left(\frac{d}{t}\right)^2 \tag{2.7}$$

If the accelerating potential V is held constant and d is fixed, then equation 2.7 yields the result that ion flight time is proportional to the square-root of the m/z (equation 2.8).

$$t = \sqrt{m/z} \text{ x constant} \tag{2.8}$$

Early TOF instruments had two problems: ions are formed with a distribution of initial kinetic energies and in different locations in the ion source. This results in ions with the same m/z arriving at the detector with different flight times, producing a mass spectrum with poor resolution. Both problems were overcome by using time-lag focusing (delayed extraction)[78] and a reflectron (Figure 2.8).[9] In time-lag focusing the ions are allowed to drift for short time before acceleration to make sure that after acceleration they reach the detector at the same time. The reflectron is an electrical mirror in which faster ions will penetrate and spend more time than slower ions of the same m/z. Both will be time-focussed at the detector.

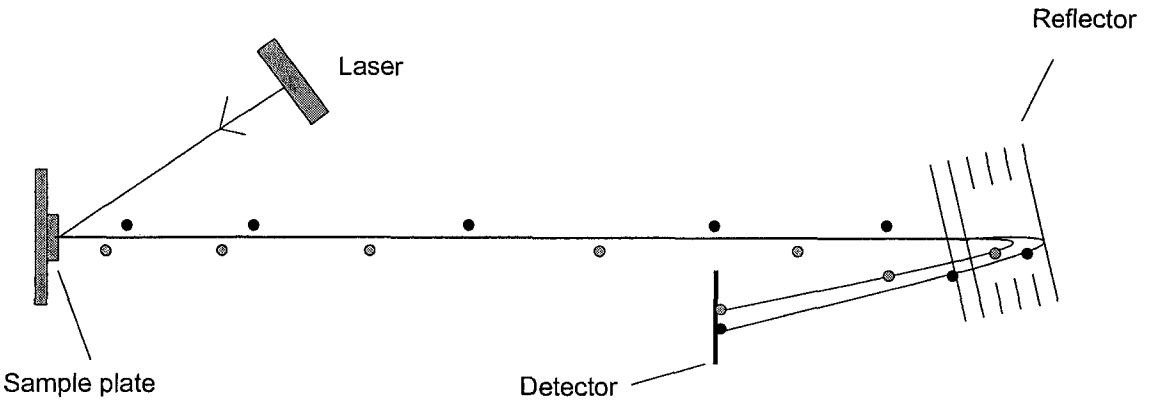

Figure 2.8: Reflectron TOF with MALDI source.

2.3 Molecular mechanics / molecular dynamics[79]

Molecular mechanics (MM), is also known as a force field method. Unlike moelcular orbital methods, in MM nuclei and electrons are not defined explicitly, but rather in the form of atoms with partial charges. MM is based on the concept that the properties of a chemical group are transferable. Therefore, the force constant of a C—C single bond stretching motion is generally the same from one molecule to another, provided the molecules are chemically similar.[80] This gives us the ability of modeling large molecules based on the parameters developed from small molecules.

The energy, V, of a molecule is expressed by:

$$V = \sum_{bonds} \frac{k}{2}(I - I_0)^2 + \sum_{angles} \frac{k}{2}(\theta + \theta_0)^2 + \sum_{torsions} \frac{V_n}{2}(1 + \cos(n\omega - \gamma))$$
$$+ \sum_{i=1}^{N} \sum_{j=i+1}^{N} \left(4\varepsilon_{ij} \left[\left(\frac{\sigma_{ij}}{r_{ij}} \right)^{12} - \left(\frac{\sigma_{ij}}{r_{ij}} \right)^{6} \right] + \frac{q_i q_j}{4\pi\varepsilon_0 r_{ij}} \right) \quad (2.9)$$

The first term in equation (2.9) accounts for the bond strain between two atoms (bond stretching). The second term is the contribution of molecule angles (bending). A harmonic potential is used to model both terms since a Morse potential is too costly for large molecules. In both terms k is the respective force constant, I represents bond length and θ the bond angles. The third term deals with the bond torsions. V_n is the "barrier height" for a bond, n is the multiplicity of the torsion (maxima and minima), ω is the value of torsion and γ is the phase factor used to position the maxima and minima. The last term accounts for non-bonding interactions. The Lennard-Jones potential is used for van der Waals interactions. The Lennard-Jones potential has an attraction part $\left(\frac{\sigma_{ij}}{r_{ij}} \right)^6$ and a repulsive part $\left(\frac{\sigma_{ij}}{r_{ij}} \right)^{12}$ where ε is the depth of the well and σ is the collision diameter. The last term is a Coulomb potential to account for electrostatic interactions, where q is the charge of the atom, ε_0 is the permittivity of free space and r is the distance between I and j.

In MD modeling, the conformation of a molecule is generated by integrating Newton's laws of motion. The result is a trajectory that shows how the particle position

and velocities change with time. The way MD generally works can be summarized in the following steps:[80]

1- Select an initial position and velocity for the atoms

2- Compute the momentum and force for each atom.

3- Then compute new positions and velocities after short time. The time step in MD must be short (1 fs, vibrational frequency) to have conformations close to each other.

4- Repeating the previous steps long enough for the system to reach equilibrium (typical equilibrium times are on the order of one hundred picoseconds in step of 1fs).

5- When the system reaches equilibrium, the atomic coordinates are saved every few iterations, resulting in a list of coordinates over time called a trajectory.

Conformation is the three-dimensional structure that molecules adopt. Simulated annealing methods are used to find the global energy minimum conformation for a molecule. The temperature of a molecule is varying systematically between high and low temperature, 300 to 800 K for instance, called an annealing cycle. The high temperatures allow the molecule to pass high energy barriers and as result occupy lower energy conformation. One should obtain several simulated annealing runs and only decide on the lowest energy conformation after it has been generated many times.

3

Experimental and Computational Procedures

3.1 Polymerization Reaction Procedures

Free radical polymerization was used to synthesis: poly(methyl methacrylate) (PMMA), poly(butyl acrylate/vinyl acetate) (PBA/PVAc), poly(methyl methacrylate/vinyl acetate) (PMMA/PVAc) and poly(butyl acrylate/methyl methacrylate) (PBA/PMMA). Butyl acrylate (BA) and methyl methacrylate (MMA) (Aldrich) were washed three times with 10% sodium hydroxide in water (wt/wt.-%), followed by three washes with distilled, deionized water and were dried over calcium chloride. The washed monomers (BA and MMA) and vinyl acetate (VAc) (Aldrich) (Figure 3.1) were purified by vacuum distillation. The initiator azodiisobutyronitrile (AIBN, Polyscience Inc.) (Figure 3.2) was recrystallized three times in methanol. The chain-transfer agent (CTA) dodecanethiol or butanethiol (Aldrich) (Figure 3.2), the polymerization solvent toluene (BDH Ltd.), acetone, deuterated chloroform, sodium chloride (NaCl) and lithium chloride (LiCl) were used without further purification.

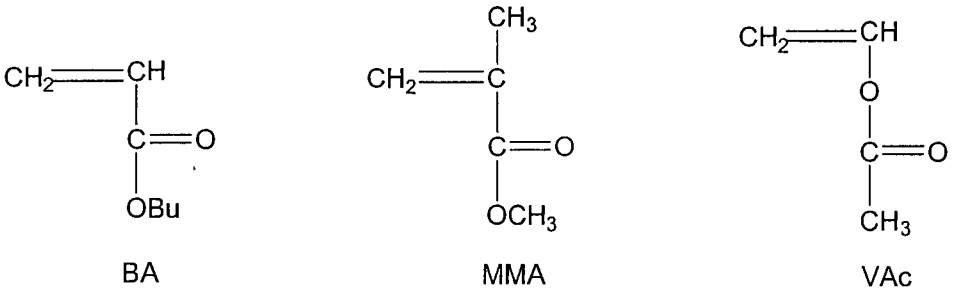

Figure 3.1: The monomers used in the reactions

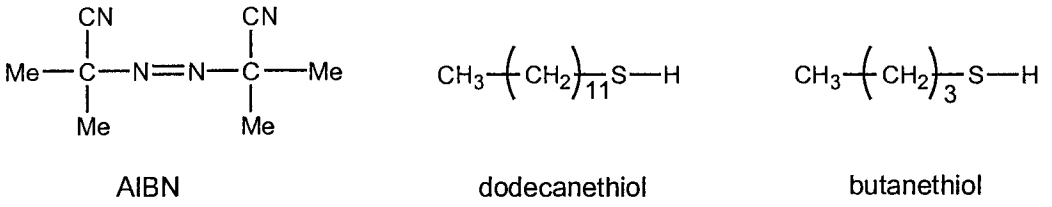

Figure 3.2: Initiator (AIBN) and dodecanethiol and butanethiol (CTA)

The reaction mixture containing one or two different monomers (4 to 11 wt/wt.-%) was pipetted into glass ampoules. The ampoules were degassed by four freeze-pump-thaw cycles (Figure 3.3), sealed and heated to 60-61°C. To stop the polymerization process at a given reaction time (or percent conversion), the ampoules were transferred to an ice bath. Solvent was evaporated at room temperature and atmospheric pressure, and the polymers were dried under vacuum for 12 hours. Oligomers of molecular weight up to 2000 Da were produced.

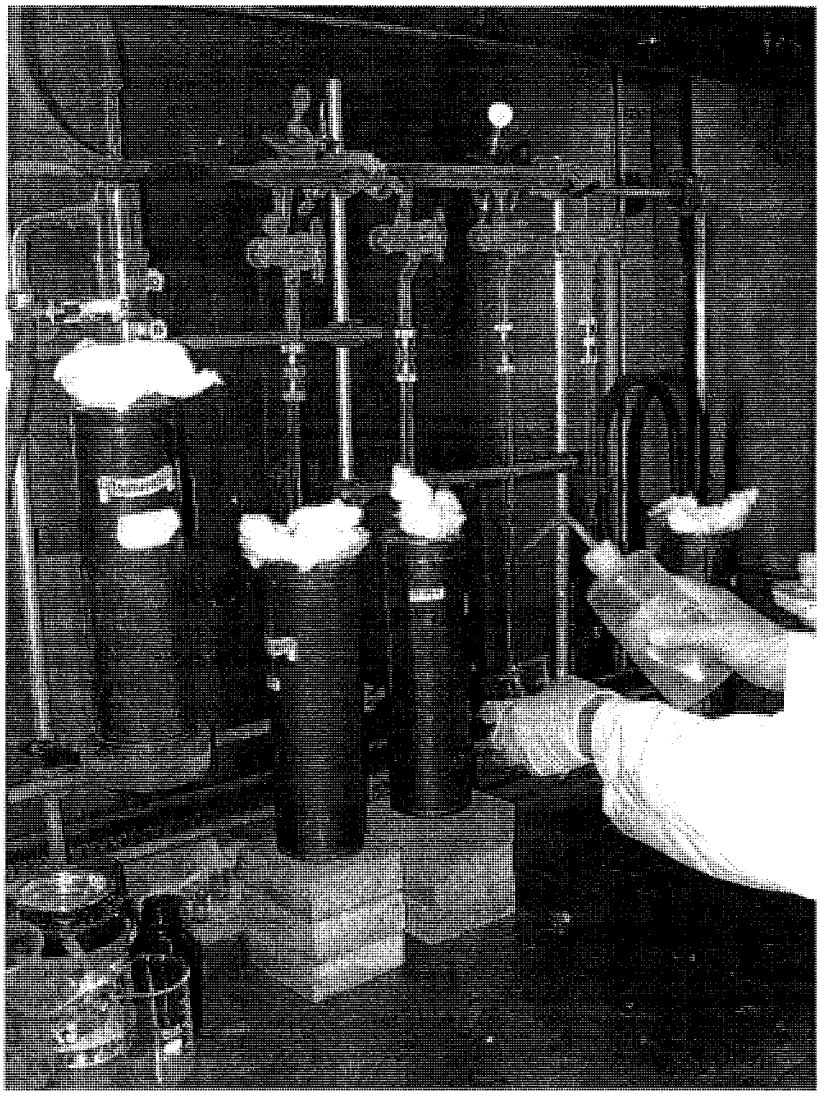

Figure 3.3: The reaction set-up

A JAVA™ based polymerization simulator developed by Badeen and Dubé,[7] was used to predict the results of free radical polymerization and thus to determine appropriate reaction conditions (monomer, initiator and chain-transfer agent concentrations) to produce the desired product average molecular weight. In addition, the compositions of PBA/PMMA copolymers were probed by changing CTA and initiator concentrations.

Reaction mixture information is listed in Table 3.1. The mass conversion (C) of each copolymer was calculated by gravimetry using equation (3.1).

$$C(\%) = \frac{w_{copolymer}(g)}{V_{ampoule}(mL) \times C_{mon}(g\,mL^{-1})} X\ 100 \qquad (3.1)$$

where $w_{copolymer}$ is the weight of the dried copolymer, $V_{ampoule}$ is the total volume of the reaction mixture and C_{mon} is monomer concentration of the reaction mixture. Additional to the synthesized polymers, standard PMMA and polystyrene (PS) were purchased from Polymer Laboratories (Shropshire, UK) and poly(butyl acrylate) (PBA) from Polymer Source Inc. (Montreal, QC, Canada)

Table 3.1: Reaction conditions

Monomers	(wt/wt-%)[a]	CTA (mol L^{-1})	AIBN (mol L^{-1})	Reaction No.
MMA[b]	4	0.02	0.03	
BA/Vac[c]	11/11	0.02	0.05	
MMA/Vac[c]	7/7	0.02	0.05	
BA/MMA	5/5	0.02	0.03	i
		0.03	0.03	ii
		0.05	0.03	iii
		0.02	0.05	iv

[a] The balance of the reaction mixture is toluene
[b] only used in chapter 5
[c] synthesized and analyzed by a previous masters student.[81]

3.2 ^{1}H-NMR Spectroscopy

Proton NMR experiments were performed using a 500 MHz NMR (Varian Inova, CA, USA). 15 mg of the desired copolymer was dissolved in deuterated chloroform. The group alpha to the oxygen atom of the ester side-chain was monitored for quantitation: the group $-OCH_2$ of BA ($\delta \approx 4.0$ ppm), $-OCH_3$ of MMA ($\delta \approx 3.5$-3.6 ppm), and the α-hydrogen in VAc ($\delta \approx 4.9$ ppm) (as an example see Figure 3.4).[82,83] The integration of the peaks obtained by NMR were scaled according to the number of hydrogen atoms in the group of interest: 1/2, 1/3, and 1 for BA, MMA, and VAc, respectively.

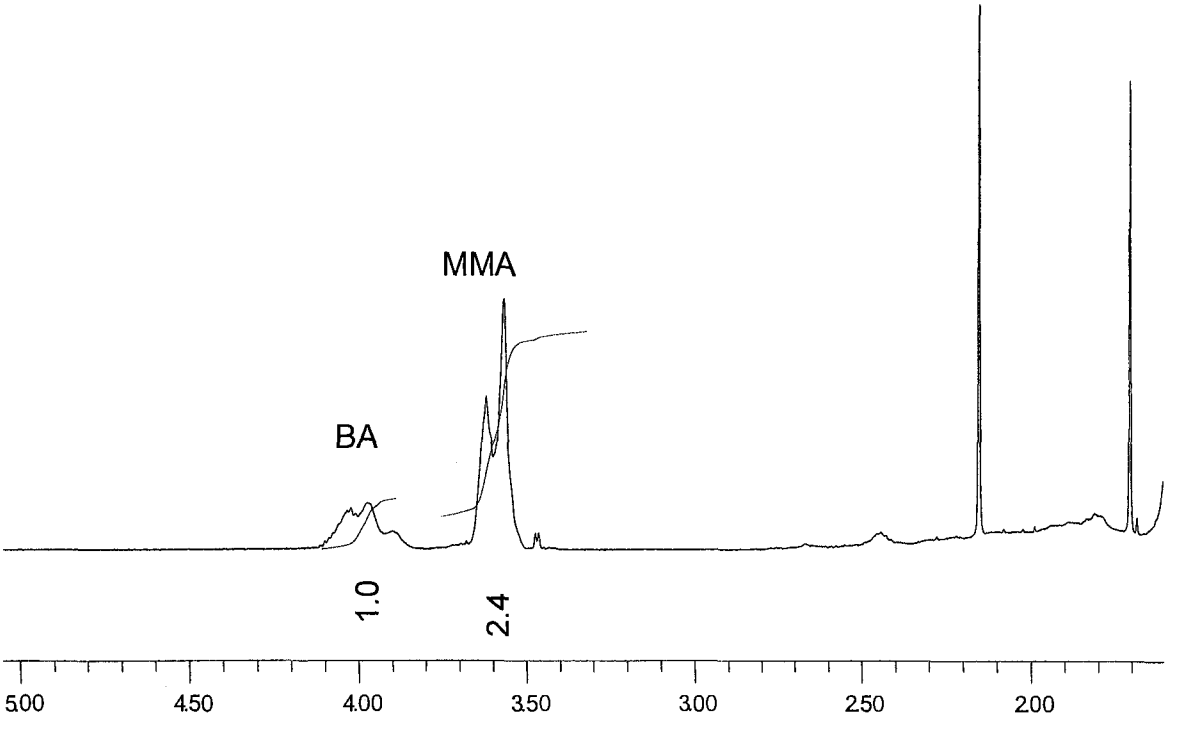

Figure 3.4: NMR spectrum of PBA/PMMA synthesized by free radical polymerization, showing the group $-OCH_2$ of BA and $-OCH_3$ of MMA used to quantifying each monomer.

3.3 ESI-MS, MS/MS

ESI-MS experiments were performed using a Micromass Quattro LC triple quadrupole mass spectrometer (Waters Micromass, Manchester, UK) equipped with a Z-spray ion source. Polymer samples were dissolved in acetone and water (9:1) to a concentration of 1 mg mL^{-1} along with 0.25 mg mL^{-1} of LiCl or NaCl. Positive ESI capillary was operated between 4.0-4.95 kV and sample cone voltage was set to 180 V. The solutions were introduced into the mobile phase (9:1 acetone: water) (v/v) which was pumped at a rate of 60 μL min^{-1}. For PS polymer (chapter 5), 1 mg mL^{-1} was introduced with $AgNO_3$ (0.25 mg mL^{-1} in 9:1 acetone : water) at a flow rate of 30 μL min^{-1}.

For the attachment of peptides or amino acids to polymers (Chapter 6 and 7), polymer and amino acid or peptide were dissolved in acetonitrile and water (8:2) (v/v) to make a ratio of 1:1 or 1:280 (c/c) polymer : amino acid or peptide. Several drops of 5% formic acid were added. Sample cone voltage was reduced from 180 to 40 V. The solutions were introduced into the system by syringe pump at a rate of 40 μL min^{-1}. Different amino acids were used: Glycine (Gly), Alanine (Ala), Leucine (Leu), Phenylalanine (Phe), Tryptophan (Trp), Aspartic acid (Asp), Lysine (Lys) and Arginine (Arg) (Sigma-Aldrich). Also two different peptides were used Diglycine (DiGly) and Triglycine (TriGly) (Sigma-Aldrich). For CID experiments, argon was used as collision gas with pressure from 1.0 X 10^{-4} to 2.0 X 10^{-3} mBar depending on the experiment. Details of the conditions will be given for each experiment.

3.4 MALDI-MS

MALDI-MS experiments were performed using a Bruker OmniFLEX time-of-flight (TOF) mass spectrometer (Bruker Daltonics, Billerica, MA, USA). The MALDI-TOF is equipped with a nitrogen laser (λ= 337.1 nm, Thermo Laser Science) producing pulse widths of < 4 ns and a maximum power of 200 μJ. Positive ion mass spectra were acquired using the TOF in reflecting mode and an accelerating voltage of 19 kV (and a reflecting lens voltage of 20 kV). Each final mass spectrum was the sum of 300 single-shot mass spectra collected from five different regions of the same sample spot. Bruker Xmass^{TM} software was used to process the data. Each copolymer sample was dissolved in THF with a 2,5-dihydroxybenzoic acid (DHB)/copolymer/trifluoroacetate (6:1:0.33) mixture. 1 μL was spotted on the MALDI target. The mass spectrometer was operated with greater than unit mass resolution

3.5 MM/MD Procedures

Molecular mechanics/molecular dynamics (MM/MD), semi-empirical and density functional theory calculations were performed to predict the structure of the polymer ions in the gas phase and the relative energies of PMMA ion fragmentation products observed by collision-induced dissociation mass spectrometry. The Cerius2 modeling environment [84] was used to model structures of PMMA ionized with sodium ions and PS ionized with silver ions ranging from their 5mers to their 12mers. Atomic charges were assigned by

the Cerius2 program. The charges of any added groups or atoms were estimated from HF/6-31G(d) calculations. To study the conformation of the polymer ions, equilibration and annealing dynamics were performed. During the equilibration phase energy-minimized structures of the ionized polymers were run for 100 ps (1 fs step size) at constant NVT (constant number of moles, volume and temperature: 300K) to determine the equilibrium structures. The lowest energy equilibrium structures were then submitted to between 100 and 1000 annealing cycles (at constant NVT) in which the temperature was varied from 300 to 800 K in increments of 100 K and then down to 300 K. One thousand steps (1 ps) of dynamics were done at each temperature increment and the model was minimized to 0 K after each complete annealing cycle. Annealing cycles were continued until the energy of the structures reached a low energy plateau.

3.6 Molecular Orbital Calculations

Standard ab initio molecular orbital calculations[85] were performed using the Gaussian 98[86] suite of programs. The geometries of the lowest energy conformations of the 5mer and 12mer of PMMA(HH) from the annealing runs were optimized, and vibrational frequencies calculated, using AM1 semi-empirical theory.

3.7 RRKM Calculations

RRKM modelling of the microcanonical rate constant, k(E), used the standard expression:[87]

$$k(E) = \frac{\sigma N^{\ddagger}(E - E_0)}{h\rho(e)} \tag{3.2}$$

Where $N^{\ddagger}(E\text{-}E_0)$ is the transition state sum-of-states above the 0 K activation energy,E_0, and $\rho(E)$ is the density of states of the reactant ion at an internal energy E. Transition state sums-of-states and reactant densities-of-states were calculated by direct count according to the algorithm of Beyer and Swinehart.[88] For the simple-bond cleavage reactions, the transition state frequencies were estimated using the reactant ion frequencies, less one mode to represent motion over the col. This motion was chosen to be a C—C stretching frequency of magnitude 1075 cm^{-1}.

To determine the effect of chain length on the average vibrational energy and RRKM rate constant in PMMA(HH) ions a set of "monomer" vibrational frequencies were developed that could be multiplied by the number of repeat units in a given PMMA polymer ion. This set of frequencies was obtained from the AM1 calculated harmonic frequencies for a single methyl methacrylate molecule ionized by Na^+ and are listed in Table 3.2. Three frequencies corresponding to motion of the sodium ion were removed from the monomer list. To obtain the frequencies for a $PMMA_n(HH)+Na^+$ ion, the monomer frequencies were repeated n times and the three metal ion modes were added. The resulting log $k(E)$ vs E curves for the four main C—C bond cleavage reactions (in which the $\Delta S^{\ddagger}(600K)$ was set arbitrarily to + 25 J K^{-1} mol^{-1}) in the resulting 5mer and 12mer were compared to those obtained using the actual calculated 5mer and 12mer AM1 frequencies to obtain a scaling factor of 0.87 for the monomer and metal ion modes.

Table 3.2. Repeat Unit Harmonic Vibrational Frequencies Used in the RRKM Modeling of $PMMA_n(HH)+Na^+$ (n = 5 - 12)

	Harmonic Vibrational Frequencies (cm^{-1})
Monomer modes	19, 104, 130, 134, 148, 220, 255, 307, 352, 511, 631, 695, 897, 938, 973, 979, 1097, 1126, 1157, 1164, 1167, 1235, 1291, 1302 1311, 1311, 1320, 1322, 1322, 1326, 1355, 1365, 1373, 1472, 1954, 2871, 2919, 2921, 2923, 2926, 2934, 2942, 3006, 3009, 3009
Scaled Monomer modes	17, 90, 113, 117, 129, 192, 222, 267, 306, 444, 549, 604, 781, 816, 847, 852, 954, 979, 1007, 1012, 1015, 1075, 1123, 1133, 1140 1141, 1148, 1150, 1150, 1154, 1179, 1188, 1194, 1281, 1700, 2498, 2540, 2541, 2543, 2546, 2553, 2560, 2615, 2618, 2618
Metal Ion modes	33, 49, 54
Scaled metal ion modes	27, 41, 45

4

Characterization of Synthetic Copolymers

4.1 Introduction

The composition and chemical structure of copolymers influence the physical and chemical properties of the materials from which they are made. It is also important to understand the kinetics of copolymer formation which affect the nature and distribution of the final polymerization products. It is well known that copolymer composition will change over the course of a reaction since each monomer has its own specific homo- and cross-propagation rate constants. The outcome of free radical polymerization can be predicted based on the reactivity ratios of the reacting monomers, i.e., will each monomer prefer to react with itself or with each other? Methods used to estimate the copolymer reactivity ratios involve a variety of statistical approaches,[89] but all rely on one important piece of information: the measured ratio of each monomer bound in the product copolymer, typically obtained from infrared (IR) and nuclear magnetic resonance (NMR) spectroscopies.[9,20] The structure of a copolymer can be defined as the sequence of the monomeric subunits forming the polymer chain together with the nature of the end

groups. NMR and IR spectroscopies give a bulk picture of a copolymer sample whereas mass spectrometry has the potential to provide molecular level information.

In this study we have examined the performance of ESI-MS and MALDI-MS for determining the composition (monomer ratios) and structure (end group analysis) relative to ^{1}H NMR and theoretical predictions (from a JAVA™-based polymerization simulator, developed by Badeen and Dubé)[7] for three different families of copolymers: poly(butyl acrylate/vinyl acetate) (PBA/PVAc), poly(methyl methacrylate/vinyl acetate) (PMMA/PVAc) and poly(butyl acrylate/methyl methacrylate) (PBA/PMMA). Butyl acrylate and vinyl acetate are copolymerized for the fabrication of adhesives and sealants related to the paper, textile and wood industries and are used in acrylic latex paints. Methyl methacrylate is a component of acrylic latex paint and lubricating oil and is also used in shatterproof glass and contact lenses.

Monomer ratios were calculated from ESI and MALDI data using the peak height for the monoisotopic ^{12}C peak for each oligomer ion. The abundance of each monomer was set equal to the product of the peak intensity multiplied by the number of each monomer in that ion, divided by the total number of monomers. Ratios of products with different end-groups were determined by summing the abundance of all oligomers containing a particular end-group and dividing. Based on replicate measurements the average standard deviation for ESI-MS data was 10%, while for MALDI-MS it was 5%.

4.2 Results and Discussion

4.2.1. Copolymer Composition

One copolymerization each was carried out for BA/VAc and MMA/VAc while four BA/MMA copolymerizations were explored (Table 3.1). PBA/PVAc and PMMA/PVAc copolymers were analyzed only by ESI-MS where PBA/PMMA copolymers were analyzed by ESI-MS and MALDI-MS. Each copolymerization was studied as a function of the mass percent conversion of the monomer to polymer. For the BA/MMA copolymerizations, the concentrations of CTA (dodecanethiol) and the initiator (AIBN) were varied to see if there is any effect on the end-group composition.

4.2.2 PBA/PVAc

A representative ESI mass spectrum of the PBA/PVAc copolymerization products (corresponding to 29% mass conversion) is shown in Figure 4.1. Oligomers of seven different products are observed: homopolymer of butyl acrylate (nBA); five copolymers each having a different BA composition (x) and from one to five units of VAc (y); and homopolymer of VAc (nVAc) (which was only observed at high conversion and so not visible in Figure 4.1). The end groups of the copolymers and BA homopolymers are a hydrogen atom and dodecylthio from the CTA, while for VAc homopolymers the dodecylthio has been replaced by α-cyanoisopropyl from the initiator. The mass of one oligomer of each distribution is listed in table 4.1.

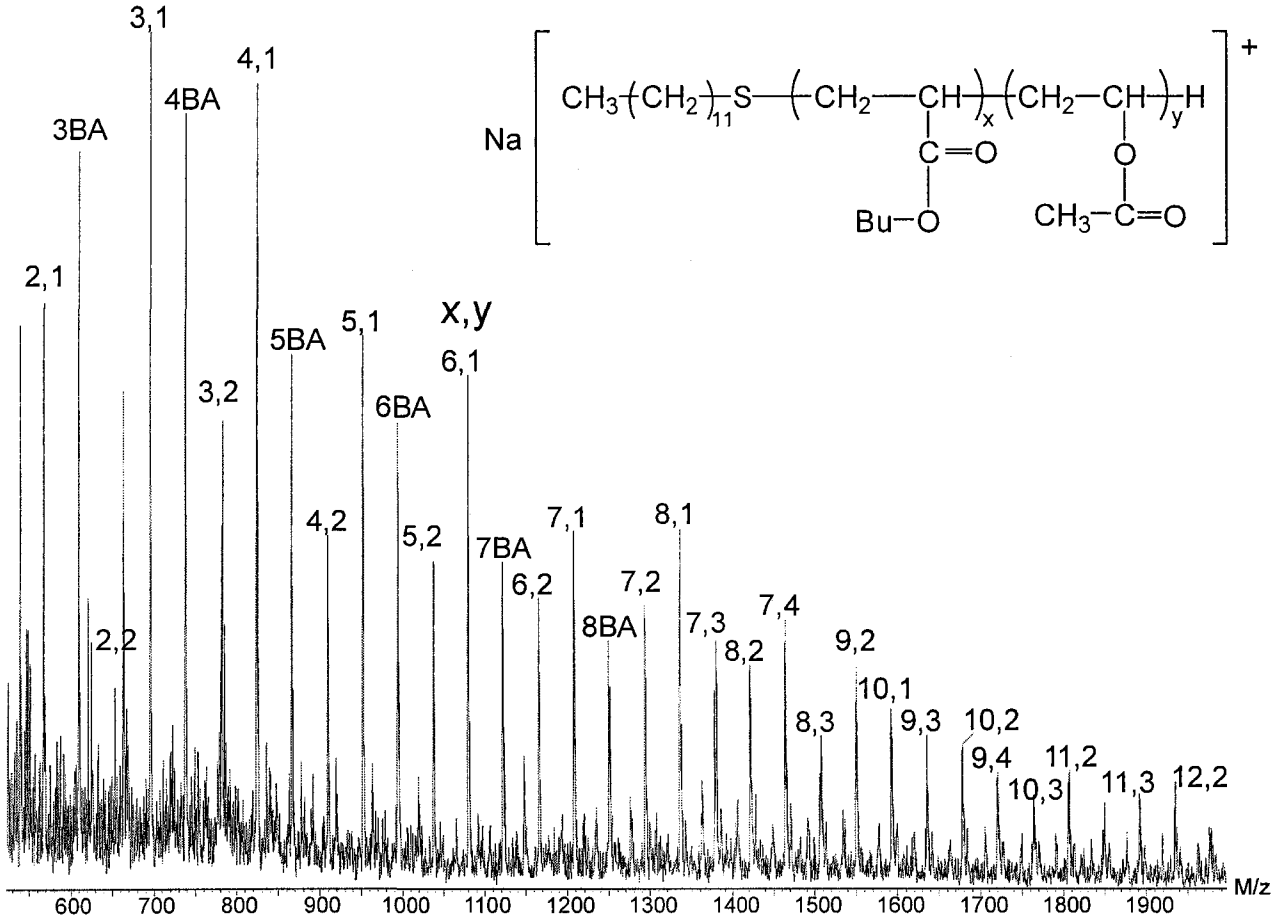

Figure 4.1: ESI mass spectrum of the PBA/PVAc copolymer mixture at 29 % conversion ionized with sodium. Homopolymer of BA (nBA) and five distributions of copolymer are observed, labeled according to number of BA (x) and VAc (y) present. The end groups of the copolymers and BA homopolymers are a hydrogen atom and dodecylthio from the CTA.

Table 4.1: The mass of one oligomer of each distribution in PBA/PVAc copolymer

m/z[a]	# BA	# VAc	End-groups
609	3	0	CTA[b]-H
567	2	1	CTA-H
653	2	2	CTA-H
739	2	3	CTA-H
697	1	4	CTA-H
1039	3	5	CTA-H
866	0	9	α-cyanoisopropyl-H

[a] Ionized with Na^+
[b] CTA= dodecylthio

The overall composition of the copolymer products changed over the course of the copolymerization due to the large difference between the reactivity ratios (r) of BA and VAc (Table 4.2).[82,83] Initially, BA reacts with itself to produce homopolymer of BA (nBA) and with VAc to produce the copolymers of PBA/PVAc. The relative abundance of copolymer decreases slightly as the polymerization process goes to completion. Since BA is consumed by homopolymer early in the reaction, the abundance of VAc homopolymer increases over time (Figure 4.2). One should note that the composition data in all figures (except Figure 4.4) show cumulative rather than instantaneous results. The VAc homopolymer is terminated with α-cyanoisopropyl from the initiator since it is formed later in the copolymerization when most of the CTA has been consumed.

Table 4.2: Reactivity ratios of monomers

Copolymer (r_1-r_2)	Reactivity ratio		
	r_1	r_2	r_1r_2
BA/VAc[83]	5.938	0.026	0.154
BA/MMA[82]	0.297	1.789	0.531
MMA/VAc[82]	24.0254	0.02611	0.6272

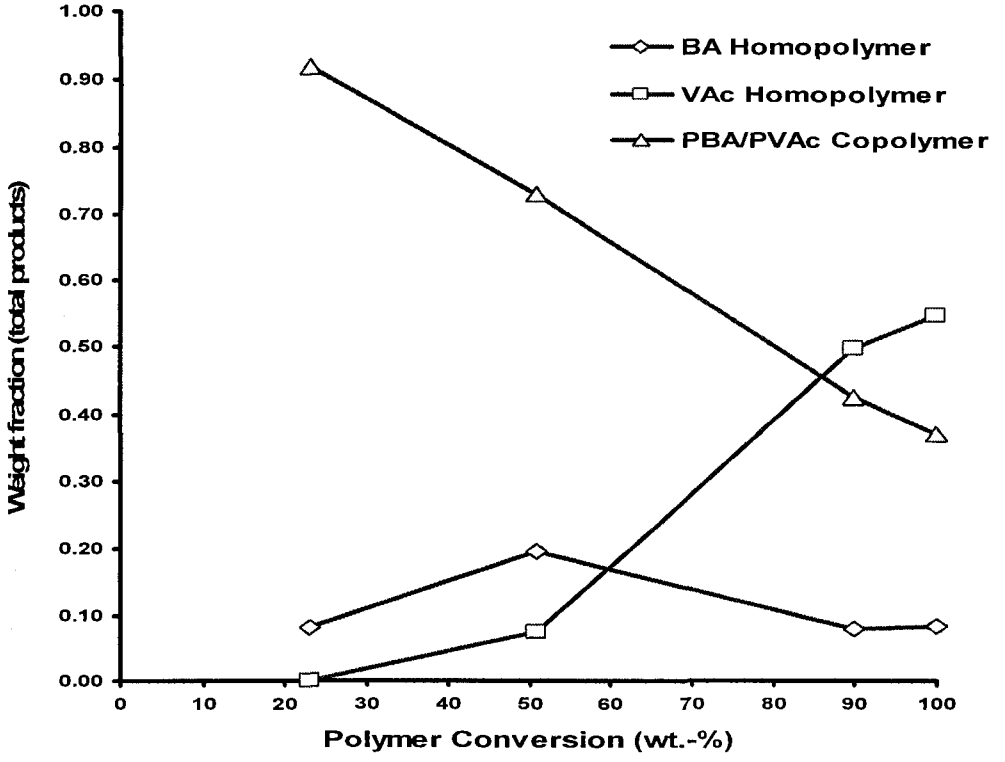

Figure 4.2: Weight fraction of BA homopolymer (◊), VAc homopolymer (□), and PBA/PVAc copolymer (Δ) as function of polymer conversion obtained by ESI-MS.The composition data is the cumulative composition.

Figure 4.3 shows the relative abundance of the five types of copolymers as a function of mass conversion, and aside from those containing five VAc monomers, they all show a fairly consistent decrease over the course of the copolymerization. The small increase in the BA/VAc (y, 5) copolymer may be due to the fast initial self-reaction of BA coupled with the depletion of BA in the reaction system. One should recall that the BA and VAc in the reaction mixture were in equal amounts (see Table 3.1). Thus, as is consistent with previously reported kinetic data,[82,83] one should expect that the BA was more or less completely consumed at about 70% conversion and this would result in the exclusive production of VAc homopolymer (Figure 4.4). The most abundant copolymers of PBA/PVAc are those containing one and two units of VAc, with the former being dominant.

4.2.3 PMMA/PVAc

A representative ESI mass spectrum of the reaction products from the copolymerization of methyl methacrylate and vinyl acetate is shown in Figure 4.5. Six classes of copolymerization products are observed and are characterized by different end groups and monomer composition. Three major distributions A, B, and C of MMA homopolymers were found (Figure 4.5, 26% mass conversion). In addition, three lower abundance products D, E, and F were observed (see inset of Figure 4.5) that consist of PMMA/PVAc copolymers each containing one VAc monomer and varying numbers of MMA. Unlike PBA/VAc, where all of the synthesized copolymer oligomers had common

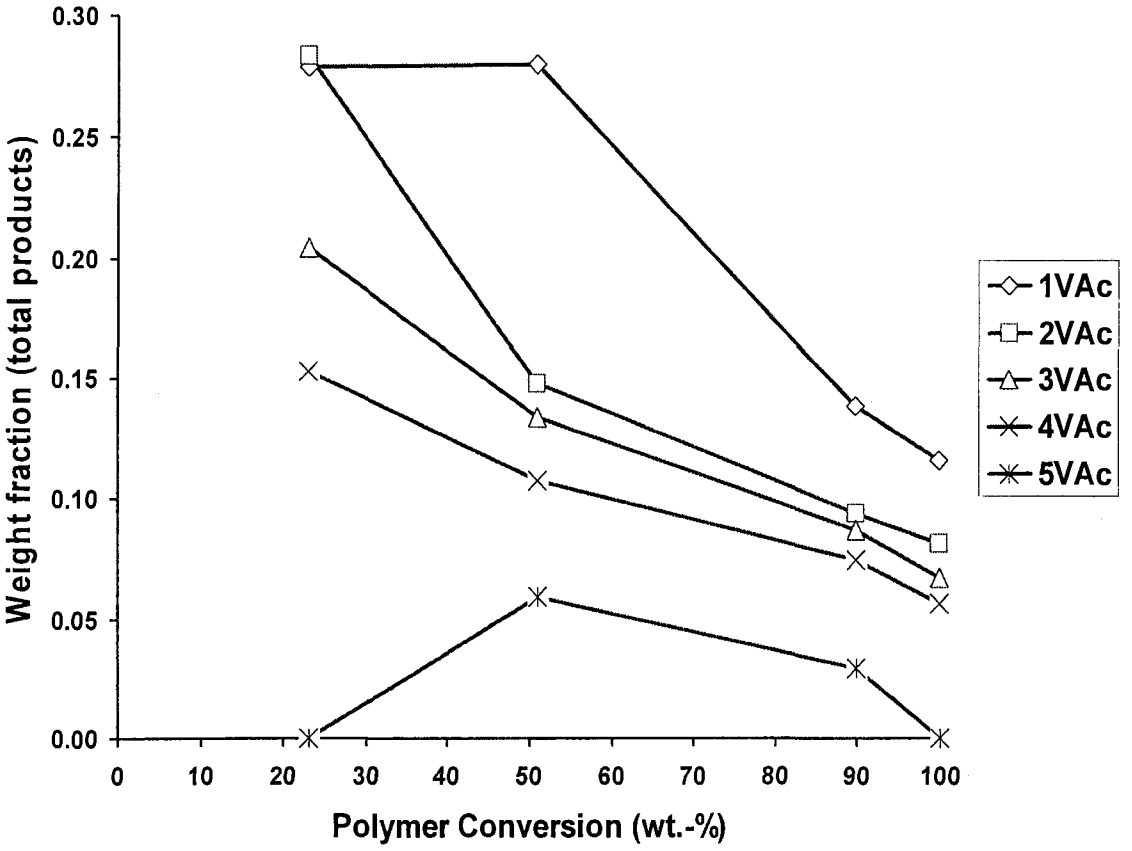

Figure 4.3: Weight fraction of the different PBA/PVAc copolymers as function of polymer conversion obtained by ESI-MS. The copolymers contain from one to five VAc and various number of BA units. The number before VAc presents the number of VAc units in the copolymer. The y axis presents weight fraction of the total product and the composition data is the cumulative composition.

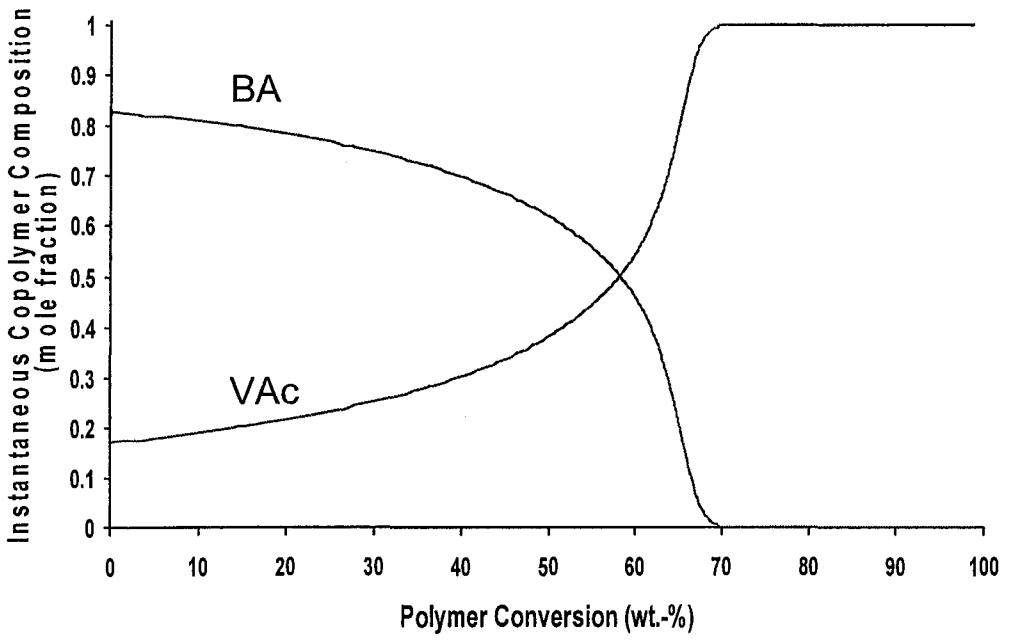

Figure 4.4: The instantaneous copolymer composition for PBA/PVAc as function of polymer conversion predicted by the polymerization simulator.

end groups, there is significant end-group variation in this copolymerization. Products A and D have hydrogen and dodecylthio as end groups, distributions B and E have end-groups of butenyl (C_4H_7) and hydrogen and distributions C and F have end groups of hydrogen and α-cyanoisopropyl. The mass of one oligomer of each distribution listed in table 4.3.

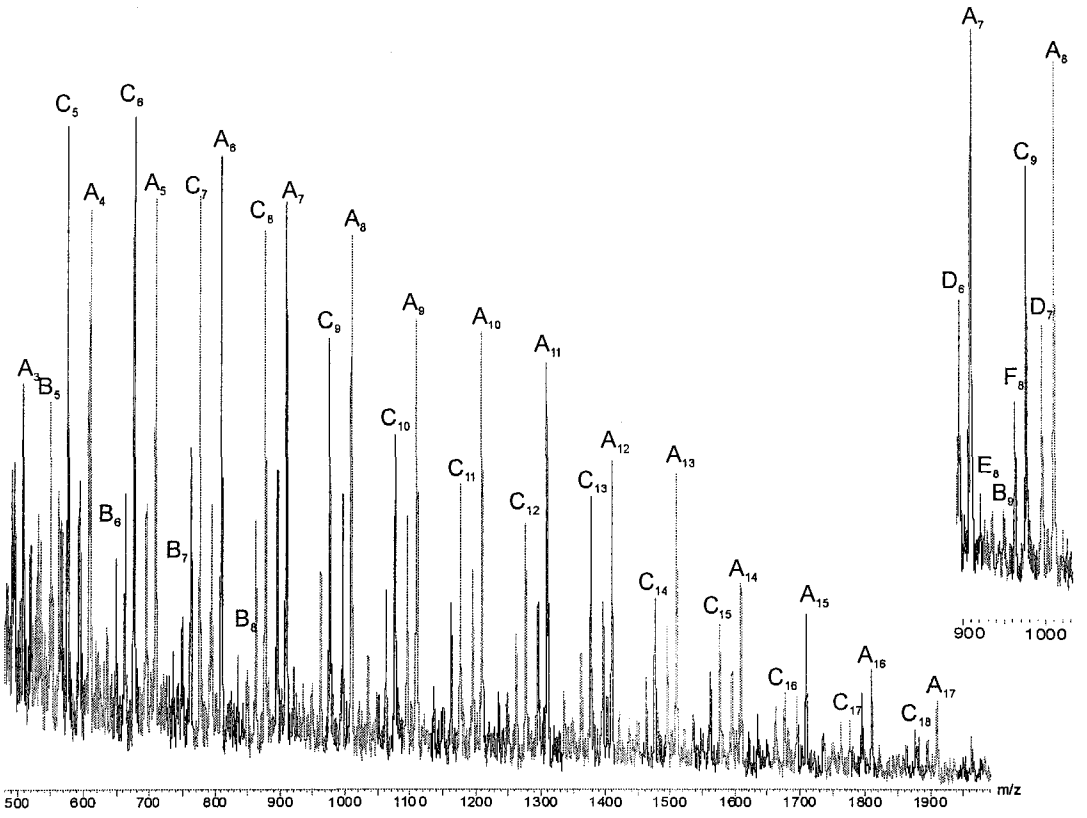

Figure 4.5. ESI mass spectrum of the PMMA/PVAc copolymer mixture ionized with lithium at 29 % completion. Three homopolymers of MMA (A, B and C) and three copolymers (D,E and F) are present: the latter contain one VAc and various number of MMA. The inset shows the labeling of the copolymers D, E and F. Products A and D have hydrogen and dodecylthio as end groups, while distributions B and E have end-groups of butenyl and hydrogen and distributions C and F have hydrogen and α-cyanoisopropyl.

Table 4.3. The mass of one oligomer of each distribution in PMMA/PVAc copolymer

m/z[a]	Code	# MMA	# VAc	End-groups
909	A_7	7	0	CTA[b]-H
949	B_9	9	0	Butenyl-H
976	C_9	9	0	α-cyanoisopropyl-H
995	D_7	7	1	CTA-H
935	E_8	8	1	Butenyl-H
962	F_8	8	1	α-cyanoisopropyl-H

[a] Ionized with Li^+

[b] CTA= dodecylthio

Over the course of the copolymerization there is very little composition change with the homopolymer of MMA always being the dominant product (Figure 4.6). As was discussed for the PBA/PVAc copolymers, the widely different reactivity ratios for PMMA/PVAc (see Table 4.2) result in MMA homopolymer being the dominant product early in the copolymerization, with more PMMA/PVAc copolymers formed as the copolymerization proceeds. This continues until the MMA is depleted and the production of VAc homopolymer ensues.

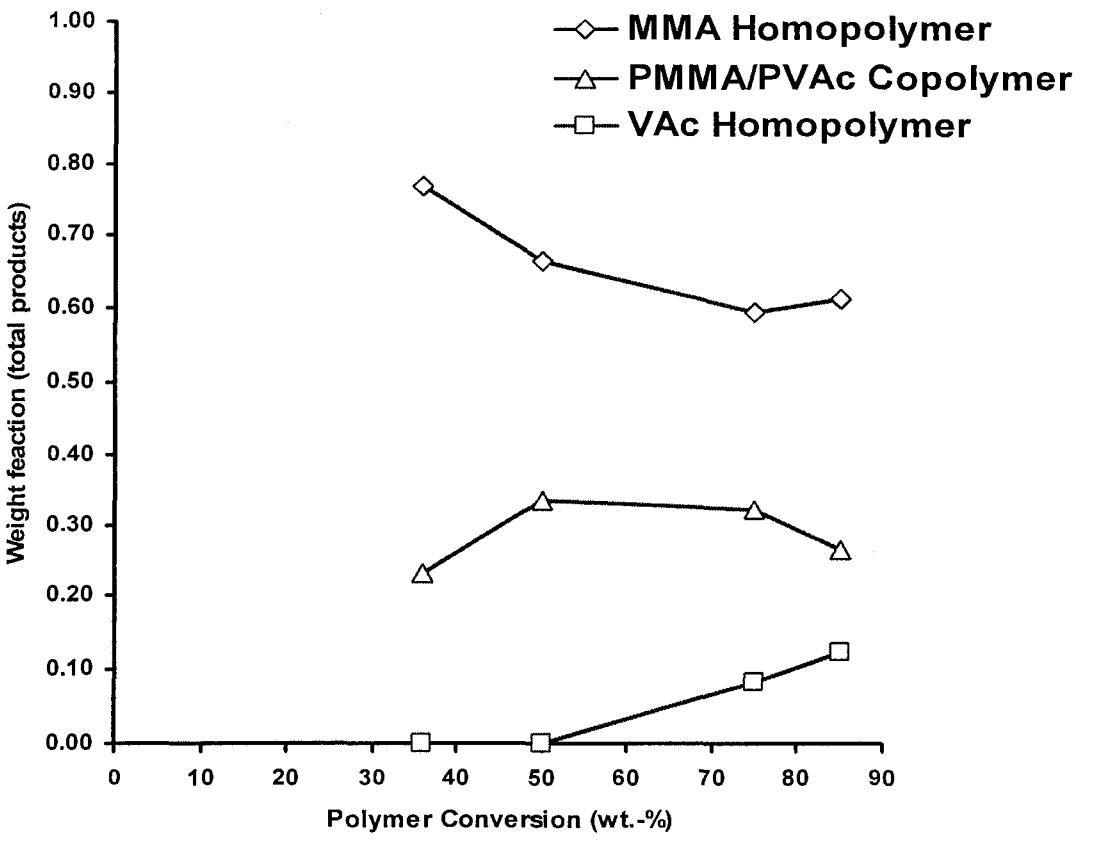

Figure 4.6: Weight fraction of MMA homopolymer (◊),VAc homopolymer (□), and PMMA/PVAc (Δ) copolymer as function of polymer conversion obtained by ESI-MS (cumulative composition).

If we examine the relative abundance of the homopolymers of MMA with different end groups, we find that those oligomers having hydrogen and butenyl group termination increase in abundance over the course of the copolymerization at the expense of those terminated by hydrogen and dodecylthio (Figure 4.7). The presence of hydrogen and butenyl end groups is consistent with termination by disproportionation and H atom abstraction reactions which are significant for MMA polymerizations.[90] The hydrogen

and dodecylthio terminated oligomers result from the presence of CTA. As the copolymerization progresses, the CTA becomes depleted and, as a result, one finds that the CTA-ended oligomers are less common. Similar results are found for the copolymers (Figure 4.8).

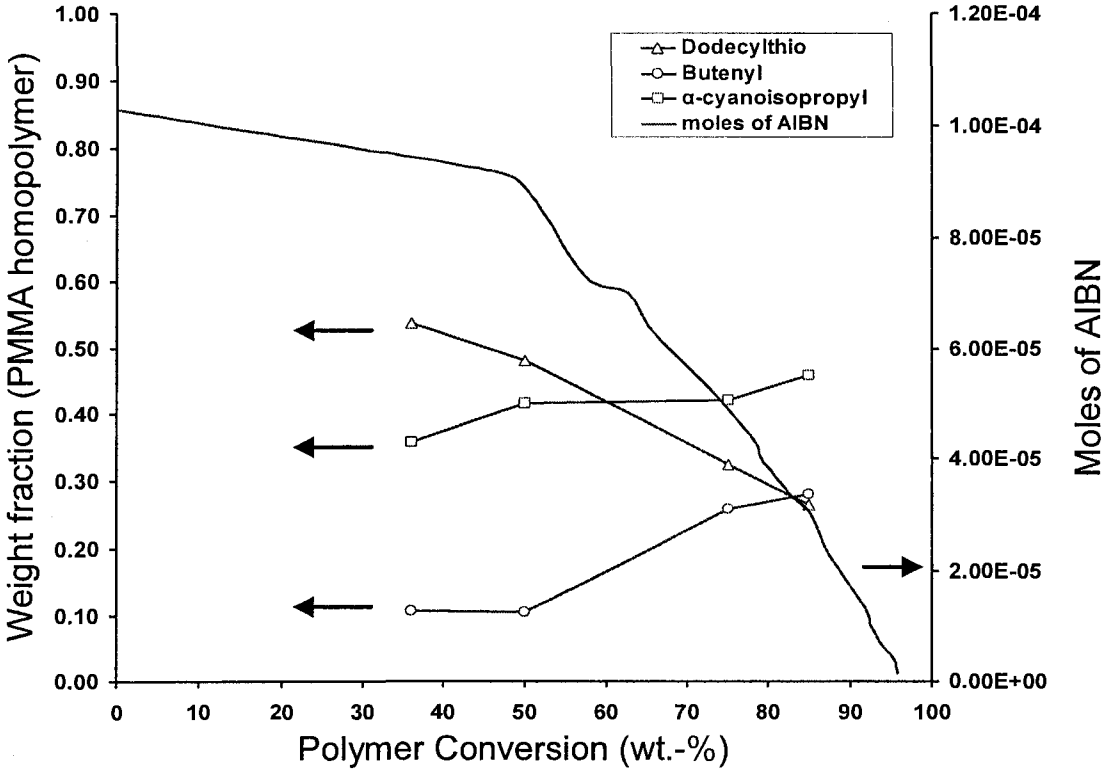

Figure 4.7: Weight fraction of the different MMA homopolymers as function of polymer conversion obtained by ESI-MS: end groups hydrogen and dodecylthio (Δ), butenyl and hydrogen (○), and hydrogen and α-cyanoisopropyl (□). Also plotted (right y-axis) are the moles of AIBN (–) over the course of reaction predicted by the polymerization simulator.

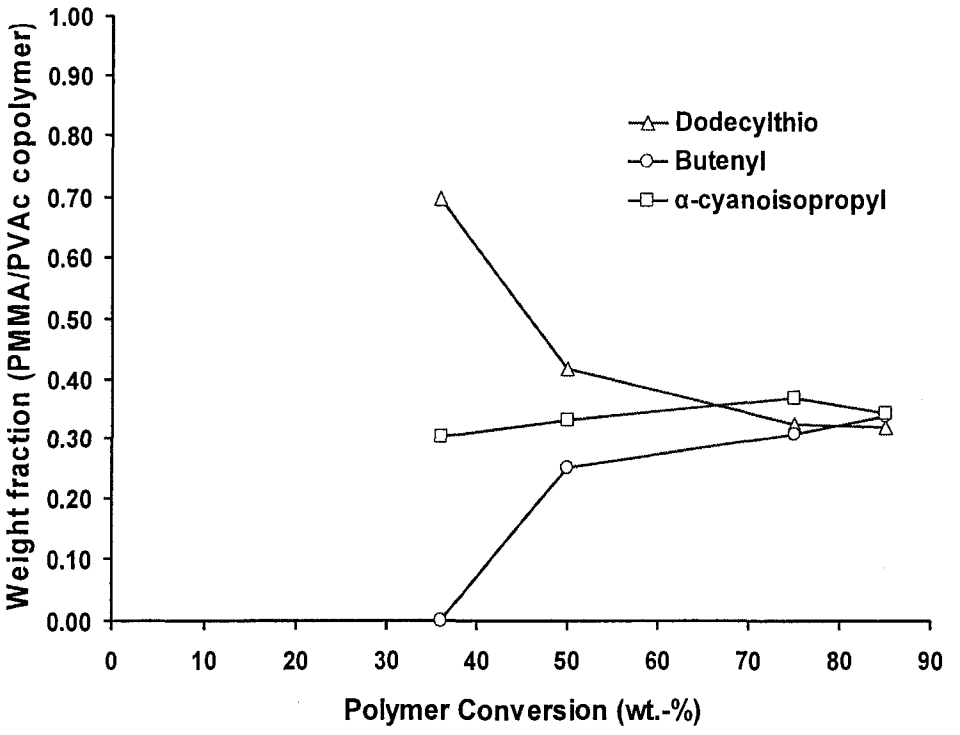

Figure 4.8: Weight fraction of the different PMMA/PVAc copolymers as function of conversion obtained by ESI-MS: end groups hydrogen and dodecylthio (Δ), butenyl and hydrogen (○), and hydrogen and α-cyanoisopropyl (□).

4.2.4 PBA/PMMA

The composition of the copolymer was studied by both ESI-MS and MALDI-MS. Similar distributions of the products were observed in the both methods. Figure 4.9 contains a typical ESI mass spectrum for the copolymerization products of BA and MMA. The two major products classes differ by their end-groups. Distribution A has hydrogen and dodecylthio end groups while in distribution B the dodecylthio has been

replaced by α-cyanoisopropyl from the initiator. Each class consists of oligomers containing between one and six BA monomers with varying numbers of MMA monomers. The mass of one oligomer of each distribution listed in table 4.4.

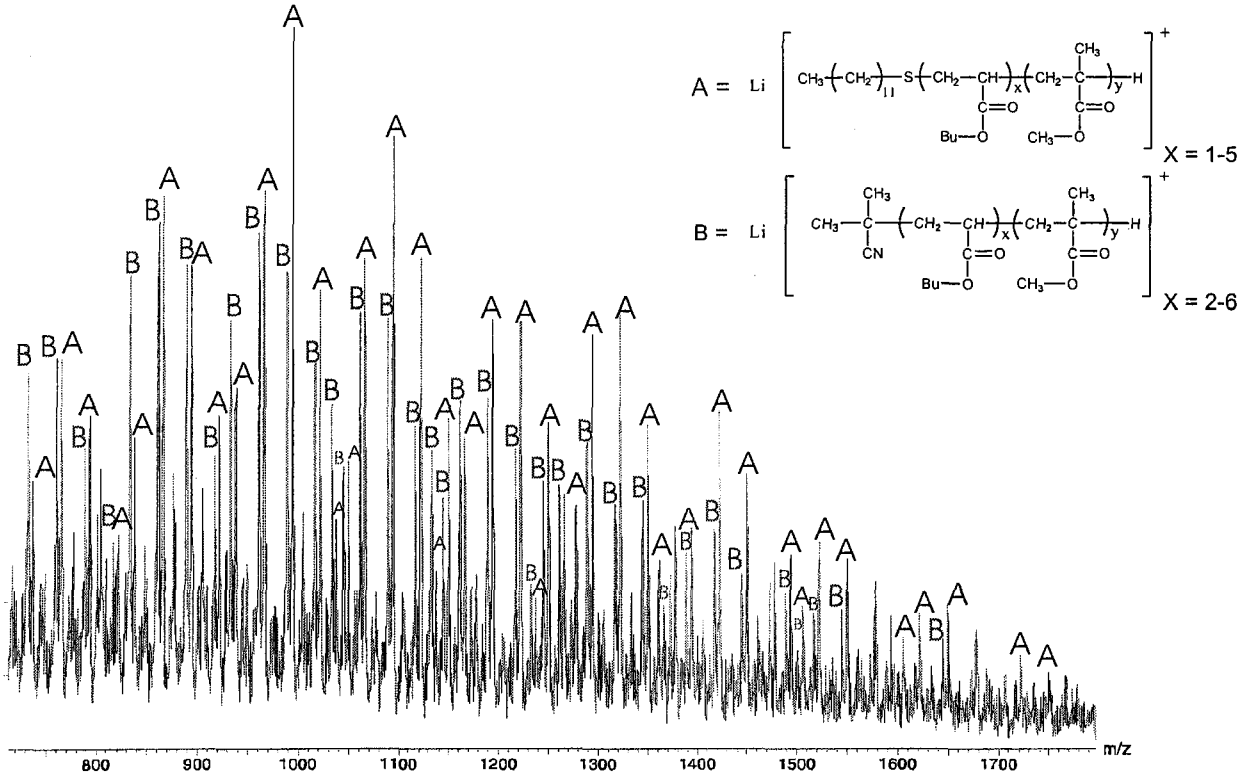

Figure 4.9. ESI mass spectrum of the PBA/PMMA copolymer mixture ionized with lithium. Two major distributions of copolymer are labeled according to end group nature: distribution A has hydrogen and dodecylthio end groups while in distribution B the dodecylthio has been replaced by α-cyanoisopropyl from the initiator.

Table 4.4. The mass of one oligomer of each distribution in PBA/PMMA copolymer

m/z[a]	Code	BA	MMA	End-groups
1037	A1,7	1	7	CTA[b]-H
1065	A2,6	2	6	CTA-H
1093	A3,5	3	5	CTA-H
1021	A4,3	4	3	CTA-H
1049	A5,2	5	2	CTA-H
1004	B1,8	1	8	α-cyanoisopropyl-H
1032	B2,7	2	7	α-cyanoisopropyl-H
1060	B3,6	3	6	α-cyanoisopropyl-H
1088	B4,5	4	5	α-cyanoisopropyl-H
1016	B5,3	5	3	α-cyanoisopropyl-H
1044	B6,2	6	2	α-cyanoisopropyl-H

[a] ionized with Li^+

[b] CTA= dodecylthio

Four different reactions were carried out employing different CTA and initiator concentrations (reactions i-iv, see Table 3.1). The dodecanethiol concentration was raised from 0.02 to 0.05 mol/L over reactions (i), (ii) and (iii), while for reaction iv the AIBN concentration was increased. Product distributions A and B were observed for all reaction conditions except in the case of (iii) which yielded only copolymer products of class A. The ratio of the two product classes are plotted vs. mass conversion in Figure 4.10 and listed in Table 4.5.

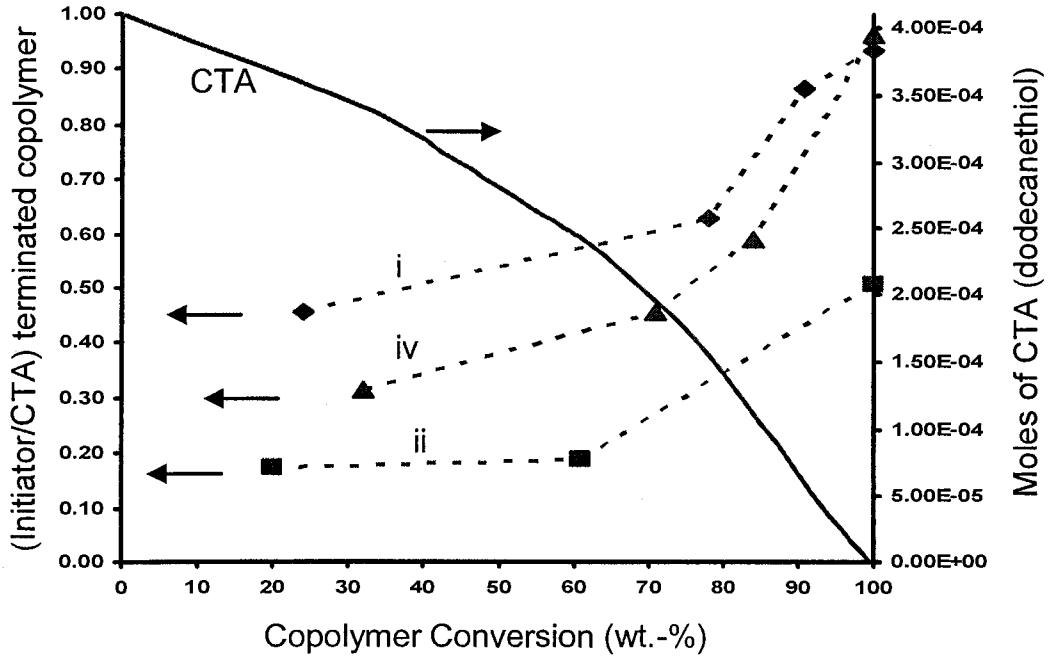

Figure 4.10: Ratios of different PMMA/PBA copolymers (A and B distributions) as function of copolymer conversion obtained by ESI-MS for reaction i (♦), ii (■) and iv (▲). The moles of dodecanethiol (CTA) (–) over the course of reaction predicted by the polymerization simulator program also plotted. The composition data reflects cumulative composition.

Early in reaction (i) (24% conversion) the copolymer formed with a dodecylthio end-group is twice as abundant as that containing an α-cyanoisopropyl end-group. The copolymerization favours class A copolymers even more as the dodecanethiol concentration is increased in reaction (ii) until finally in reaction (iii) it is the only product observed (at least > 99%). As the reactions proceed to completion the copolymers containing α-cyanoisopropyl increase in relative abundance. This is consistent with the change in

Table 4.5. Ratios of PMMA/PBA copolymer with α-cyanoisopropyl from the initiator as end group to that with dodecylthio from CTA as end group obtained by ESI-MS and MALDI-TOF.*

Reaction i			Reaction ii			Reaction iv		
Conversion (%)	Ratio		Conversion (%)	Ratio		Conversion (%)	Ratio	
	ESI-MS	MALDI-MS		ESI-MS	MALDI-MS		ESI-MS	MALDI-MS
24	0.46	0.64	20	0.18	0.43	32	0.32	0.64
78	0.63	0.85	61	0.19	0.43	71	0.46	0.59
91	0.87	1.00	N/A	N/A	N/A	84	0.59	0.82
100	0.94	N/A	100	0.51	0.57	100	0.97	0.98

* For reaction iii only dodecylthio end group copolymers were observed.

dodecanethiol concentration over the course of the copolymerization predicted by the polymerization simulator program (Figure 4.10). As expected, increasing the initiator concentration does not affect the copolymer composition (reaction (iv)) and the final composition was found to be indistinguishable from that obtained for reaction (i).

The products of reaction (i), (ii) and (iv) were also analyzed using MALDI-TOF mass spectrometry. The results are summarized in Table 4.5. The overall trends for the ratio of product classes A and B are similar to those obtained by electrospray ionization; however, the magnitudes of the product class ratios are significantly different. It is

possible that this is caused by the different MALDI efficiencies of the two different end groups terminated copolymers a phenomenon which was been observed with other polymers.[19,69,70,72] The ESI results were found to be independent of solution composition (notably salt concentration) and as will be seen in 4.2.6 section, tend to agree well with ^{1}H NMR. Overall, the MALDI results showed much less variation in composition than was found with ESI over the course of the copolymerizations.

4.2.5 Matrix Effects on PBA/PMMA Quantitation by MALDI

The influence of matrix on PBA/PMMA copolymer composition was subsequently investigated.[91] Results show that when H_2O/Acetonitrile 1:1 was used as solvent only one distribution (B) was observed (Figure 4.11). A single polymerization product was divided into nine separate samples for MALDI-MS analysis. Each was prepared with a different matrix-to-copolymer mixture (c/c) ((mg/mL)/(mg/mL)) (Table 4.6).

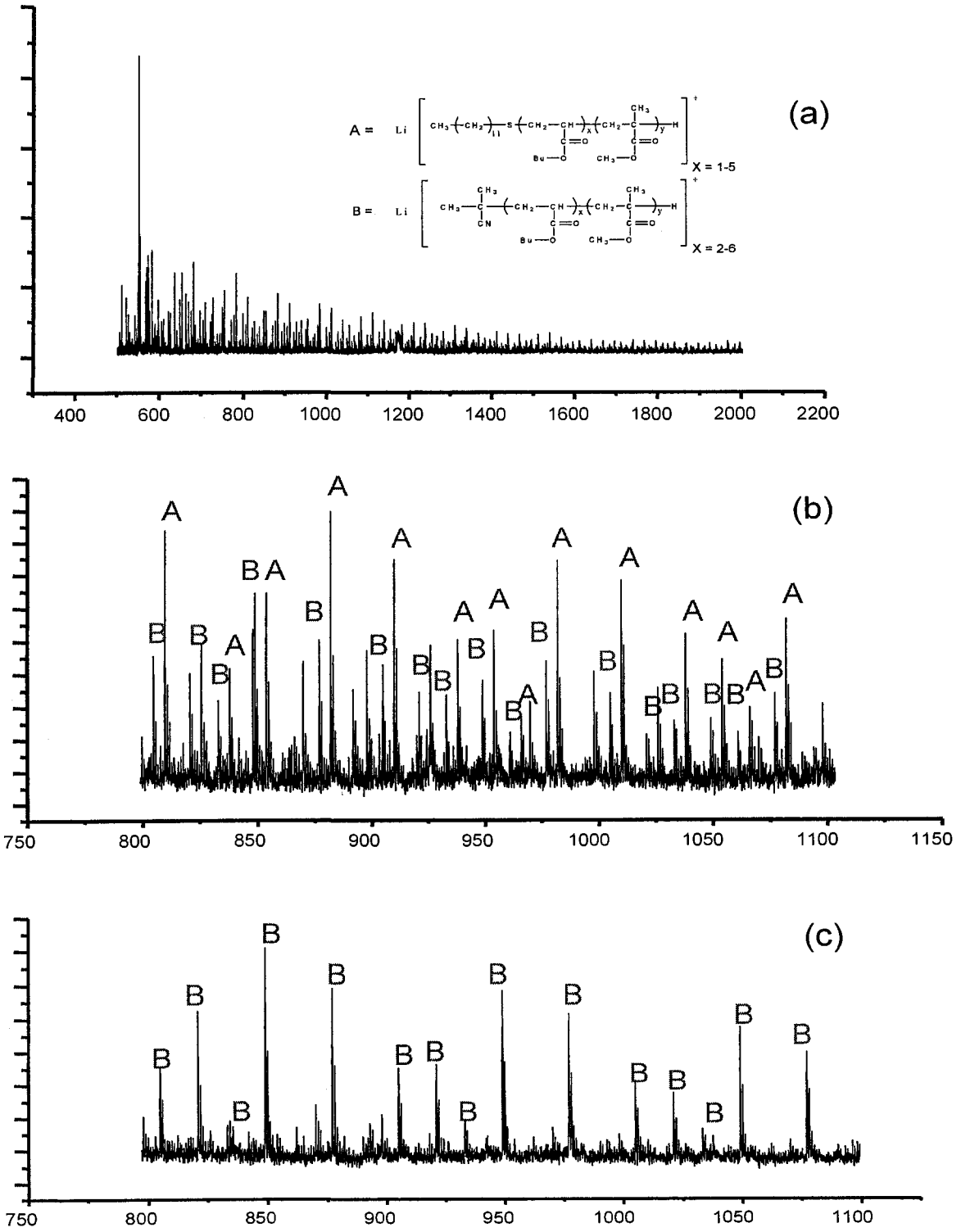

Figure 4.11: MALDI-MS spectra of PBA/PMMA copolymer (a) full spectrum, (b) blow up of (a), (c) only distribution B was observed when H_2O/Acetonitrile 1:1 was used as solvent

Table 4.6: The ratio of different PBA/PMMA copolymers for different matrix:copolymer

Sample ID	Matrix : copolymer	R[a]
a	4 : 1	0.480 ± 0.005
b	5 : 1	0.53 ± 0.03
c	6 : 1	0.515 ± 0.001
d	7 : 1	0.67 ± 0.02
e	9 : 1	0.62 ± 0.04
f	11 : 1	0.63 ± 0.02
g	20 : 1	0.640 ± 0.003
ESI-MS		0.510 ± 0.007

[a] Error bars reflect the standard deviation in the average of two mass spectra collected for each mixture.

No mass spectrum could be obtained for a 1:1 matrix-to-copolymer mixture. At a ratio of 3:1, both products were observed (distribution A and B) but the signal intensity was not sufficient to do quantitative analysis of the different distributions. With a 4:1 mixture, both distributions were observed in the ratio (R) of 0.480 ± 0.005 (B/A). This ratio increases with increasing matrix in the sample preparation step until a plateau is reached at R ~ 0.67 ± 0.02 when the matrix to copolymer ratio is 7:1 (Table 4.6). ESI-MS gives a ratio of the two end-group terminated copolymers of 0.510 ± 0.007, consistent with the MALDI results at intermediate matrix-to-analyte compositions (samples b and c).

The matrix concentration in MALDI sample preparation for PBA/PMMA synthetic copolymer has an influence on the observed ratio of the different copolymer reaction products. This effect is profound even within a small range of matrix concentrations. It is therefore useful to estimate the ratio of copolymers terminated by different end groups with complementary techniques such as ESI-MS, depending on what is suitable for the copolymer, since MALDI alone may lead to erroneous results.[91]

4.2.6 Monomer Ratios

Figures 4.12 - 4.14 show plots of the predicted mole fraction of MMA or BA against mass conversion for PBA/PMMA (reaction i), PBA/PVAc and PMMA/PVAc, respectively. The experimental results from ^{1}H NMR, ESI-MS and MALDI-MS (only for PBA/PMMA (i)) are also plotted in the graph. The large composition drift of the MMA/VAc and BA/VAc reaction mixtures can be confirmed by the decrease in mole fraction of MMA or BA over the course of the copolymerization. The monomer reactivity ratios for PBA/PMMA copolymers are similar and each is close to the inverse of the other.[82] According to Billmeyer,[2] a random copolymer should be expected when the reactivity ratio of one monomer is equal to the inverse of the other monomer as both of the monomer radicals can react equally with themselves or each other. The experimental ESI and NMR results and the theoretical predictions from the polymerization simulator indicate that MMA tends to react first (Figure 4.12).

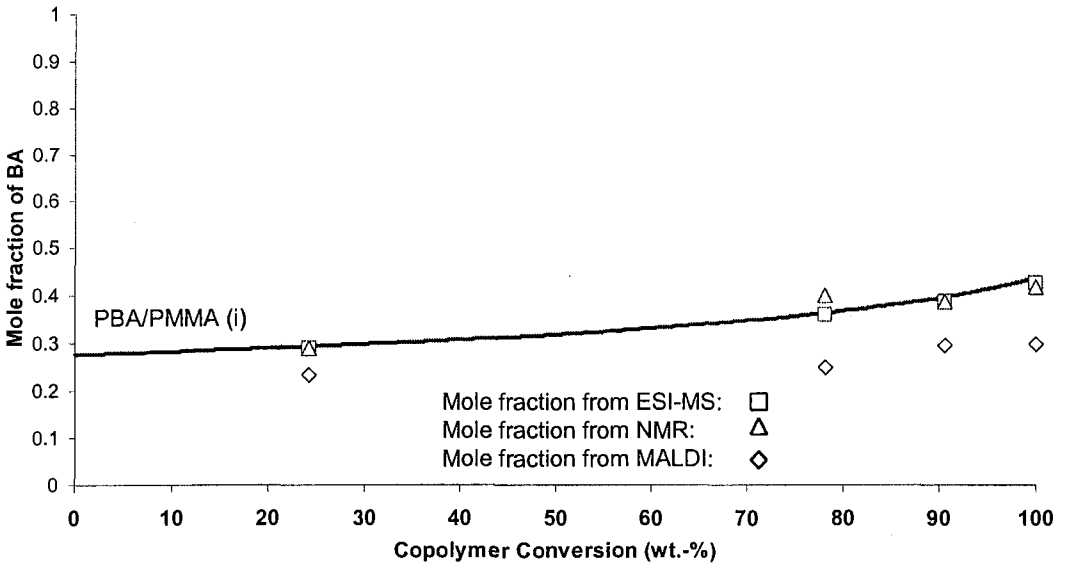

Figure 4.12: Mole fraction of BA obtained by the polymerization simulator, ESI-MS, ^{1}H NMR and MALDI-MS as a function of copolymer conversion for PBA/PMMA (reaction i).

All three are in excellent agreement. The mole fractions of BA obtained by MALDI-MS show a similar trend but are lower. Reports in the literature suggest that MALDI is biased toward high molecular weight (MW) oligomers.[92,93] This was confirmed in the present study by examining the ratio of oligomer peak intensities summed between m/z 500-1200 with that for m/z 1200-1800 for four different reaction times. The ratios from ESI gave 1.73, 2.06, 2.12 and 2.07 where MALDI gave 1.12, 0.99, 0.91 and 1.02 which showed that MALDI-MS consistently gave results skewed to higher m/z. Since high MW oligomers contain more MMA, the monomer ratios of BA are underestimated. One suggested reason for this bias is that low MW oligomers volatilize off the target prior to analysis.[92] To test this, the mole fraction of BA for a single sample

was determined at three different residence times in the ion source: 19 min., 45 min. and 57 min. The same ratio was obtained each time, and thus the low BA mole fraction results are not due to the higher vapour pressure of low MW oligomers. They can only be due to different MALDI ionization efficiencies for oligomers of different chain lengths.

For the PBA/PVAc system, the ESI-MS and NMR results confirm that the PBA homopolymerization occurs at the beginning of the copolymerization as expected by kinetic data and the polymerization simulator. All three approaches quite agree, with the ESI data qualitatively reproducing the composition drift during the copolymerization as predicted by the polymerization simulator (Figure 4.13).

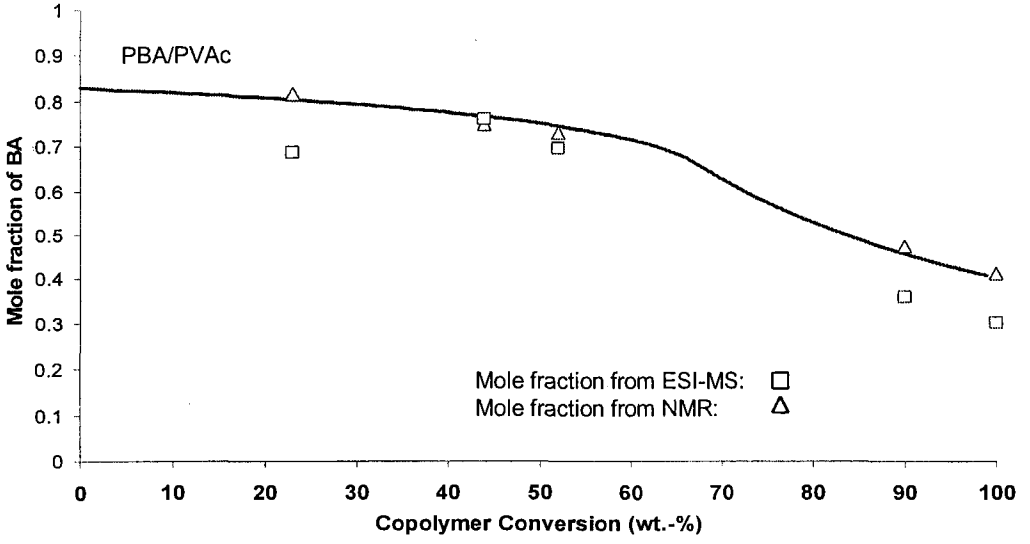

Figure 4.13: Mole fraction of BA obtained by the polymerization simulator ESI-MS and ^{1}H NMR as a function of copolymer conversion for PBA/PVAc copolymers. The solid lines are the theoretical prediction of the BA mole fraction for PBA/PVAc and the composition data is the cumulative composition.

According to the reactivity ratios in table 4.2, the copolymerization of MMA and VAc should lead to homopolymer of MMA during the early stages of the polymerization.[94] Both monomer radicals prefer to react with MMA and thus MMA is consumed much faster from the reaction mixture than VAc. All three approaches agree on the general trend over the course of the copolymerization, but there are some discrepancies during the composition drift over the completion of the copolymerization (Figure 4.14). According to the NMR experiments, the copolymers at high conversion were not perfectly dry; the presence of toluene was observed at 3.6 and 7.1 ppm. It is possible that the polymerization simulator overestimated the polymer conversion close to the completion (the solvent might be harder to evaporate because of the high viscosity of the sample). ESI-MS can be less accurate in this case because of the large number of low intensity peaks observed in the mass spectra. The NMR results also have a significant uncertainty associated with them since the signal at 4.9 ppm corresponding to VAc in the copolymer was quite small and can be overestimated if impurities are present in the same region of the spectrum.

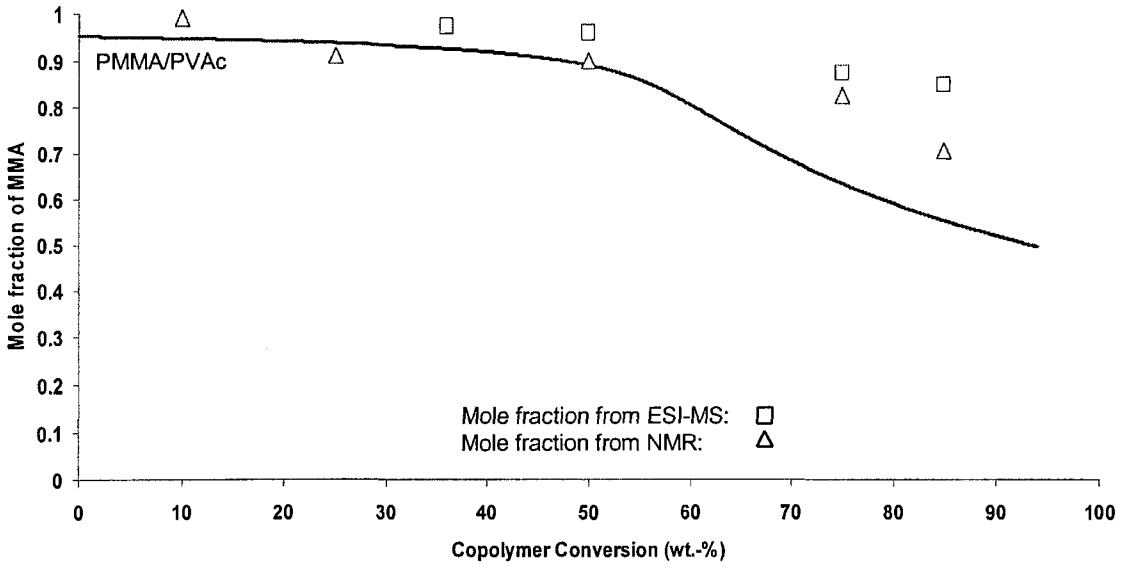

Figure 4.14: Mole fraction of MMA obtained by polymerization simulator, ESI-MS and ^{1}H NMR as a function of copolymer conversion for PMMA/PVAc copolymers.

4.3 Conclusion

ESI-MS and MALDI-MS can be used to track the composition changes that occur during copolymerization of PBA/PVAc, PMMA/PVAc and PBA/PMMA. It is possible to obtain molecular-level information on the distribution of these different types of copolymers, their end groups and on the overall monomer ratios. The former appear to agree fairly well with proton NMR results and with the predictions of the polymerization simulator modelling program. The advantage of ESI-MS is for the end-group analysis, which in the present case was impossible by NMR, and in the molecular-level information on copolymer composition. The increase in intensity of low-mass distributions of products may lead to a decrease in the accuracy of the measurement of

monomer ratios by ESI-MS. ESI-MS and MALDI-MS produced different monomer and copolymer end group ratios for PBA/PMMA due to inherent ionization efficiency differences in MALDI-MS.

5

Effect of Gas-Phase Polymer Ion Conformation on MS/MS mass spectra

5.1 Introduction

Peptide and polymer ion chains can access a wide variety of conformations at ambient temperatures and upon activation by collisions with a target gas or surface.[95-99] The average internal energy deposited into small peptides ions upon low eV collisional activation has been shown to increase with peptide ion size. For a centre-of-mass collision energy, E_{cm}, of 5 eV and gas pressure corresponding to a collision number of 5, Laskin and Futrell found that the average internal energy deposited into protonated dialanine ions AAH^+ was ~ 2.75 eV; the value increased to 4 eV for $AAAH^+$ and 4.5 eV for protonated pentaalanine, $AAAAAH^+$.[98] Meroueh and Hase found that the percent energy transfer for single collisions with Ar of extended β-sheet polyglycine molecules generally increased with number of atoms (chain length) at low E_{cm} (1 eV), but was insensitive to chain length at higher E_{cm}.[96] Helical α-alanine polypeptides did show an almost linear increase in percent energy transfer with increasing size. So, not only overall molecule size is important, but also molecular conformation.

We have examined the unimolecular decomposition of oligomers of poly (methyl methacrylate), PMMA, ionized by Na^+ and polystyrene, PS, ionized by Ag^+ by combining low energy collision-induced dissociation (CID) and a variety of computational techniques. Three different types of PMMA end groups we studied: PMMA terminated by two hydrogen atoms, PMMA(HH), by α-cyanoisopropyl from the initiator and H, PMMA(InH), and butylthio and H, PMMA(BtH). PMMA polymers have been the subject of considerable investigation since Jackson and Scrivens published detailed tandem mass spectrometry experiments and, along with Bowers, proposed decomposition mechanisms for the ions.[40-43] Figure 5.1 shows a typical CID mass spectrum of a 12mer of PMMA terminated by two hydrogen atoms ($PMMA_{12}$(HH)) ionized with Na^+ at a collision energy less than 200 eV (laboratory frame). The mass of each fragment ion in Figure 5.1 will depend on the nature of the terminating groups. Scrivens, Jackson and Bowers[42] interpreted the observed fragment ion types and distributions by demonstrating through molecular mechanics/molecular dynamics (MM/MD) simulations that the ionized PMMA molecules adopt cyclic structures with as many acetate oxygen atoms as possible interacting with the Na^+ ion. The first step in the dissociation pathway was suggested to involve the opening of this ring conformation to form linear chains with the Na^+ associated with methacrylate substituents either near the hydrogen-terminal end (H-end) or methyl-terminal end (Me-end) of the polymer (see the scheme in Figure 5.1). Fragmentation along the polymer backbone would result in the observed product ion distributions. The CID mass spectra of ionized polystyrene (PS) exhibit a similar distribution of fragment ions to that seen for PMMA.[48] However, ionized PS chains were found to adopt extended conformations with the metal ion

associated between two adjacent benzene rings.[49] So, depending on the conformation of the various ionized polymers, we might expect to see evidence for differing internal energy deposition in their respective CID mass spectra. All collision energies reported here are centre-of-mass (E_{cm}) energies (unless otherwise stated) and were obtained from the laboratory frame energies (E_{lab}) with the equation:

$$E_{cm} = E_{lab}\left(\frac{M_{Ar}}{M_{Ar} + M_{ion}}\right) \tag{5.1}$$

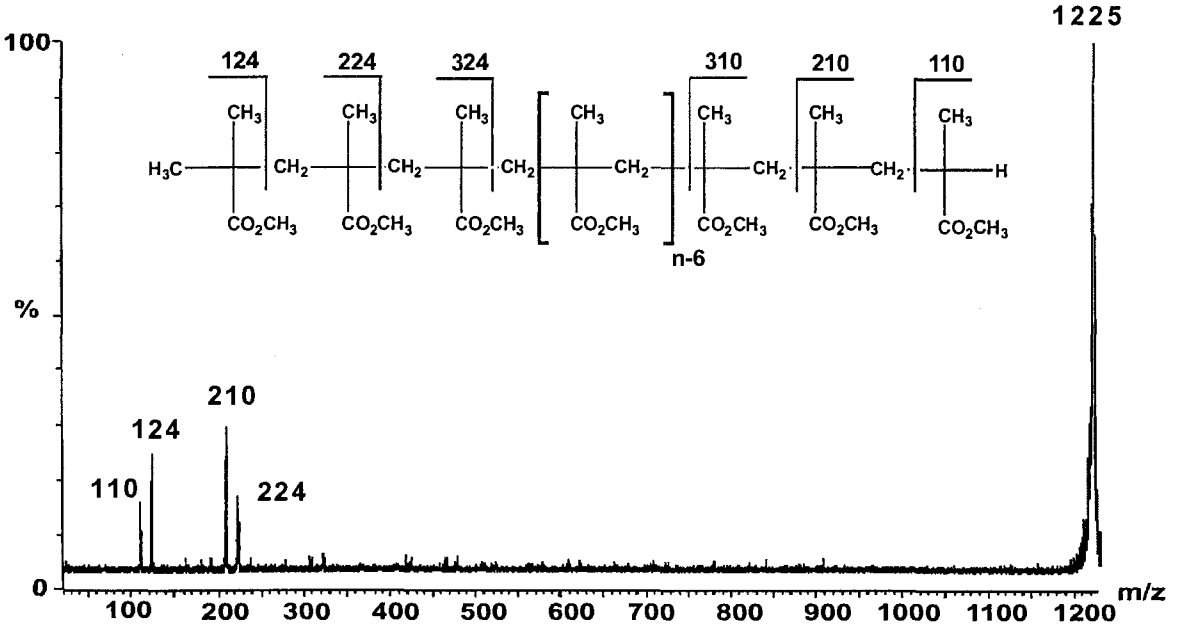

Figure 5.1: Collision-induced dissociation mass spectrum of $PMMA_{12}(HH)+Na^+$ at a laboratory frame collision energy of 180 eV (E_{cm} = 5.7 eV). Inset shows the proposed bond cleavage reactions giving rise to the observed peaks.

5.2 Results and Discussion

The 5.7 eV E_{cm} CID mass spectrum of $PMMA_{12}(HH)+Na^+$ is shown in Figure 5.1 and is consistent with observations by Scrivens and Jackson under conditions of higher collision energy.[40] The four most significant dissociation channels produce ions with m/z 110, 124, 210 and 224 which correspond to the progressions $[87+n(100)+Na^+]$ (A) and $[101+n(100)+Na^+]$ (B). Each MMA monomer ($-CH_2-C(CH_3)CO_2CH_3$) has a mass of 100 Da and the only difference between the two progressions corresponds nominally to which terminal end group is part of the fragment ion, $CH_3-C(CH_3)CO_2CH_3$ (101 Da) or $HC(CH_3)CO_2CH_3$ (87 Da).

The relative fragment ion abundances for $PMMA_5(HH)+Na^+$ through $PMMA_{12}(HH)+Na^+$ under identical collision conditions (i.e, the same E_{cm} of 5.7 eV and the same number of collisions as judged by setting the gas pressure to achieve 30% transmission for each precursor ion) are listed in table 5.1. Na^+ loss is the dominant product observed for the small oligomers $PMMA_3(HH)+Na^+$ and $PMMA_4(HH)+Na^+$ but it becomes insignificant for $PMMA_5(HH)+Na^+$ and higher. For each oligomer, the loss of Na^+ becomes dominant as the E_{cm} increases. As the size of the polymer ions increase so do the number of vibrational modes and hence density of states. However, the energy required to break each C—C bond will remain relatively constant with increasing size. Normally this would result in smaller unimolecular dissociation rate constants and lower fragment ion abundances for the higher molecular weight homologues (illustrated by the plot of the RRKM rate constant as a function of ion internal energy in Figure 5.2).

Clearly this is not observed in the current experiments since the relative total fragment ion abundance (R) increases with polymer size (Table 5.1).

Table 5.1. Relative CID Ion Abundances for $PMMA_n(HH)+Na^+$ for E_{cm} = 5.7 eV and 30% Ion Beam Transmission

				Ion Relative Abundance [a] m/z							
n	#vib[b]	$<E_{vib}>$[c]	E_{lab}[d]	MNa^+[e]	110	124	210	224	310	324	R[f]
5	228	100	81	0.84	0.05	0.11	0.00	0.00	0.00	0.00	0.16
6	273	119	95	0.80	0.03	0.10	0.04	0.03	0.00	0.00	0.20
7	318	137	109	0.69	0.10	0.13	0.04	0.03	0.00	0.00	0.31
8	363	156	123	0.62	0.10	0.15	0.09	0.03	0.00	0.00	0.38
9	408	174	138	0.61	0.11	0.14	0.12	0.04	0.01	0.02	0.39
10	453	193	152	0.58	0.09	0.14	0.12	0.04	0.01	0.02	0.42
11	498	212	166	0.57	0.08	0.14	0.13	0.05	0.01	0.02	0.43
12	543	230	180	0.60	0.06	0.12	0.14	0.06	0.00	0.01	0.40

[a] Fragment ions involving H-transfer were not fully resolved and so were summed into the adjacent peak.

[b] Number of vibrational modes.

[c] Average thermal vibrational energy at 298 K calculated using standard monomer frequencies as outlined in RRKM calculation 3.7 (kJ mol^{-1}).

[d] Laboratory frame collision energy corresponding to E_{cm} = 5.7 eV (eV).

[e] Precursor ion.

[f] Σ (fragment ion abundances) / Σ (total ion abundance). Numbers may not sum to one due to rounding errors.

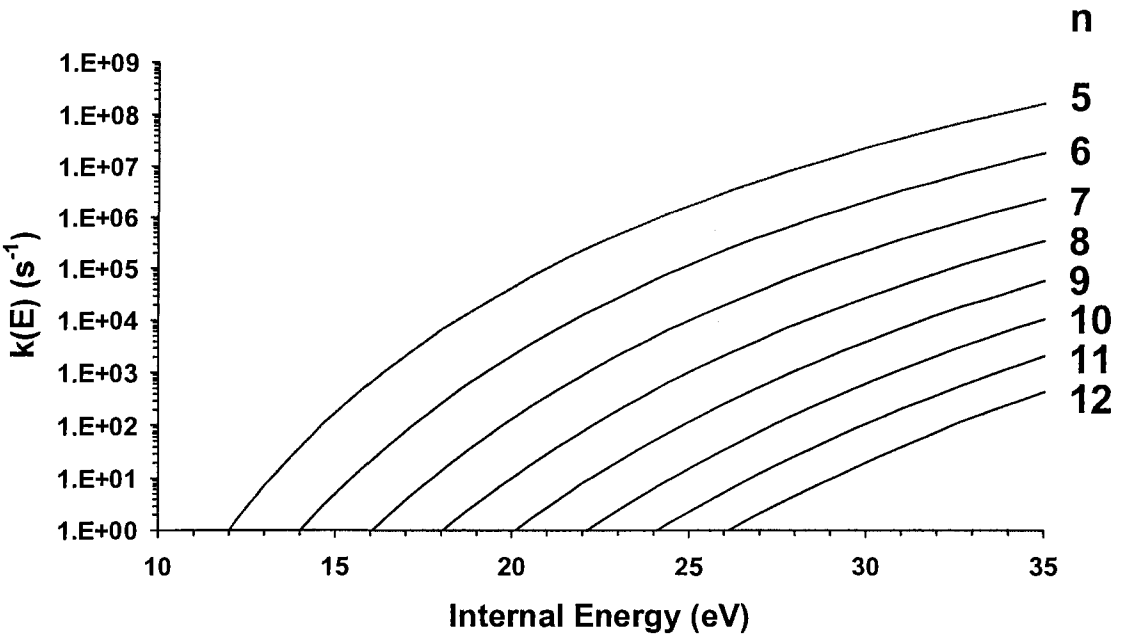

Figure 5.2: RRKM log $k(E)$ vs E curves for the formation of m/z 110 from $PMMA_n(HH)+Na^+$ (n = 5 - 12). The $\Delta S^{\ddagger}$ was arbitrarily chosen to be +25 J K^{-1} mol^{-1} and the bond strength was assumed to be the same for all chain lengths.

Table 5.1 lists the average thermal vibrational energy for each ion at 298 K and Figure 5.3 shows the internal energy distributions at that temperature. An increased thermal energy with molecular size cannot be the sole factor governing R since Figure 5.2 shows that for the 12mer to dissociate on the timescale of the experiment the ions must have more than 30 eV of internal energy, a result similar to that found by Marzluff et al. for small deprotonated peptides.[95] All of the ions take ~ 18 - 19 μs to travel the length of the central hexapole at the E_{lab} values listed in table 5.1, and so to make observations of fragment ions the internal energy of the precursor ions must be such that

the unimolecular decay rate constant is greater than 10^4 s^{-1}. Clearly, an internal energy difference of only 2 eV from thermal vibrational energy would be insufficient to produce the changes in R listed in table 5.1.

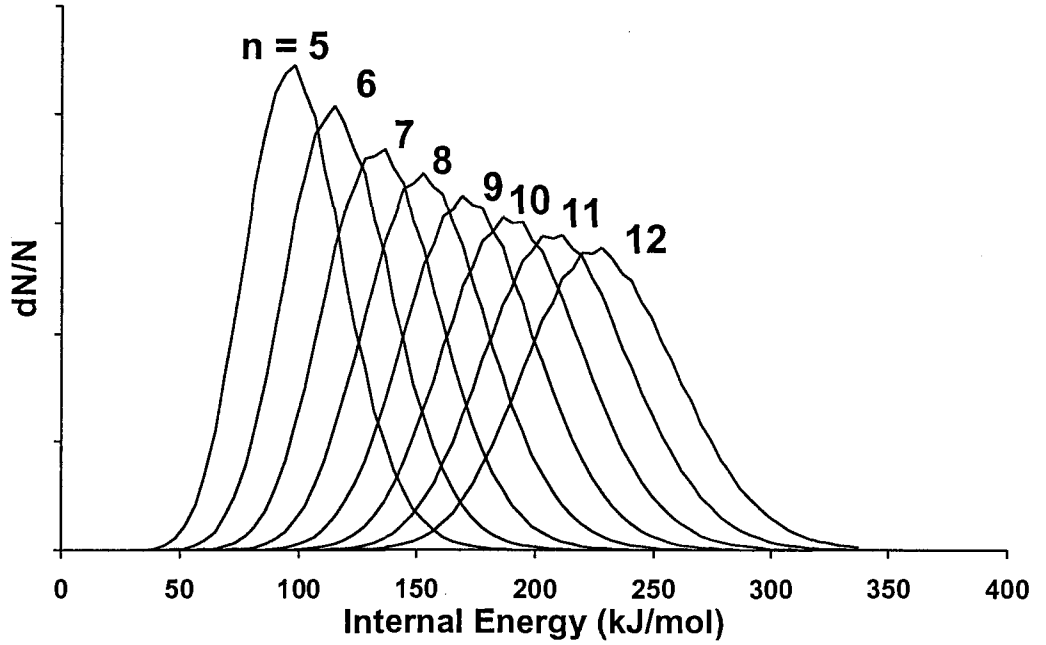

Figure 5.3: Calculated 298 K thermal energy distributions for $PMMA_n(HH)+Na^+$ (n = 5 - 12).

Assuming a common internal energy deposition for all chain lengths, the effective unimolecular rate constant (k_{eff}) for the formation of m/z 110 for collisionally activated polymer ions was calculated by multiplying the 0 K $k(E)$ values by the post-collisional internal energy distribution, $P(E,E_{cm})$ and integrating over all internal energies above threshold. This latter distribution was obtained by assuming a common 30 eV internal energy deposition on top of the ions' 298 K thermal internal energy distributions. The resulting k_{eff} (in s^{-1}) values for the 5mer through 12mer, 4264, 435, 54, 8, 1, 0.24, 0.05 and 0.01, respectively, are inconsistent with the experimental results in table 5.1 that

show the total fragment ion abundance increasing in going from the 5mer to the 12mer. Increasing the common internal energy deposition will not change this trend; what has to change is the efficiency of the energy transfer with chain length. Only if the internal energy transfer increases significantly with chain length will the k_{eff} for the 12mer ever out-compete that of the 5mer and give the experimental result.

In addition, a plot of R vs chain length shows that the total fragment ion abundance does not uniformly increase with chain length, but plateaus at n = 10 (Figure 5.4). The discontinuity in the rise in R coincides with a change in the conformation of the polymer ions at this n value.

The shorter PMMA chain lengths are virtually linear structures (Figure 5.5). For n = 8, the lowest energy conformation has the metal ion complexed near one end of the oligomer leaving the other end free to change conformation. Once n is greater than nine, completely cyclic conformations are most stable and adopt a general structure similar to the 12mer shown in Figure 5.5. So, it appears that the cyclic conformations of the larger polymer ions generally undergo less efficient energy transfer than the smaller extended polymer ions. Once a cyclic conformation is reached at the 10mer, the R value plateaus as now the increasing density of states of the ions competes with increasing energy deposition. Similar results are obtained for $PMMA_n$(InH) (Figures 5.4 and 5.5). The lowest energy conformations of $PMMA_n$(BtH) tend to be less well defined. At large chain lengths, it appears that the bulky butanethiol end group prevents the fully cyclic conformation from forming. Here R increases gradually, but consistently, with

increasing chain length. Both $PMMA_n$(InH) and $PMMA_n$(BtH) exhibit CID mass spectra that contain peaks due to fragment ions that can be classified in the same categories as those found for $PMMA_n$(HH).

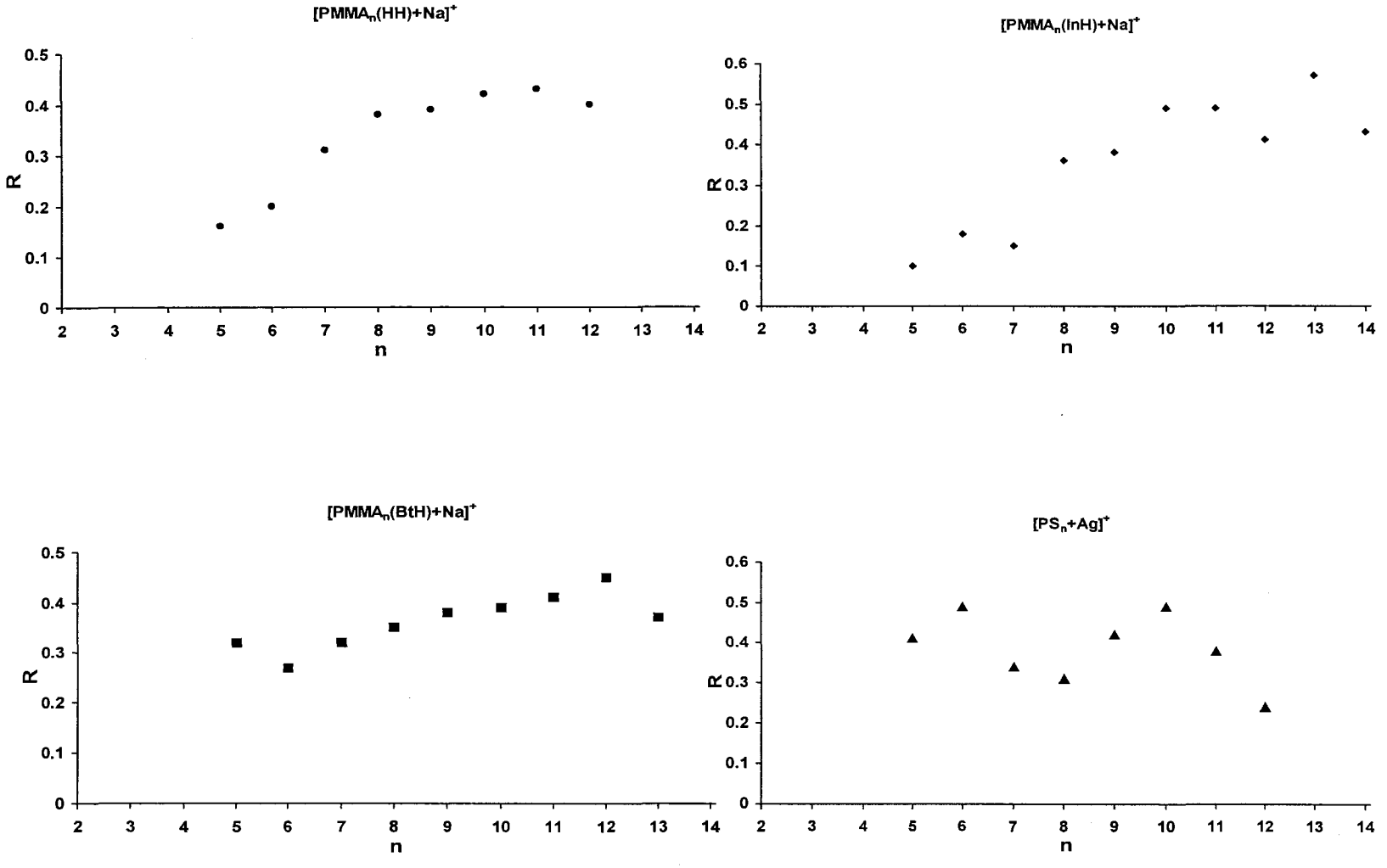

Figure 5.4: Plots of the relative fragment ion intensity ratio R vs chain length for PMMA(HH), PMMA(InH), PMMA(BtH) and PS (E_{cm} = 5.7 eV, 30% Ion Beam Transmission and ± 12%).

$PMMA_5(HH)+Na^+$

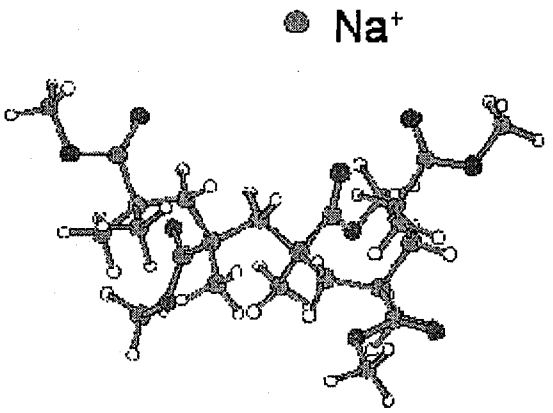

PS_5+Ag^+

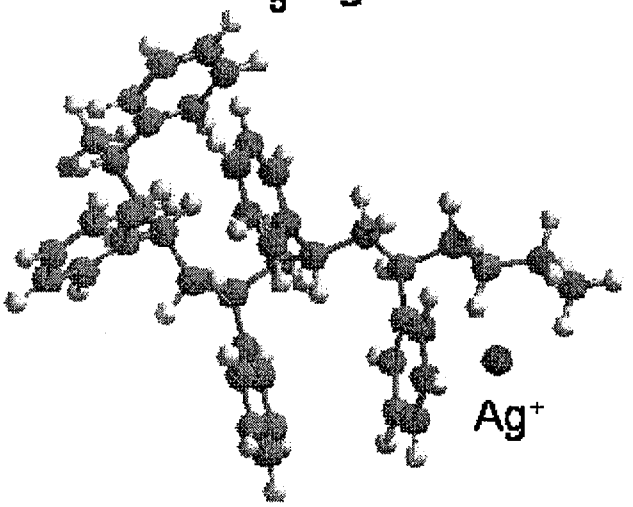

$PMMA_8(HH)+Na^+$

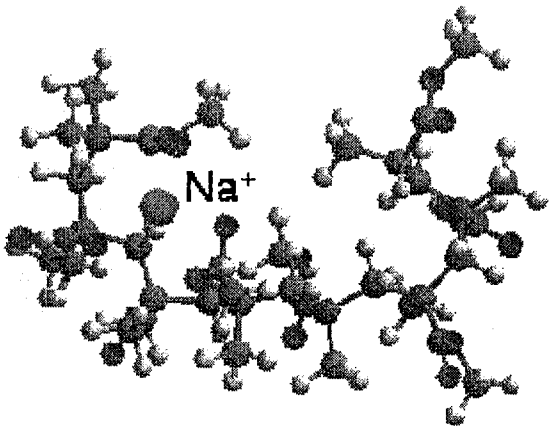

PS_8+Ag^+

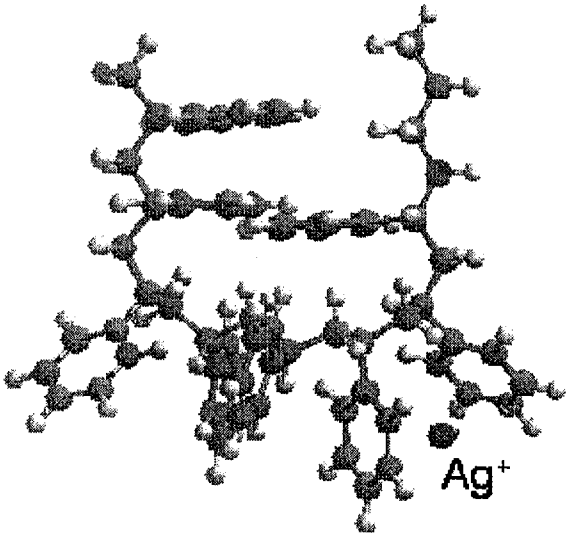

$PMMA_{12}(HH)+Na^+$

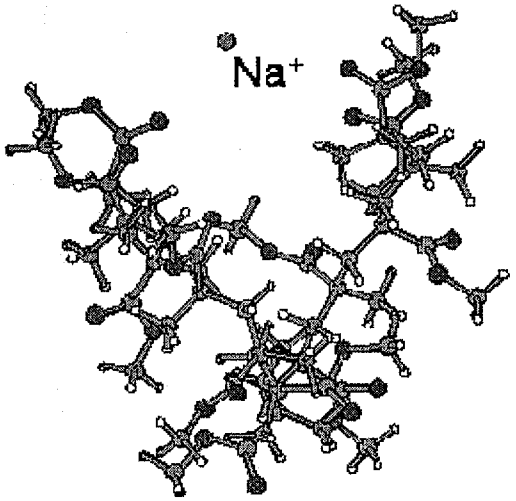

$PS_{12}+Ag^+$

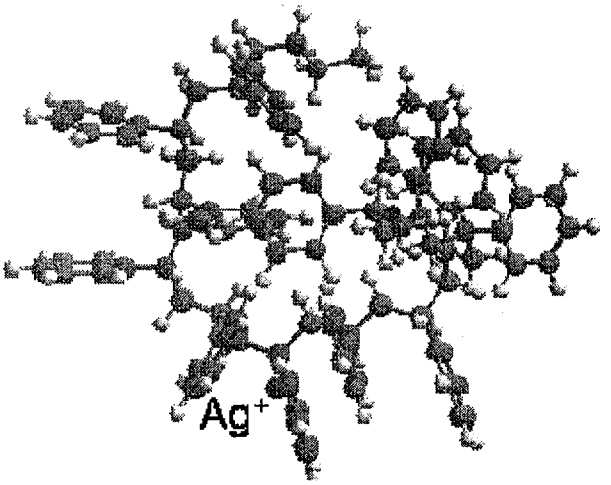

$PMMA_5(InH)+Na^+$

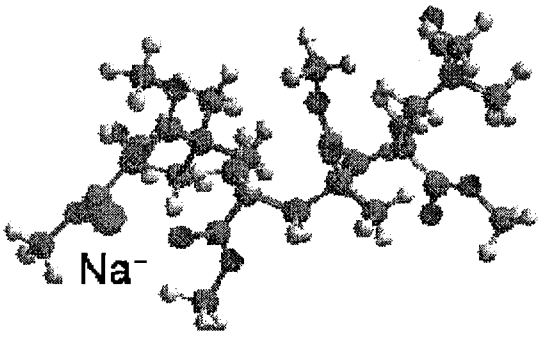

$PMMA_5(BtH)+Na^+$

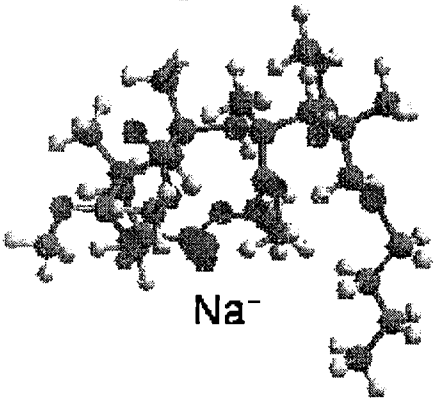

$PMMA_9(InH)+Na^+$

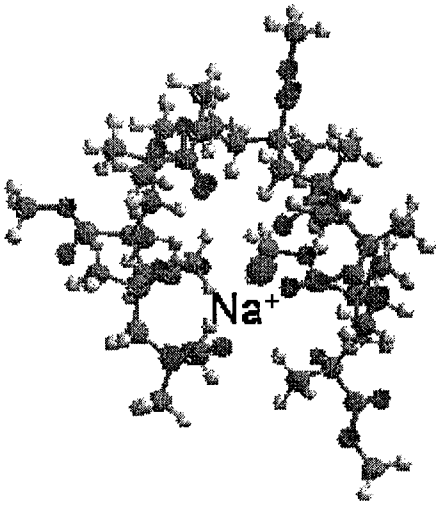

$PMMA_9(BtH)+Na^+$

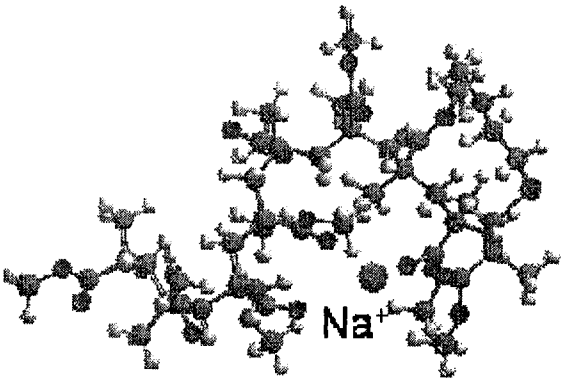

$PMMA_{12}(InH)+Na^+$

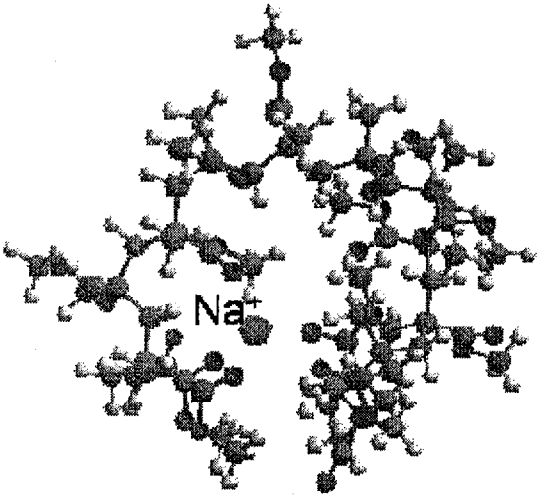

$PMMA_{12}(BtH)+Na^+$

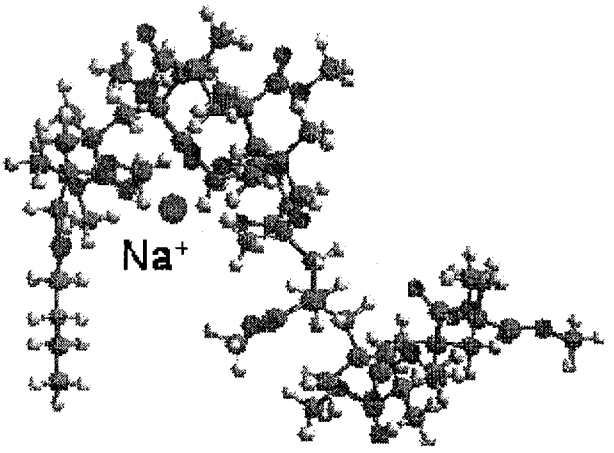

Figure 5.5: MM/MD structures for the lowest energy conformations of $PMMA_n(HH)+Na^+$ (n = 5,8,12) ions, PS_n+Ag^+ (n = 5,8,12) ions, $PMMA_n(InH)+Na^+$ (n = 5,9,12) ions and $PMMA_n(BtH)+Na^+$ (n = 5,9,12) ions. The MM/MD structures for $PMMA_n(HH)+Na^+$ (n = 5,12) were further optimized at the AM1 level of theory (shown) but no significant changes in conformation were observed.

The results for R for PS ionized with Ag^+ are qualitatively different in that no increase is observed with increasing chain length (Figure 5.4). According to the rationalization present above, this should mean that ionized PS having $n \geq 5$ adopt similar, compact conformations. Contrary to the results of MM/MD calculations in the literature for ionized PS,[49] our calculations show that most PS oligomers do indeed adopt compact conformations due to π-π and π-edge interactions of the aromatic rings (Figure 5.5). MM/MD simulations performed by Gidden et al.[49] on neutral PS oligomers predicted compact conformations similar to those we obtained for the ions (Figure 5.5). In their study the oligomers straightened out, and the functional groups aligned on one side of the oligomer, upon the addition of Li^+ and Na^+. The cross sections of these linear structures agreed better with the experimental cross sections from ion mobility experiments than those calculated for the more compact *neutral* structures. We have no explanation for the discrepancy between the previous simulations and the present results. Indeed, when we start our annealing dynamics with linear structures, they quickly undergo conformational change to those shown in Figure 5.5. A 5mer with Ag^+ complexed between two rings was found to lie some 89 kJ mol^{-1} higher in energy than the structure shown in Figure 5.5 in which Ag^+ is bound at the end of the chain. Apparently

the extra stability of binding the silver cation between two rings is less than that produced by π-π and π-edge interactions of the benzene rings. When specifically isotactic PS structures are built in the MM/MD program and ionized with Ag^+ between two adjacent aromatic rings, a more linear structure was formed (Figure 5.6) with virtually the same energy as that obtained when we started with atactic PS; however, continued annealing did not interconvert the two types of structures (they are diastereomers) and there does not appear to be a thermodynamic driving force for aligning the aromatic groups on the same side of the polymer backbone. It is not obvious why the presence of an alkali metal ion between two adjacent aromatic rings should cause aromatic side chains to break all their favorable π-π and π-edge interactions, rotate many remote C—C bonds and align on one side of the oligomers.[49] How the calculated cross sections of our compact *ionized* PS oligomers compare with the experimental values determined by Gidden et al.[49] is not known.

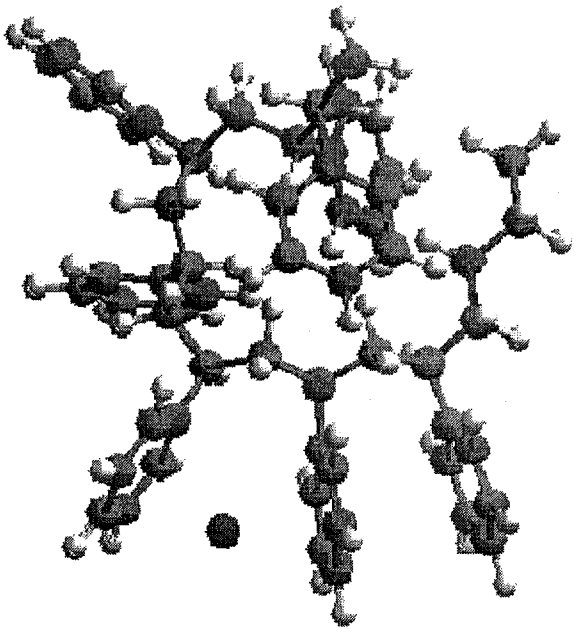

Figure 5.6: MM/MD structure for the lowest energy conformation of isotactic PS_n+Ag^+ (n = 7) ions.

According to the present set of results, it appears that compact molecular conformations undergo collisional energy transfer less efficiently than extended linear chains, presumably due to their slightly lower collision cross-sections.

5.3 Conclusion

The total relative fragment ion abundances in the CID mass spectra of oligomers of ionized PMMA and PS polymers were obtained at fixed centre-of-mass collision energies and collision numbers. The results are consistent with an increase in internal energy deposition with increasing molecular size. In addition, compact polymer ion conformations appeared to undergo less efficient energy transfer than extended structures.[100]

6

Protonating Polymer Oligomers

6.1 Introduction

While the predominant mode of ionization for peptides and proteins in mass spectrometry is protonation in solution, the same cannot be said for synthetic polymers. Typically, synthetic polymers such as poly(methyl methacrylate) are not basic enough in solution to acquire a proton from an added acid. To overcome this limitation salts incorporating metal ions are usually added to the polymer/solvent solution prior to electrospray ionization (or to the polymer/matrix solution prior to ionization by MALDI). This generates gas-phase polymer oligomers ionized by the metal ion. This has consequences for the analysis of these oligomers by collision-induced dissociation (CID) mass spectrometry. For example, Jackson and Scrivens studied poly(alkyl methacrylate) polymers, namely poly(methyl methacrylate) (PMMA) and poly(n-butyl methacrylate) (PBMA) by different mass spectrometry techniques.[37-43] In each case the CID mass spectrum was dominated by low mass-to-charge ratio (m/z) fragment ions. In the case of PMMA the fragments were proposed to be generated mainly by homolytic cleavage and 1,5 hydrogen rearrangement reactions along the polymer backbone.[40,43] Low intensity peaks at high m/z were assumed to be formed by neutral losses and fragmentation along the polymer backbone.[38] The end result was a variety of fragment ion progressions each

differing by one monomer unit. Bowers et al. proposed a mechanism that rationalized the predominance of the low m/z fragments. MM/MD simulations demonstrated that the oligomer/metal ion adduct takes on a quasicyclic structure. Upon collisional activation this ring opens, leaving the metal ion attached to either end of the oligomer. The metal ion drives the fragmentation near the end of the oligomer, producing low m/z fragments ions.[42] An alternative mechanism has been proposed by Wesdemiotis et al. in which the metal ion acts as a spectator as the oligomer undergoes what is essentially a free-radical decomposition pathway similar to that which occurs during pyrolysis.[44,101]

We wished to explore the difference protonation would make on the oligomer ion decomposition pathways. Since it is very difficult to form such species in solution, they were generated in the gas phase by using electrospray ionization to first form proton-bound complexes between the oligomers and small peptides or amino acids. As will be seen, these protonated oligomer ions undergo a unique fragmentation chemistry upon collisional activation.

6.2 Results and Discussion

6.2.1 Poly(methyl methacrylate)

The mass spectrum of PMMA ionized by protonated triglycine (TriGly) (Figure 6.1a) shows a distribution of ions with m/z (X92) representing (H-PMMA$_n$-H)(TriGly)(H^+), where n is the number of MMA units and H are the two oligomer end groups. One monomer unit of MMA is 100 Da and neutral TriGly is 189 Da. When

diglycine (DiGly) was used, the peak m/z values are reduced by 57 Da to give a progression with m/z (X35) (Figure 6.1b). Ionized PMMA oligomers ions have also been generated separately with several amino acids (Gly, Ala, Leu, Phe, Trp, Asp, Lys and Arg), each giving the corresponding distribution, which can generically be written as (H-$PMMA_n$-H) (AAH^+), where AA is the amino acid.

Figure 6.2a shows the CID mass spectrum of (H-$PMMA_{10}$-H)(DiGly)(H^+). The dominate fragment ions are at high m/z and only $DiGlyH^+$ is seen in the low m/z region of the mass spectrum. Fragmentation is completely different from that observed when alkali metal ions are used for ionization. In Figure 6.2a, an initial loss of 164 Da is observed corresponding to neutral DiGly (132 Da) plus a molecule of methanol (32 Da) from one of the monomer side chains. When DiGly is replaced by TriGly (Figure 6.2b), the initial neutral loss was 221 Da, an increase of the 57 Da mass difference between the two peptides. The loss of methanol occurs from a protonated oligomer after the initial loss of the peptide (Scheme 6.1), a sequence supported by the observation of the protonated oligomer (H-$PMMA_{10}$-H)H^+ in the CID mass spectrum at low collision energy (CE) (Figure 6.3).

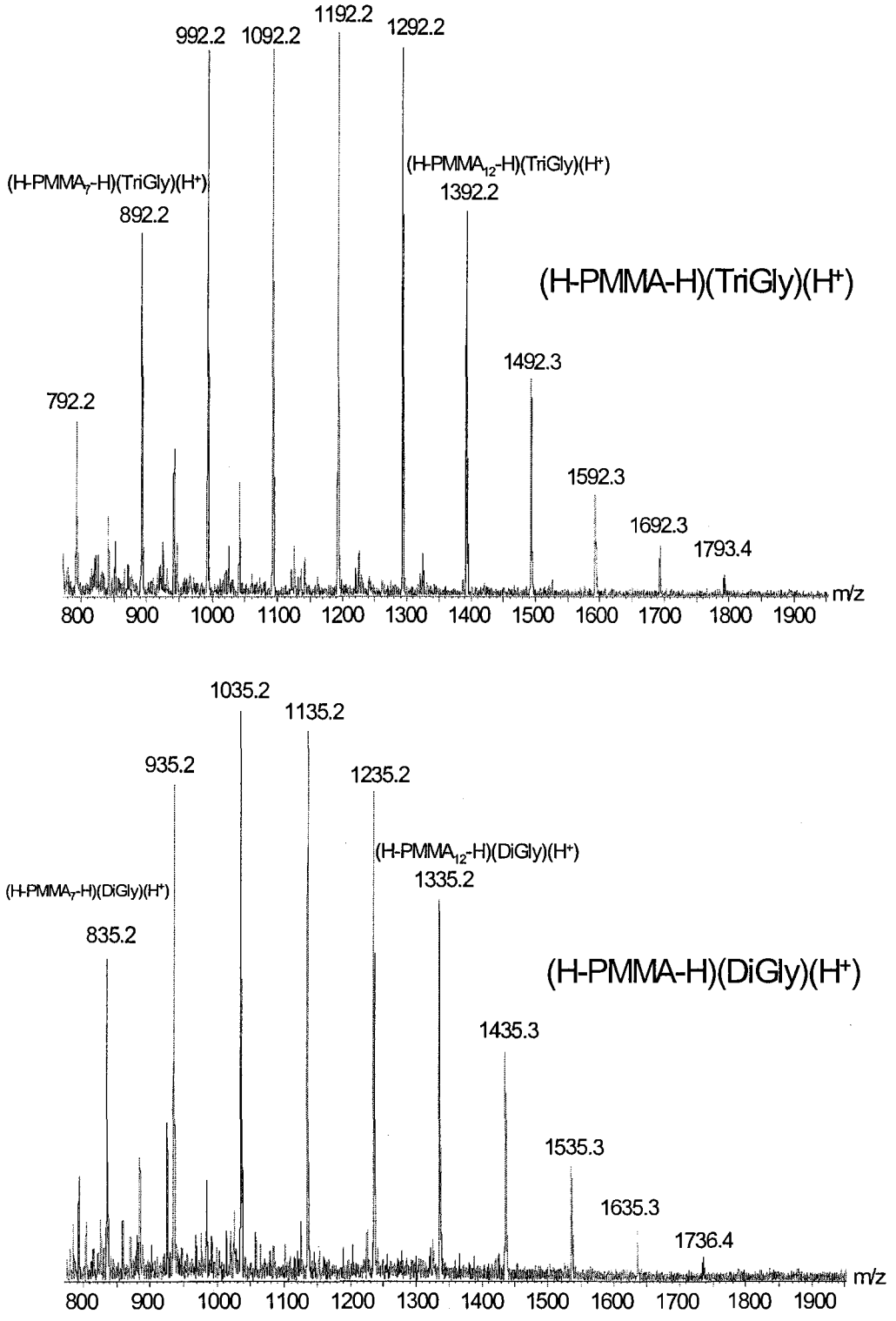

Figure 6.1(a): ESI-MS mass spectrum of PMMA ionized by protonated triglycine, (b) PMMA ionized by protonated diglycine (H-PMMA$_n$-H)(DiGly)(H^+), the minor distributions in (a) and (b) are mainly PMMA ionized by Na^+ coming from the glassware.

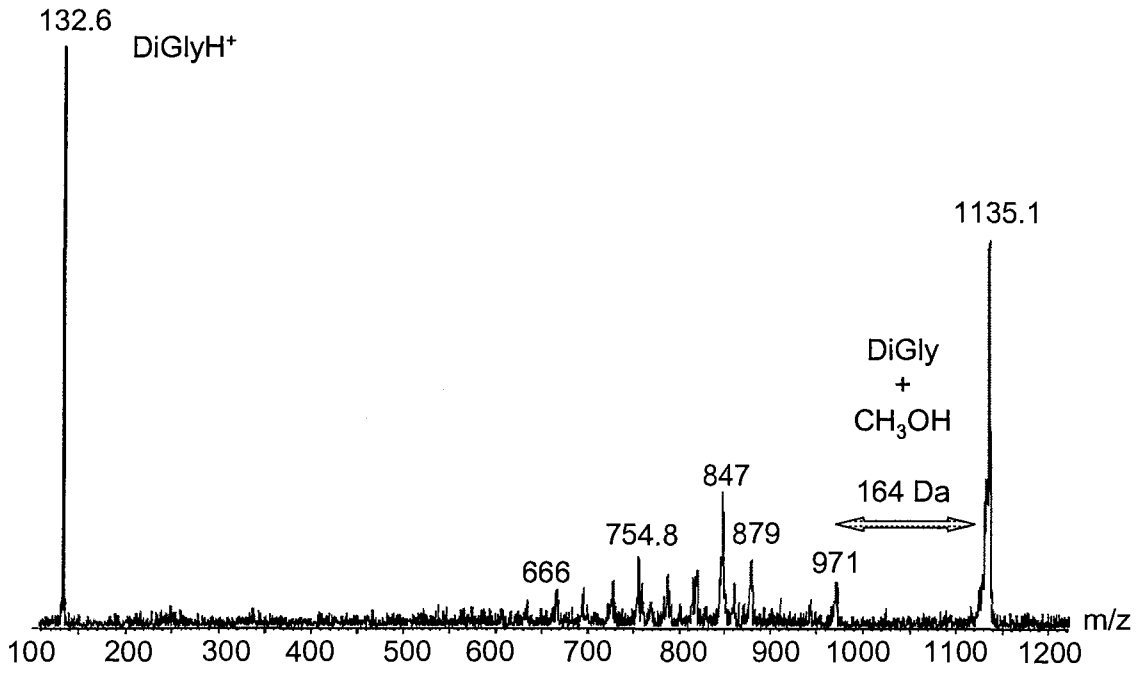

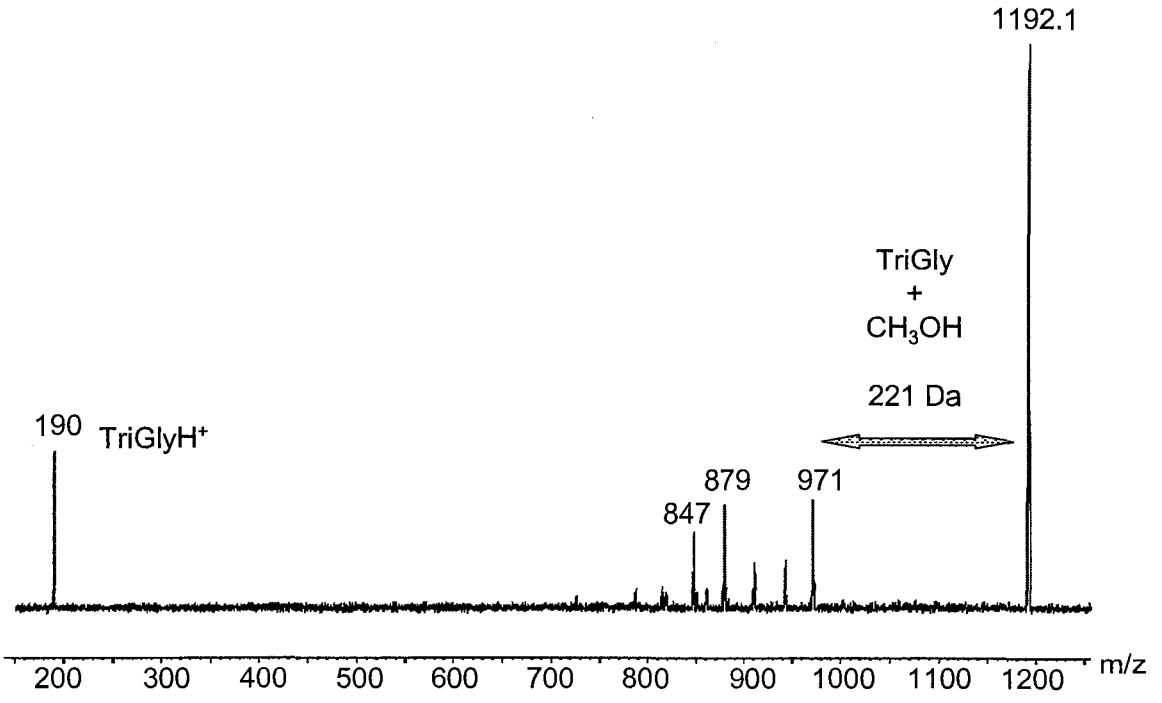

Figure 6.2(a): CID mass spectrum of (H-PMMA$_{10}$-H)(DiGly)(H$^+$), m/z 1135, (E$_{coll}$ = 100eV, pressure = 2.0 x 10^{-3} mBar). (b): CID mass spectrum of (H-PMMA$_{10}$-H)(TriGly)(H$^+$), m/z 1192, (E$_{coll}$ = 30 eV, pressure = 2.0 x 10^{-3} mBar).

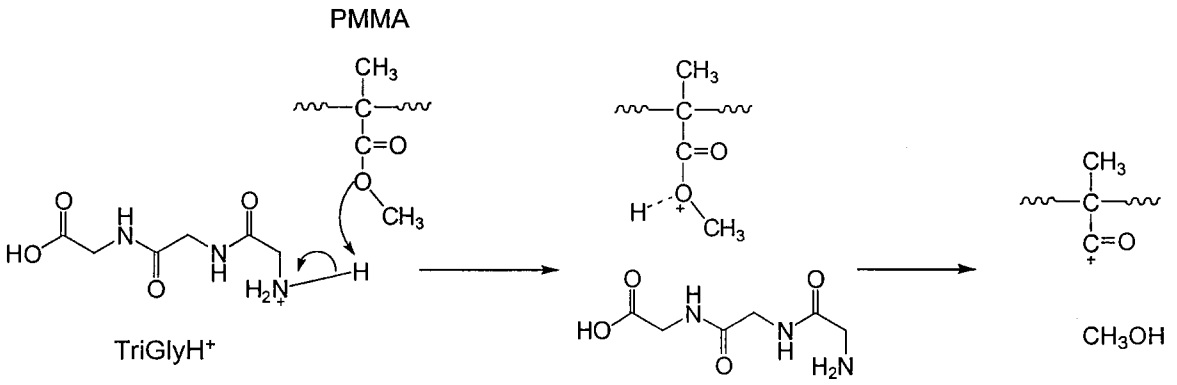

Scheme 6.1

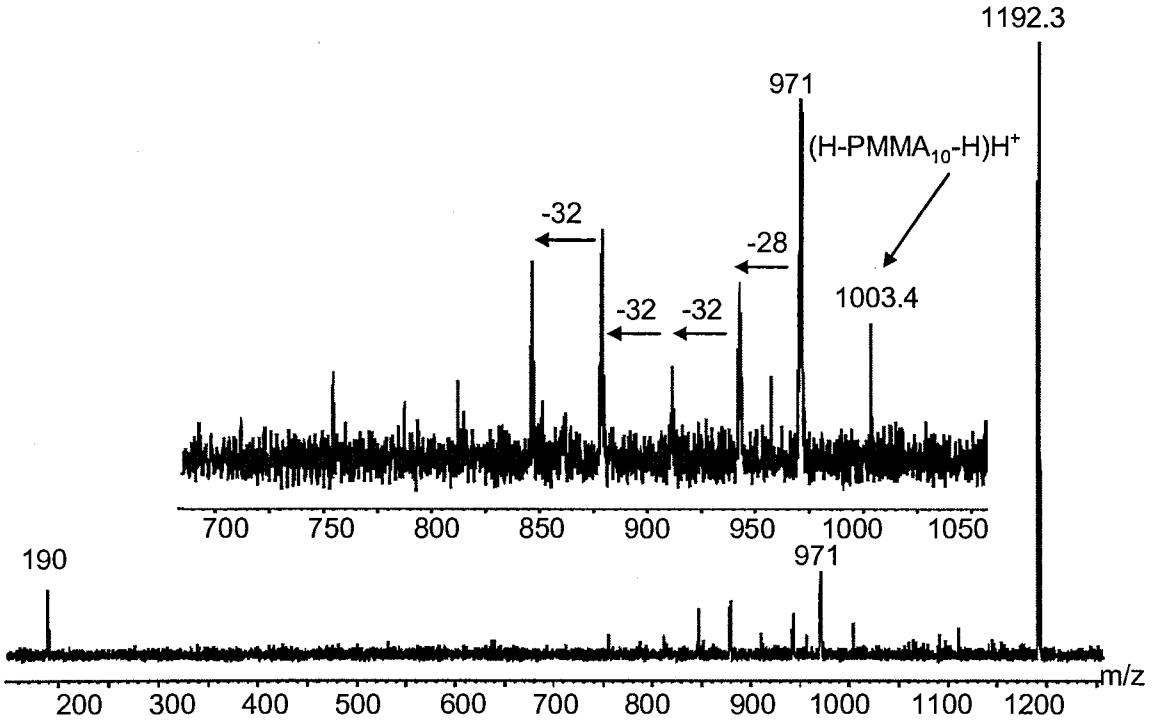

Figure 6.3: CID mass spectrum of (H-$PMMA_{10}$-H)(TriGly)(H^+), m/z 1192, (E_{coll} = 27 eV, pressure = 2.0 x 10^{-3} mBar). The expansion region shows the protonated ion (H-$PMMA_{10}$-H) H^+, m/z 1003, after the loss of the neutral TriGly

After the initial loss of methanol the resulting oligomer cation produces a mass spectrum dominated by peaks separated by 28 and 32 Da. At least the first loss of 28 Da is consistent with CO loss from an acylium ion structure. Alkyl-substituted acylium ions such as that produced from methanol loss from a methyl methacrylate monomer have a low energy threshold to CO loss [102] which is why the peak with m/z 971 in Figure 6.2 is dominant only at very low collision energy. No loss corresponding to the mass of one momoner unit (100 Da) is observed at any collision energy. Therefore, these fragmentation reactions do not happen along the backbone of the oligomer cation, but rather involve the side chains, leaving the backbone at least partially intact. Figures 6.4a and b demonstrate how the fragmentation pattern changes as a function of collision energy for $(H\text{-}PMMA_9\text{-}H)H^+$, and Figure 6.4b highlights the peak separations of 28 and 32 Da. The dominate fragment ion peaks change from high m/z at low CE to low m/z at high CE, indicating substantial consecutive fragmentation with increasing CE. This is also borne out by the CID breakdown diagram in Figure 6.5 (a-d).

From Figure 6.5a it is apparent that m/z 843, 811 and 779 originate from m/z 871. Each has a similar onset energy and a maximum at ~ 30 eV (all energies lab-frame collision energy). These fragment ions involve loss of 28 (see Scheme 6.2), 60 (possibly an intact methacrylate side chain) and 92 Da, respectively.

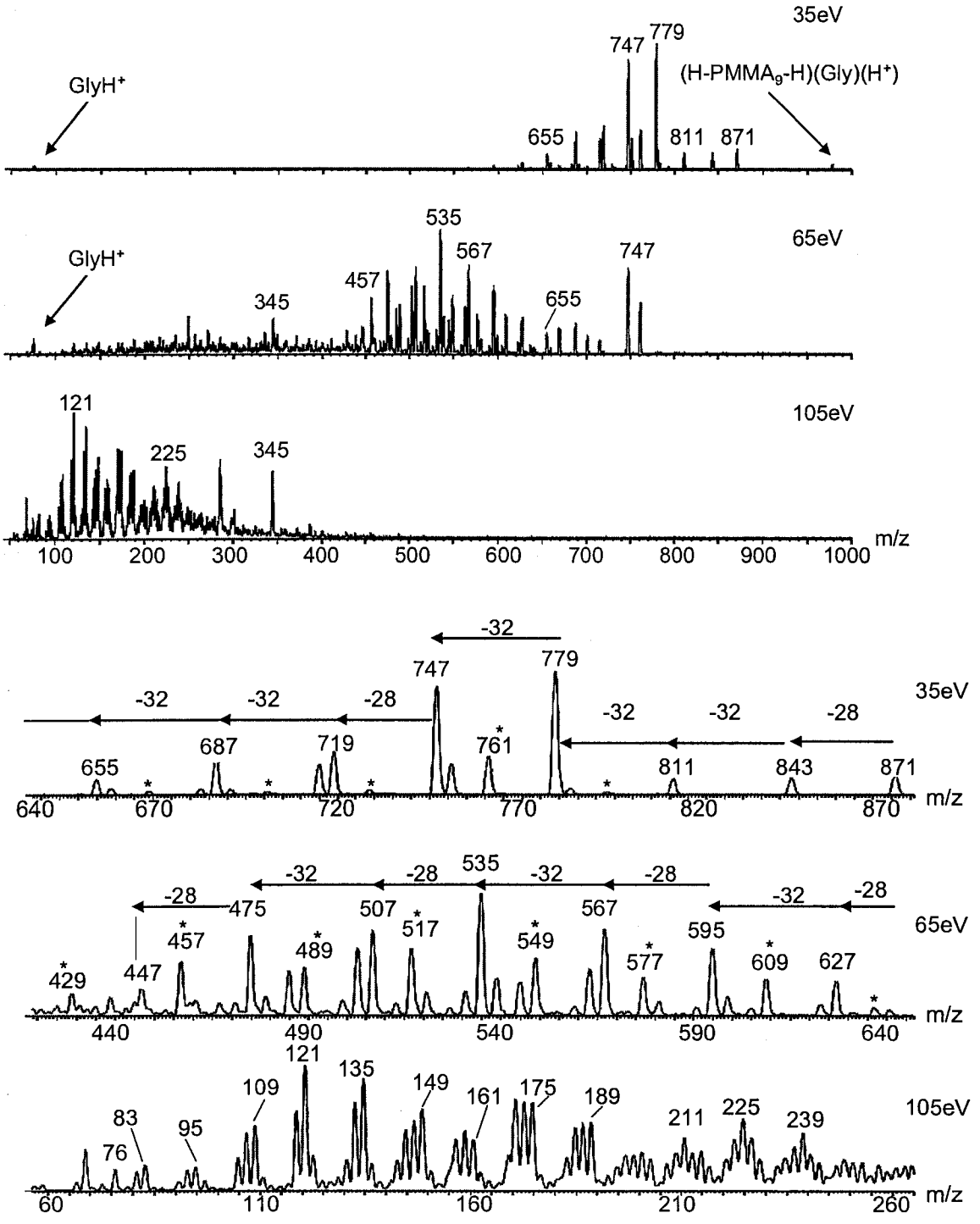

Figure 6.4(a): CID mass spectrum of (H-PMMA$_9$-H)(Gly)(H$^+$), m/z 978, at three different collision energies: 35, 65, and 105 eV (pressure = 2.0 x 10^{-3} mBar).(b): Expansion of the mass spectra in (a). The asterix (*) denotes the minor fragmentation progression in which H_2O is lost early in the sequence (see text).

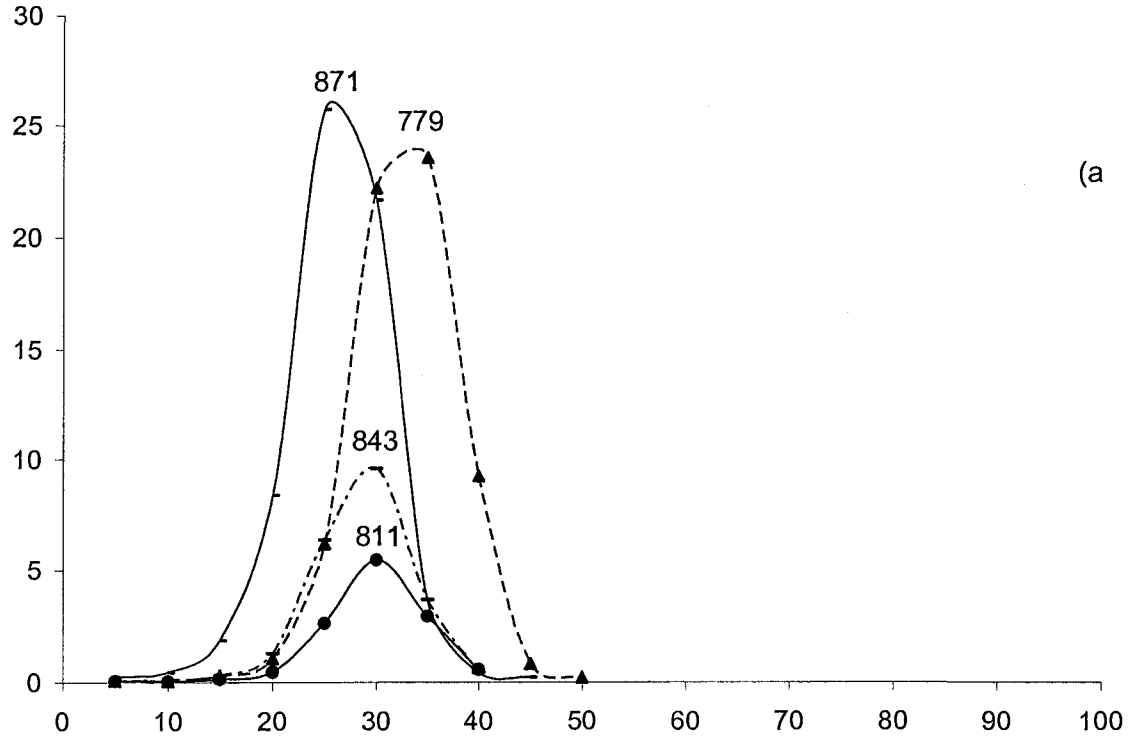
30
25
20
15
10
5
0
871
779
843
811
0
10
20
30
40
50
60
70
80
90
100

(a

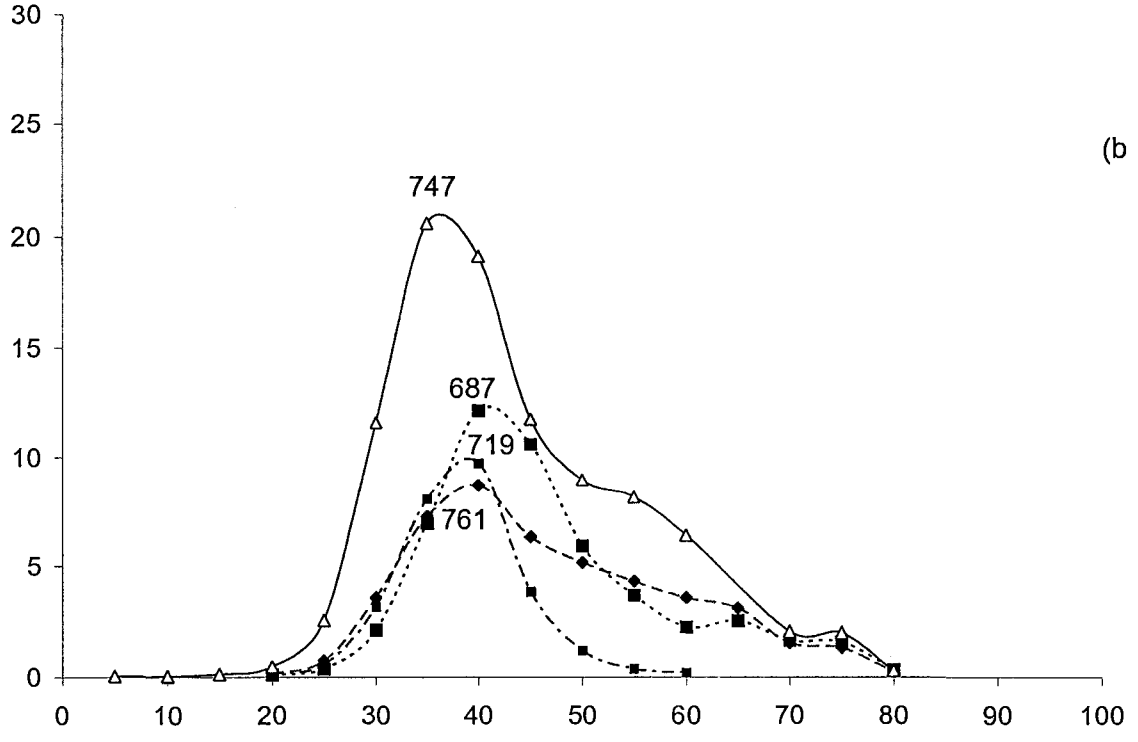
30
25
20
15
10
5
0
747
687
719
761
0
10
20
30
40
50
60
70
80
90
100

(b

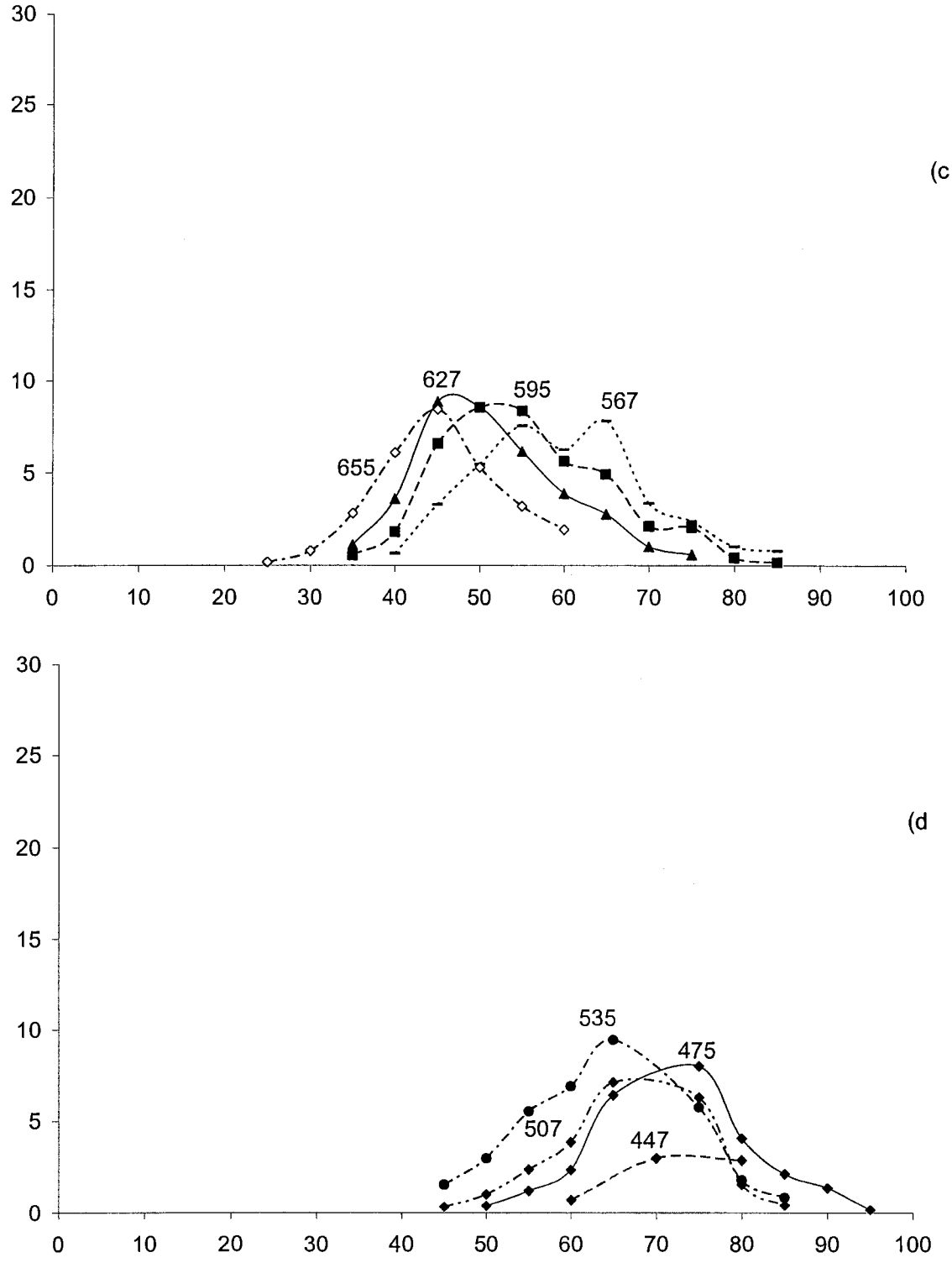

Figure 6.5. CID breakdown diagrams for (H-PMMA$_9$-H)(Gly)(H$^+$) as a function of lab-frame collision energy.

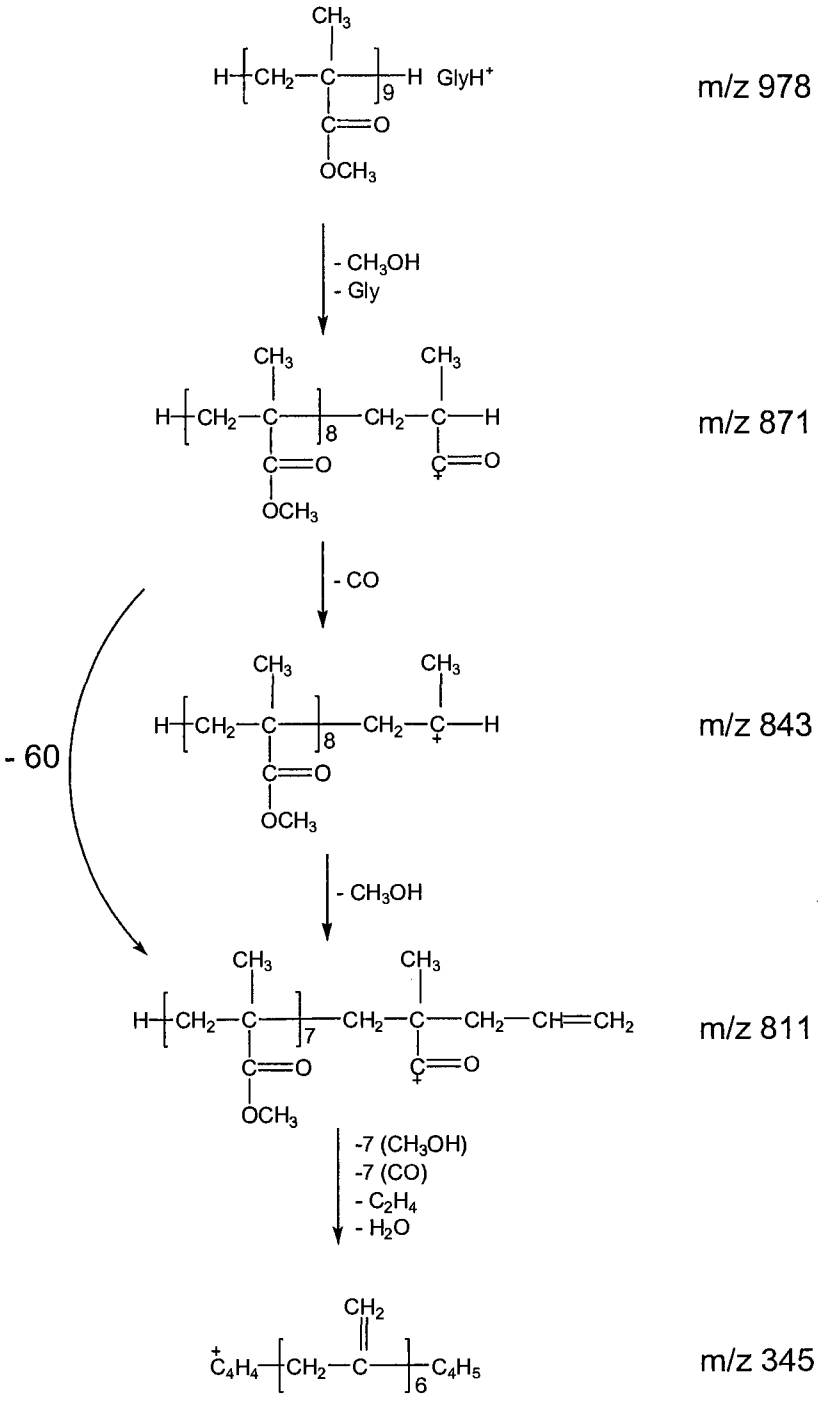
m/z 978
- CH3OH
- Gly
m/z 871
- CO
- 60
m/z 843
- CH3OH
m/z 811
-7 (CH3OH)
-7 (CO)
- C2H4
- H2O
m/z 345

Scheme 6.2

Figure 6.5b shows the breakdown curves for the next four fragment ions, m/z 761, 747, 719 and 687. They all have peak maxima around 40 eV, suggesting they are formed sequentially from m/z 843, 811 and 779. Also, the high energy tail on the curves for m/z 761, 747 and 687 are similar, suggesting they are formed competitively from a common precursor. If this precursor is m/z 779, these channels correspond to losses of 18, 32 and 92 Da, respectively. M/z 719 would correspond to loss of 60 Da from m/z 779, but at the very least the reacting configuration of this ion must be different from that producing the other three fragment ions. Figure 6.5c shows the breakdown curves for the fragment ions with maxima between 45 and 55 eV (m/z 655, 627, 595 and 567). The similar maxima and onsets for m/z 655 and 627 suggest they are formed competitively from a common precursor. One possibility would be losses of 32 and 60 Da from m/z 687. The other two ions in Figure 6.5c have maxima at higher CE, which means they could originate from m/z 655 and 627 by loss of 60 Da. This general pattern repeats itself for the last four fragment ions presented in Figure 6.5d.

Figure 6.4b is an enlargement of each mass spectrum in Figure 6.4a and at the beginning of oligomer cation fragmentation there are relatively more "losses" of 32 than 28 Da, but as the CE increases the two peak separations become more sequential (see 65 eV). Counting the initial loss of methanol, the mass spectra at 35 and 65 eV show the loss of methanol from all nine side chains of this 9-mer. Only six losses of 28 Da are observed as CE increases. There is also a lower intensity progression of fragment ions 18 Da lower in m/z due to loss of H_2O (annotated by the asterix in Figure 6.4b) from m/z 779 as discussed previously. Once the oligomer cation has lost the equivalence of all nine methoxy groups and six CO units it lands up with m/z 447 (m/z 429 has the additional

loss of H_2O). Both progressions of fragment ions undergo further loss of three units of 28 Da (and H_2O for the case of the major progression) to finally produce m/z 345, which reflects the backbone of the oligomer. This is supported by the high intensity of m/z 345 and the fact that sequential losses of 32 and 28 Da are no longer observed from this ion. Rather, peaks separated by 14 and 12 Da are observed, consistent with the fragmentation of a hydrocarbon chain (Figure 6.4b, 105 eV). The fragmentation pathways are illustrated scheme 6.2. Of course, what is presented above is only a suggested sequence of events; without the ability to independently generate each intermediate in isolation it is impossible to prove a mechanism. Attempts are complicated by the fact that the initial loss of methanol can occur from any of the monomer side chains and each of these resulting ions can fragment to its own degree. What is clear is that a simplistic arrow-pushing exercise starting with the protonated oligomer cannot account for the sequence of fragment ions. It is likely that intramolecular reactions may be involved, perhaps similar to that generating the oxazolone-based structure of the b-ion in peptide ion fragmention.

6.2.2 Poly(butyl acrylate)

Figure 6.6 shows the mass spectrum of PBA ionized by $TriGlyH^+$. Four distinct ion distributions were observed: one major (A) and three with lower abundance (B, C, and D). A, C and D are singly charged while distribution B is doubly charged. In distribution A the oligomer has butyl and hydrogen end-groups $(Bu\text{-}PBA_n\text{-}H)(TriGly)(H^+)$. Residual Na^+ produces distribution C $(Bu\text{-}PBA_n\text{-}H)(Na^+)$. Distribution B is doubly charged consisting of two protonated $TriGlyH^+$ and oligomers terminated by methoxy end-groups $(CH_3O\text{-}PBA_n\text{-}126\text{-}OCH_3)(TriGly)_2(H^+)_2$, where 126 is an

unsaturated BA unit ($C_7H_{10}O_2$) and the methoxy groups come from the terminator (CH_3OH) used in the synthesis.[103] Distribution D is PBA ionize with $TriGlyH^+$ and terminated with an 80 Da end-group and is not clearly identified. Likely this end-group originates from the alkyl lithium initiator system used to make PBA.[103,104] As for PMMA, we were able to generate proton-bound complexes of PBA oligomers with different peptides and amino acids, represented by the generic formula $(PBA_n)(AA)H^+$.

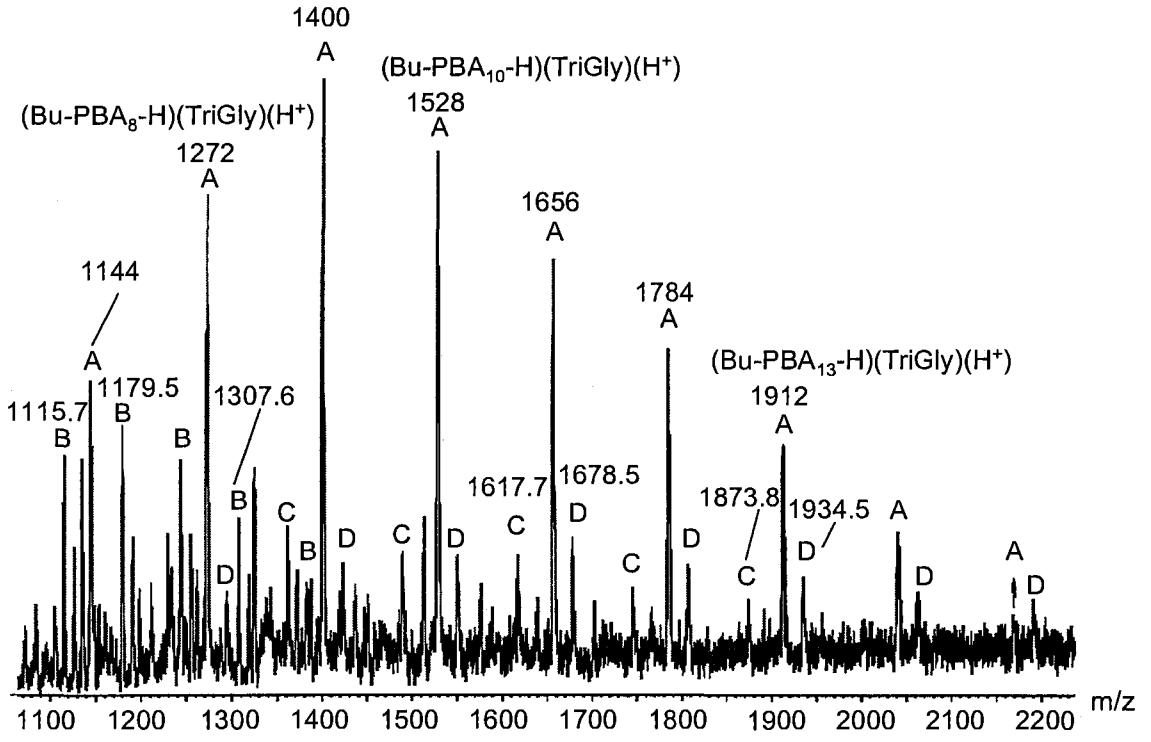

Figure 6.6: ESI-MS mass spectrum of PBA ionized by protonated triglycine. Four distinct ion distributions were observed: A: $(Bu\text{-}PBA_n\text{-}H)(TriGly)(H^+)$, B: $(CH_3O\text{-}PBA_n\text{-}126\text{-}OCH_3)(TriGly)_2(H^+)_2$, C: $(Bu\text{-}PBA_n\text{-}H)(Na^+)$ and D: PBA ionized with $TriGlyH^+$ and terminated with about 80 Da end-groups (see text).

The CID mass spectrum of (Bu-PBA$_8$-H)(DiGly)(H$^+$) (Figure 6.7a) shows a loss of 206 Da which corresponds to butanol (74 Da) and neutral DiGly. This was confirmed by observing a 57 Da increase in this loss when DiGly was replaced with TriGly (Figure 6.7b). After the initial loss of butanol and the peptide, the protonated PBA undergoes a sequential loss of 130 Da. This 130 Da is butyl ether lost from the PBA side chains and not a rearranged BA unit cleaved from the backbone. The number of butyl ether loses agrees with number of PBA side chains in the oligomer. For example, a 7-mer has seven –OBu units and since one is lost in the initial step of the fragmentation, it can only lose three butyl ether molecules (Figure 6.8). This is also true for the 8-mer. The number of butyl ether loses will increase as the number of BA units increases and is the same for oligomers with sequential odd and even number of BA units.

For comparison, the CID mass spectrum of (Bu-PBA$_9$-H)(Na)$^+$ shows this loss of 130 Da, but is dominated by butene and butanol losses (Figure 6.9). Ionizing PBA with Na$^+$ does not allow the loss of all the monomer side chains as in protonated PBA. This may be due to the competition from the other fragmentation pathways occurring along the backbone to form (BA$_n$)(Na$^+$), Figure 6.9. The loss of butene and butanol are also observed from protonated PBA, but only after the oligomer loses the maximum number of butyl ether molecules (Figure 6.8), and only as minor processes at high CE. The losses of butene and butanol likely occur by side chain reactions similar to their formation in the thermal degradation of PBA.[105,106] First, the ester butyl group will form a six-membered ring transition state which then eliminates butene, leaving an acrylic acid unit in the PBA side chain (Scheme 6.3). Secondly, butene could form in the same manner from another

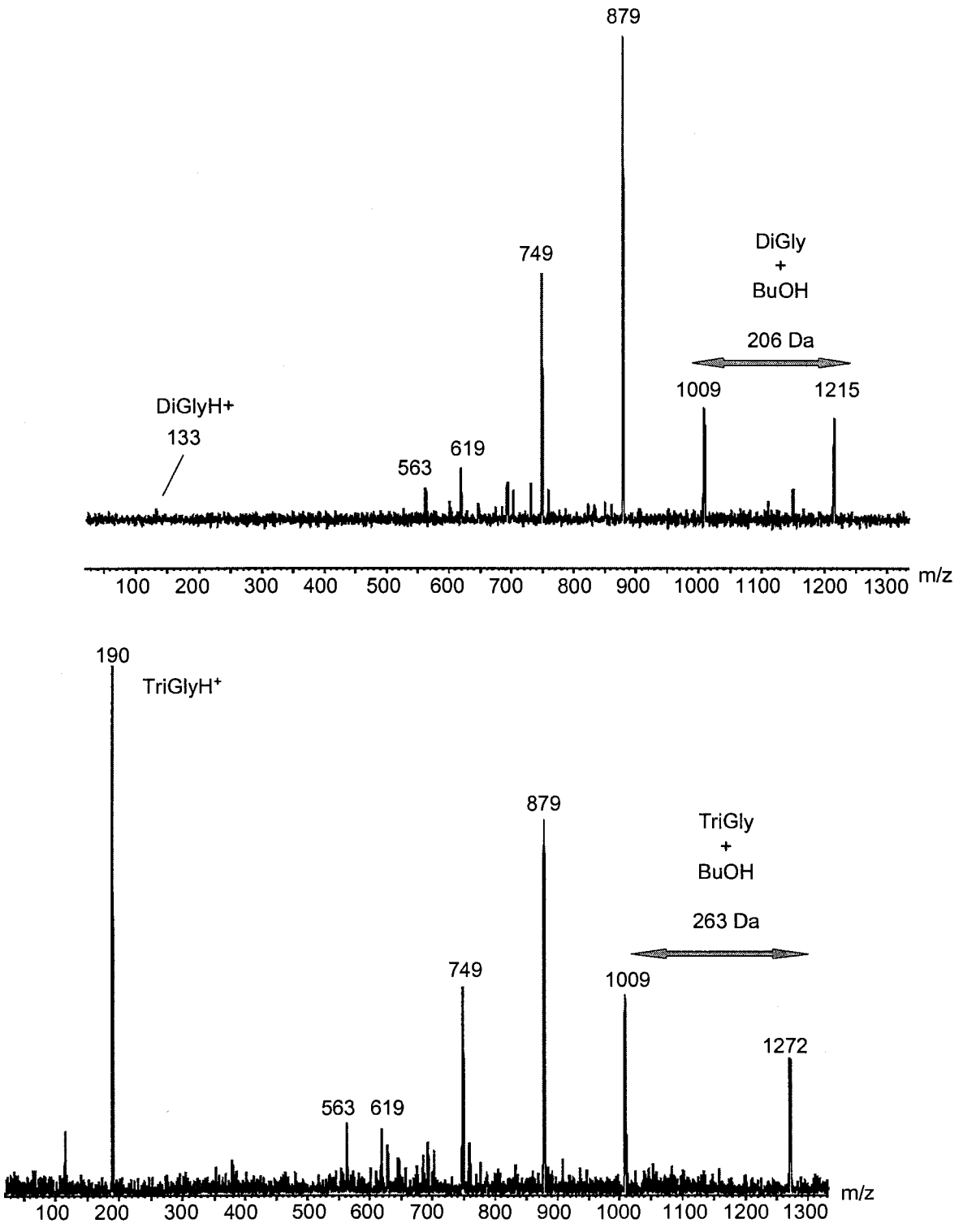

Figure 6.7(a): CID mass spectrum of (Bu-PBA_8-H)(DiGly)(H^+), m/z 1215, (E_{coll} = 30 eV, pressure = 2.0 x 10^{-3} mBar). (b): CID mass spectrum of (Bu-PBA_8-H)(TriGly)(H^+), m/z 1272, (E_{coll} = 40 eV, pressure = 2.0 x 10^{-3} mBar).

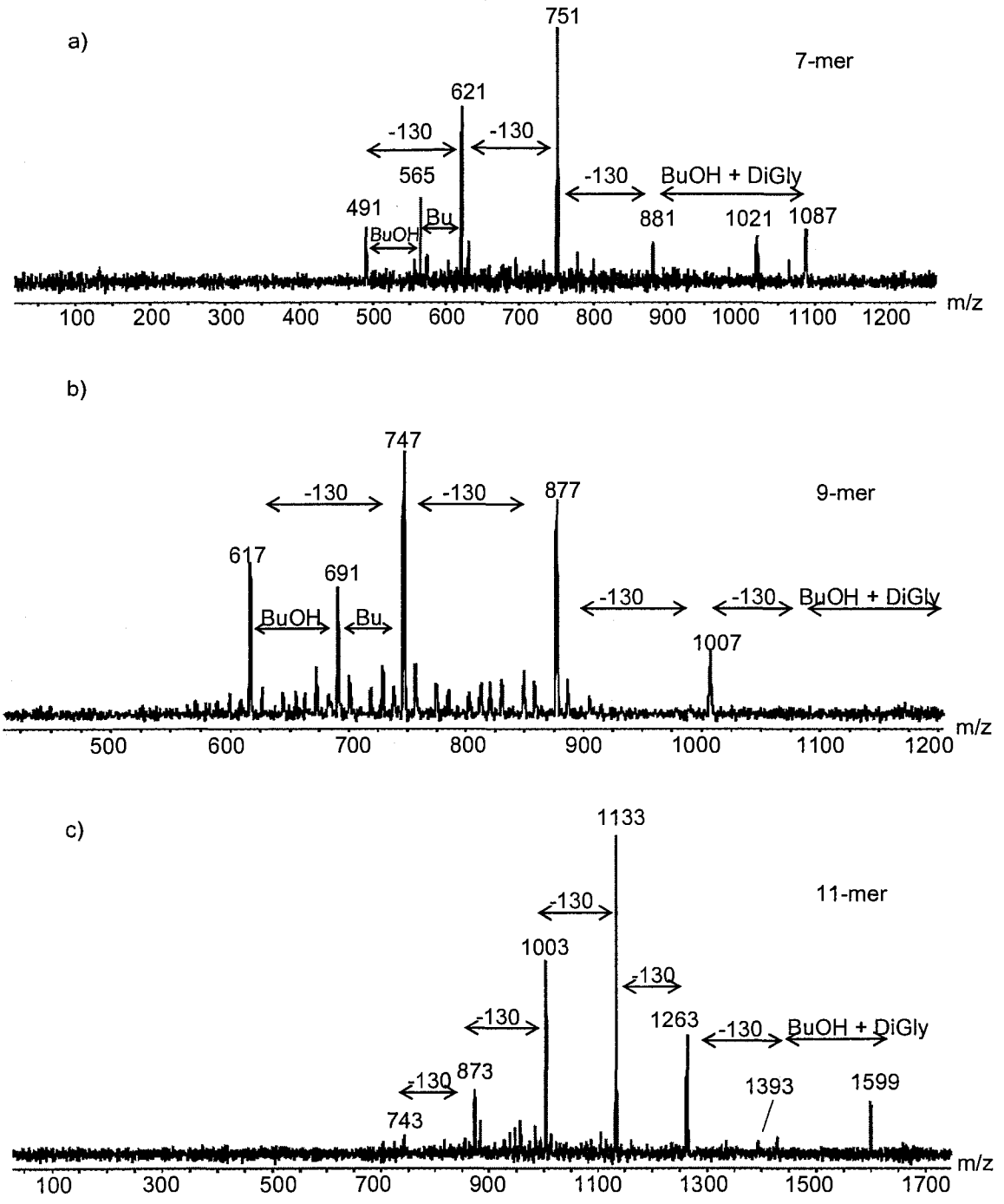
a)
751
7-mer
621
-130
-130
565
-130
BuOH + DiGly
491
Bu
881
1021
1087
BuOH
100 200 300 400 500 600 700 800 900 1000 1100 1200
m/z
b)
747
-130
-130
877
9-mer
617
691
-130
-130
BuOH + DiGly
BuOH
Bu
1007
500 600 700 800 900 1000 1100 1200
m/z
c)
1133
11-mer
-130
1003
-130
-130
1263
-130
BuOH + DiGly
-130
873
1393
1599
743
100 300 500 700 900 1100 1300 1500 1700
m/z

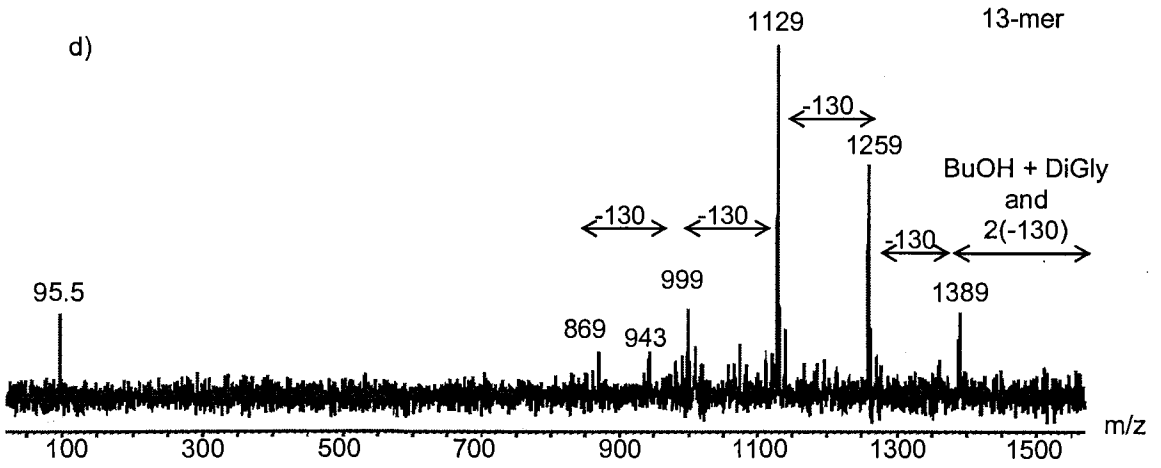

Figure 6.8: CID mass spectrum of (Bu-PBA$_n$-H)(DiGly)(H^+) for 7-mer (E_{coll} = 30 eV), 9-mer (E_{coll} = 40 eV), 11-mer (E_{coll} = 40 eV) and 13-mer (E_{coll} = 50 eV) (pressure = 2.0 x 10^{-3} mBar in each case).

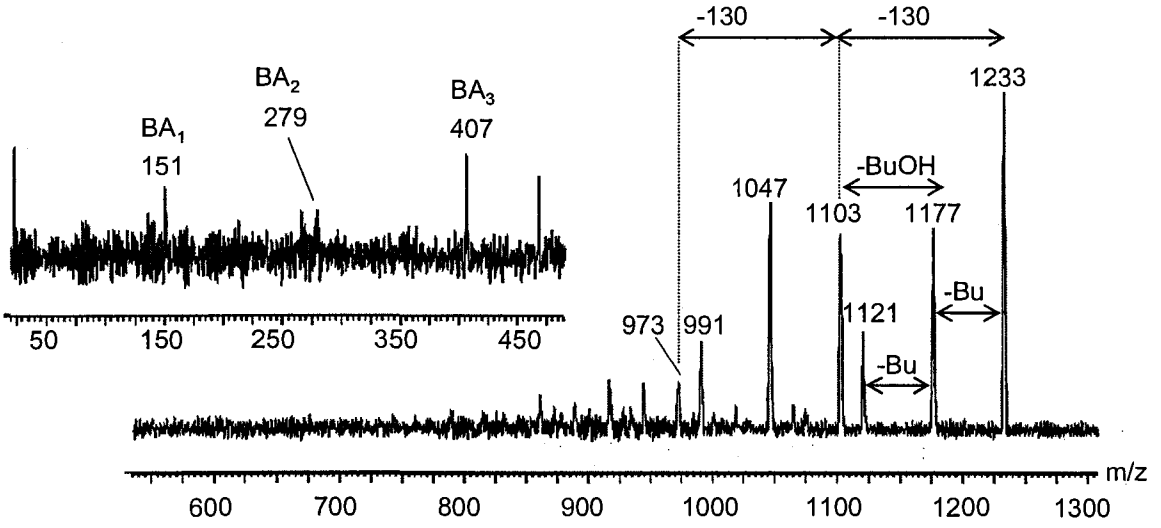

Figure 6.9: CID mass spectrum of (Bu-PBA$_9$-H)(Na^+), m/z 1233, (E_{coll} = 80 eV, pressure = 2.0 x 10^{-4} mBar), -Bu in the figure is the lost of Butene (56 Da). The inset shows the low mass.

side chain, or the acrylic acid unit reacts with a neighbouring butyl ester to form butanol and a cyclic anhydride.[105]

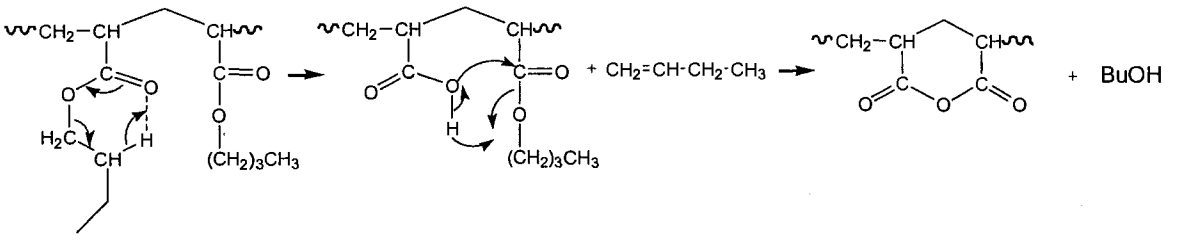

Scheme 6.3

Protonated PBA forms the cyclic anhydride in one step by the loss of butyl ether (illustrated in Scheme 6.4 for (H-PMMA$_9$-H)(DiGly)(H$^+$)). Once all side chains are lost, the resulting ion loses a series of 28 and 18 Da masses, presumably from the cyclic anhydride units (Figure 6.10).

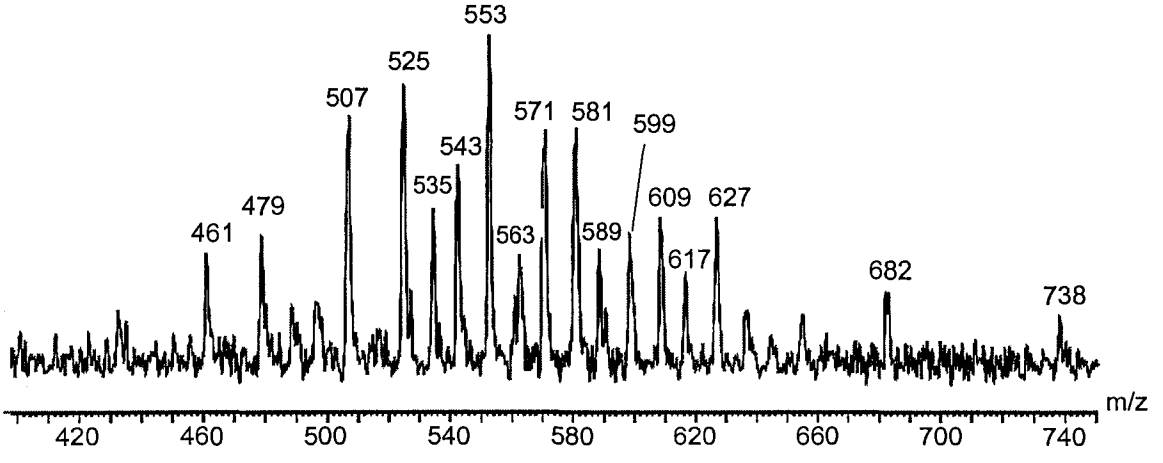

Figure 6.10: CID mass spectrum of (Bu-PBA$_9$-H)(DiGly)(H$^+$), m/z 1343, (E_{coll} = 70 eV, pressure = 2.0 x 10^{-3} mBar)

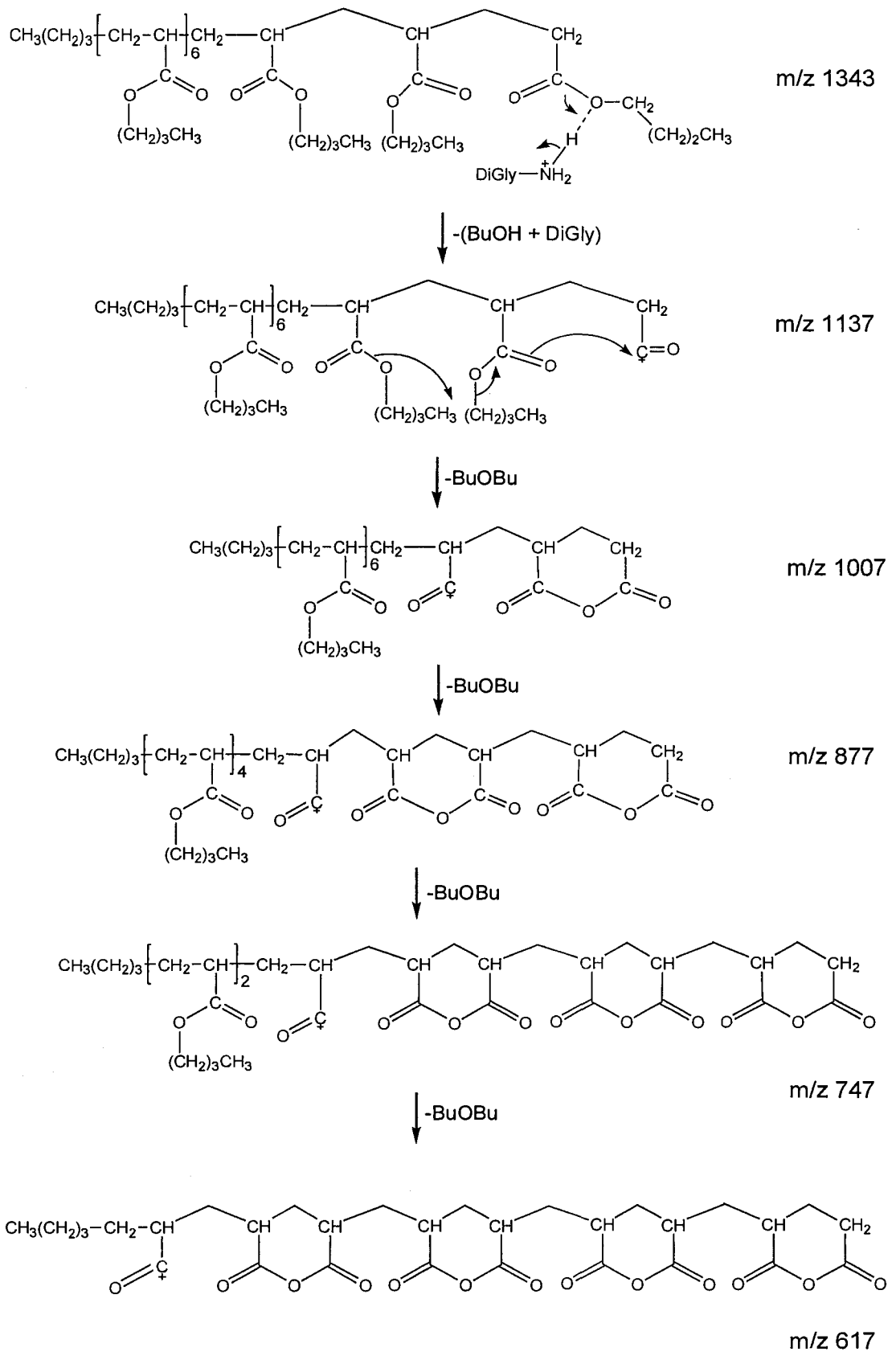

Scheme 6.4 (9-mer)

6.3 Conclusion

Protonated PMMA and PBA oligomers can be generated in the gas phase from the dissociation of proton-bound complexes of the oligomers with simple protonated amino acids and peptides. Compared to their metal ion adduct analogues, these protonated oligomers undergo a unique fragmentation chemistry upon collisional activation. Both protonated oligomers fragment primarily by eliminating neutral molecules from the monomer side chains until all that is left is the backbone hydrocarbon.

6.4 A curious aside: Doubly charged PBA ions

Figure 6.11a shows the CID mass spectrum of $(CH_3\text{-}O\text{-}PBA_{15}\text{-}126\text{-}O\text{-}CH_3)(TriGly)_2(H^+)_2$. The doubly charged ion either losses neutral TriGly to give the doubly charged PBA $(CH_3\text{-}O\text{-}PBA_{15}\text{-}126\text{-}O\text{-}CH_3)(TriGly)(H^+)_2$ m/z 1149.5 or $TriGlyH^+$ to give the singly charged $(CH_3\text{-}O\text{-}PBA_{15}\text{-}126\text{-}O\text{-}CH_3)(TriGly(H^+)$ m/z 2298. The doubly charged ion at m/z 1149.5 can lose the second neutral TriGly leaving the doubly protonated oligomer (m/z 1055) which does not undergo further fragmentation at any collision energy we explored. The two protonated TriGly of distribution B are replaced by two Na^+ when PBA is ionized with NaCl. In the CID mass spectrum of this ion (Figure 6.11b) we see the loss of the first Na^+ to form the singly charged ion, and the

doubly and singly charged ions fragment as seen for distribution A when it was ionized with Na^+ (Figure 6.9*)*.

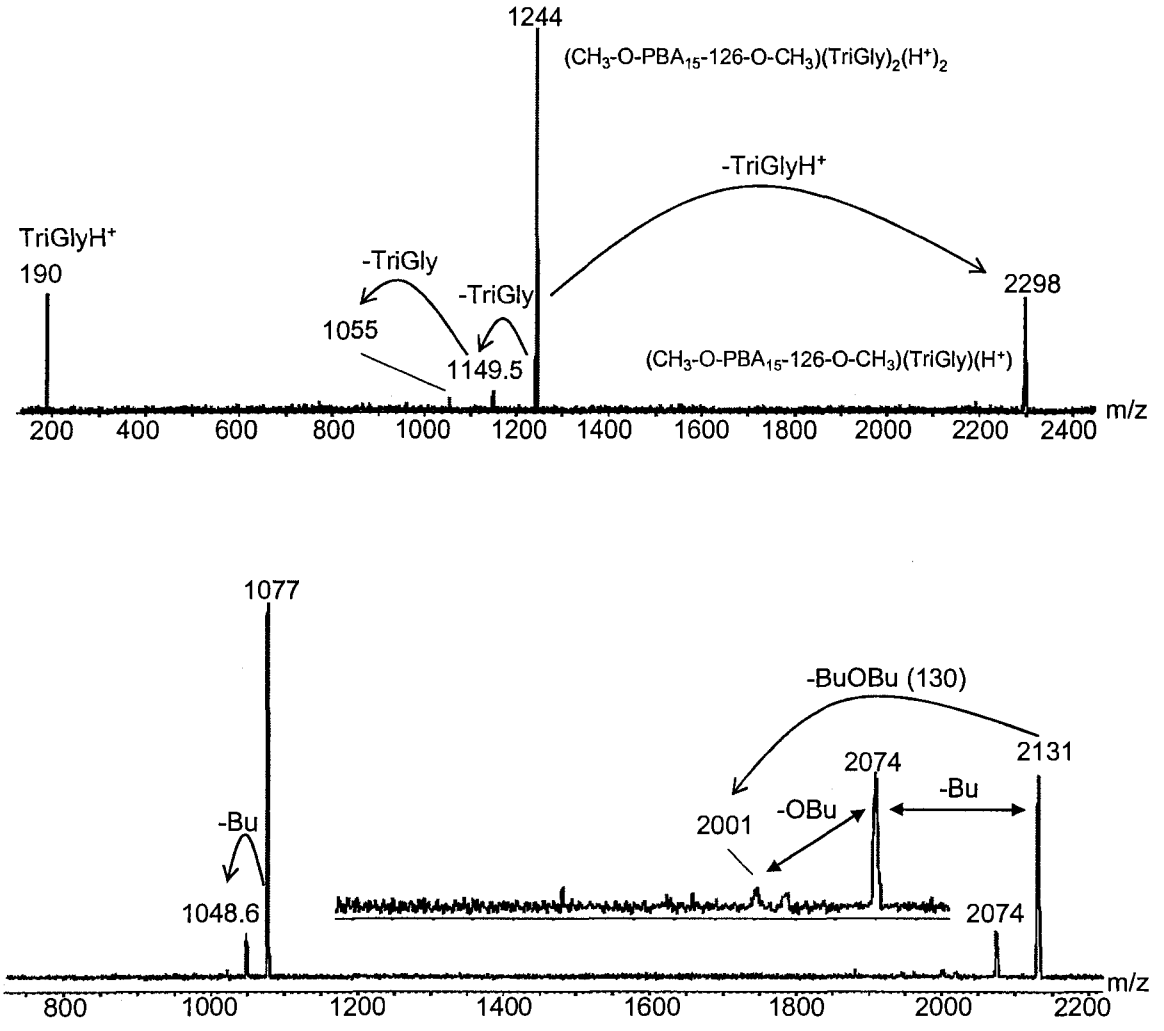

Figure 6.11(a): ESI-MS/MS spectrum of $(CH_3\text{-O-PBA}_{15}\text{-126-O-CH}_3)(TriGly)_2(H^+)_2$, m/z 1244, (E_{coll} = 40 eV). (b): ESI-MS/MS spectrum of $(CH_3\text{-O-PBA}_{15}\text{-126-O-CH}_3)(Na^+)_2$, m/z 1077, (E_{coll} = 60 eV).

7

The Proton Affinity of a Polymer: What Does That Mean?

7.1 Introduction

The proton affinity (PA) of a compound is one of the key thermochemical pieces of information that can be used to understand its chemistry. A variety of methods have been developed to determine accurate PA values, including equilibrium measurements, bracketing experiments and the kinetic method.[107] By and large, these methods have been applied to small molecules due to the need for reference bases of similar structure and PA. But what of larger, poly-functional species, such as polymers? Can one define the PA for an oligomeric compound with many of the same functional groups?

7.2 Results and Discussion

As discussed in Chapter 6, it is straightforward to generate proton-bound complexes of polymer oligomers and amino acids by electrospray-ionization (ESI) mass spectrometry. Figure 7.1 exhibits the ESI mass spectrum of poly(methyl methacrylate) oligomers ionized with protonated glycine.

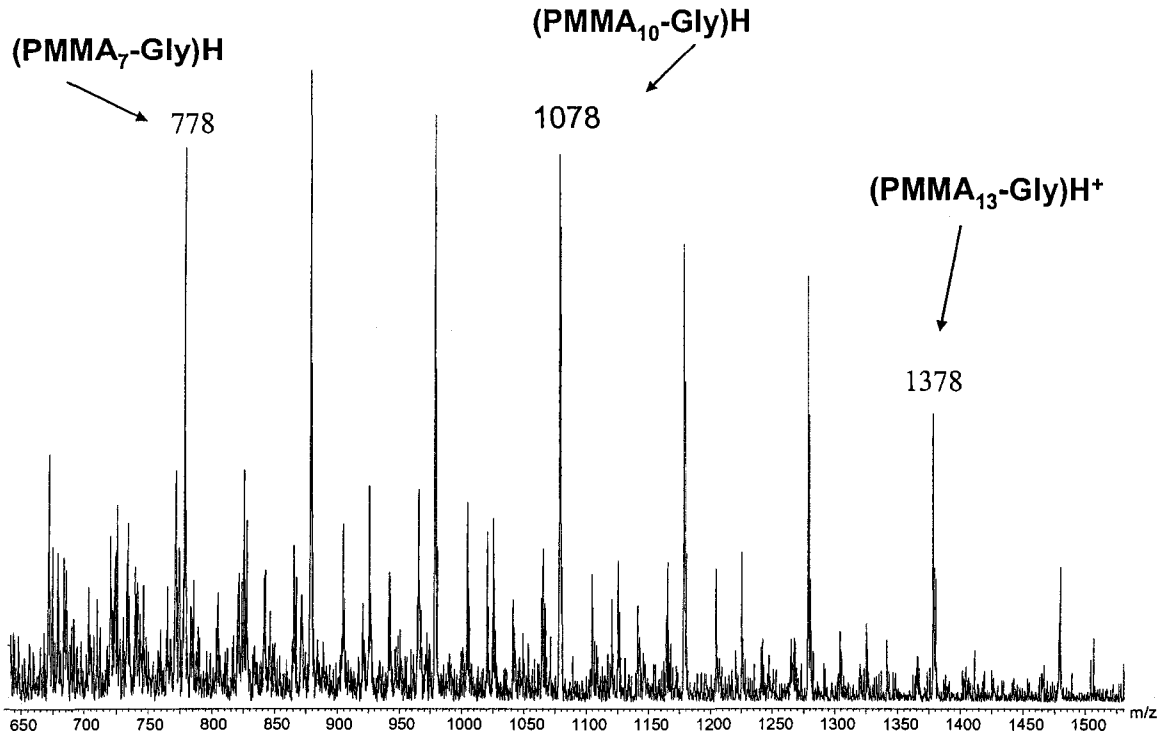

Figure 7.1. Mass spectrum of PMMA complexed with protonated glycine.

To bracket the PA of five PMMA oligomers, the collision-induced dissociation (CID) mass spectrum of each oligomer/amino acid complex (Table 7.1) was obtained at the lowest collision energy needed to see a fragment ion. This "first observed" fragment ion was either the protonated amino acid (AAH^+) or the protonated oligomer, which also sometimes appeared as the $PMMA_nH^+$-CH_3OH ion (for example, see Figure 7.2). The results are summarized in table 7.1. In some cases, both species appear at the lowest collision energy, indicating that the PA of the oligomer is similar to that of the amino acid. The data in table 7.1 place $PA(PMMA_3) = 910 \pm 10$, $PA(PMMA_4) = 910 \pm 10$, $PA(PMMA_7) = 910 \pm 10$, $PA(PMMA_{13}) = 950 \pm 20$ and $PA(PMMA_{17}) = 1000 \pm 50$ kJ mol^{-1}.

Table 7.1. Fragment ion observed at threshold in CID mass spectra of $(PMMA_n)(AA)H^+$ complexes (A=AAH^+, P = $PMMAH^+$)

	Observed Threshold Fragment Ion[a]						
oligomer	Arg (1051.0)	Lys (996)	Trp (948.9)	Phe (922.9)	Leu (914.6)	Ala (901.6)	Gly (886.5)
3mer	A	A	A	A	A / P	P	P
4mer	A	A	A	A	A / P	P	P
7mer	A	A	A	A	A / P	P	P
13mer	A	A	A / P	P	P	P	P
17mer	A	A	P	P	P	P	P

[a] Amino acid PA in parentheses (kJ mol^{-1}).

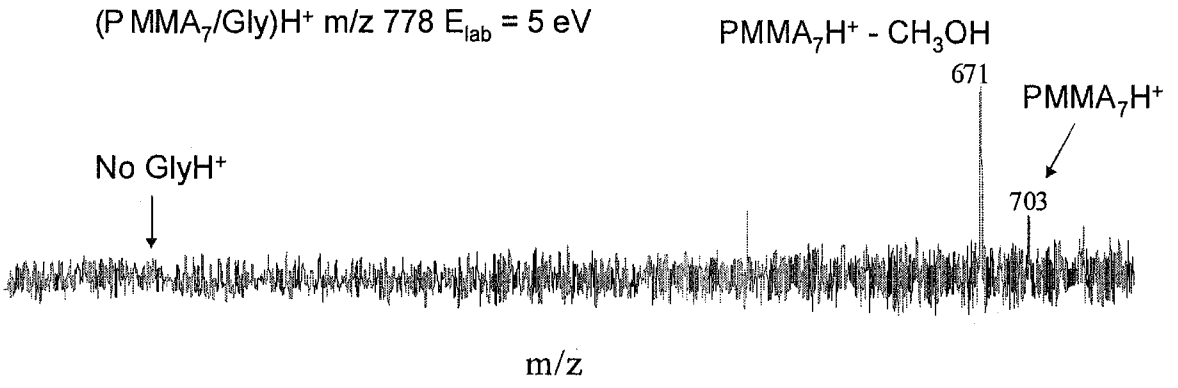

Figure 7.2. CID mass spectrum of $(PMMA_7)(Gly)H^+$ at a lab frame collision energy of 5 eV (centre-of-mass collision energy of 0.24 eV). Argon gas pressure 3 x 10^{-3} mbar.

Are these values reasonable? The PA of $tBuCO_2CH_3$, the analogue of one PMMA side chain, is only 845 kJ/mol,[108] and so even protonated glycine ($GlyH^+$) should not proton transfer. One explanation is that the proton is bound by adjacent side chains. We can estimate the impact of this on the PA. In alcohols, PA values increase upon di-OH substitution due to double H-bonding. The effect is more pronounced as the distance between the OH groups increases (i.e., increasing ring size in the protonated species) due to improved H-bonding geometry (Figure 7.3). Using this data, PA 1,5-pentanediol > pentanol by 112 kJ/mol.[108] For the series of esters PA $MeCO_2CH_3$ (822) < $EtCO_2CH_3$ (830) < $iPrCO_2CH_3$ (837) < t-$BuCO_2CH_3$ (845)[108] and so we might expect the PA of PMMA to be up to 112 kJ/mol greater than t-$BuCO_2CH_3$, i.e., ca 950 kJ/mol, if it is bi-dentate binding, similar to the measured estimates.

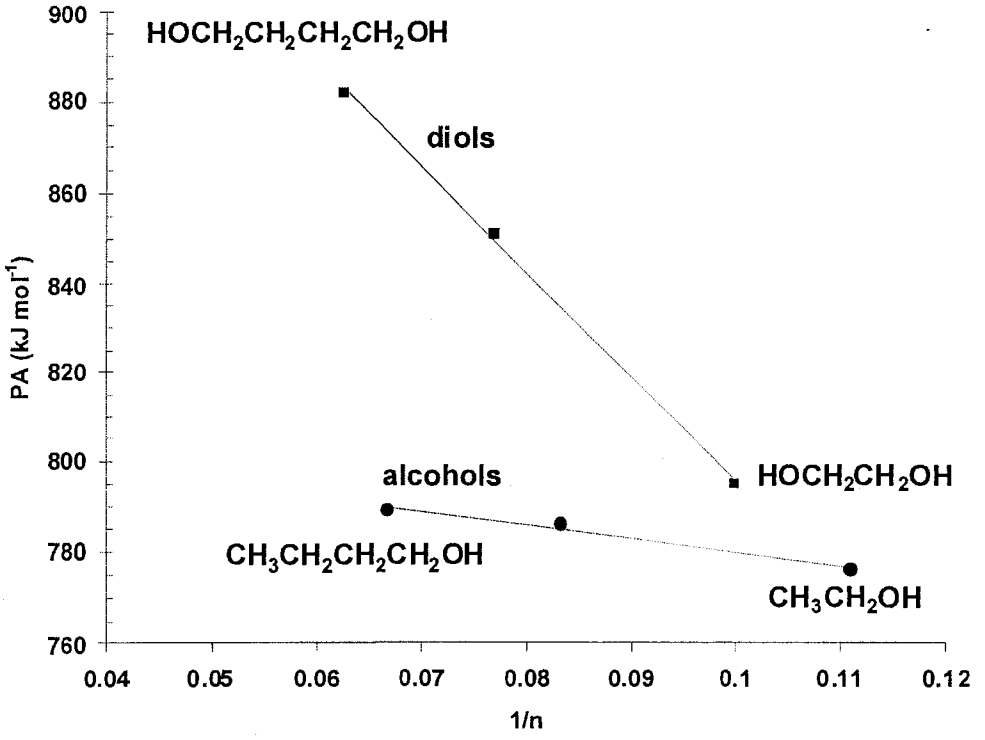

Figure 7.3. Plot of the proton affinities of primary alcohols and analogous diols as a function of 1/n, where n is the number of atoms.

If the proton is bound by two adjacent MMA side chains in every oligomer, one might expect the PA of any n-mer to be the same. This is clearly not the case in table 7.1. The ion $(PMMA_n)(AA)H^+$ decomposes by two competing pathways:

$$PMMA_n + AAH^+ \xleftarrow{k_{AAH^+}} (PMMA_n)(AA)H^+ \xrightarrow{k_{PMMA_nH^+}} PMMA_nH^+ + AA$$

The rate constant for each unimolecular decomposition can be written as:

$$k_{PMMAnH^+} = \frac{k_B T}{h} \frac{Q^t_{PMMAnH^+}}{Q_{complex}} e^{\frac{-E_{0,PMMAnH^+}}{RT}} \tag{7.1}$$

$$k_{AAH^+} = \frac{k_B T}{h} \frac{Q^t_{AAH^+}}{Q_{complex}} e^{\frac{-E_{0,AAH^+}}{RT}} \tag{7.2}$$

where Q represents the partition function for the reactant ion or transition state for a particular reaction and E_0 the 0 K activation energy. In the experiment, we are probing the relative rate constants for these two processes:

$$\frac{k_{PMMAnH^+}}{k_{AAH^+}} = \frac{Q^t_{PMMAnH^+}}{Q_{complex}} \frac{Q_{complex}}{Q^t_{AAH^+}} e^{\frac{-\Delta E_0}{RT}} \tag{7.3}$$

which simplifies to:

$$\frac{k_{PMMAnH^+}}{k_{AAH^+}} = \frac{Q^t_{PMMAnH^+}}{Q^t_{AAH^+}} e^{\frac{-\Delta E_0}{RT}} \tag{7.4}$$

The relative rate constants can be approximated by the relative peak intensities in the CID mass spectrum. At threshold, if we observe $PMMA_nH^+$ and not AAH^+, we assume a peak ratio ~ 10.

$$10 = \frac{Q^{\ddagger}_{PMMAnH^+}}{Q^{\ddagger}_{AAH^+}} e^{\frac{-\Delta E_0}{RT}} \tag{7.5}$$

ΔE_0 in this case becomes simply the difference in proton affinity (PA) of the oligomer and amino acid:

$$10 = \frac{Q^{\ddagger}_{PMMAnH^+}}{Q^{\ddagger}_{AAH^+}} e^{\frac{-\Delta PA}{RT}} \tag{7.6}$$

Each partition function in the above expression can be written out fully:

$$10 = \frac{g_{PMMAnH^+}}{g_{AAH^+}} \frac{q^{\ddagger}_{trans,PMMAnH^+}}{q^{\ddagger}_{trans,AAH^+}} \frac{q^{\ddagger}_{rot,PMMAnH^+}}{q^{\ddagger}_{rot,AAH^+}} \frac{q^{\ddagger}_{vib,PMMAnH^+}}{q^{\ddagger}_{vib,AAH^+}} e^{\frac{-\Delta PA}{RT}} \tag{7.7}$$

Here *g* represents the reaction degeneracy for the two reactions. The proton can sit in n-1 possible locations if bound in a bidentate fashion between adjacent side chains in an n-mer oligomeric chain, and this will raise the rate constant for this channel. Since the two transition states have the same mass, the translational partition functions will cancel. Even though the geometry of the two transitions states will differ near the location of the proton, the rotational partition function will be dominated by the moments of inertia of the oligomer chain, and so it should be safe to cancel these as well:

$$10 = \frac{g_{PMMAnH^+}}{g_{AAH^+}} \frac{q^{\ddagger}_{vib,PMMAnH^+}}{q^{\ddagger}_{vib,AAH^+}} e^{\frac{-\Delta PA}{RT}} \tag{7.8}$$

Without explicit information about the transition states and their vibrational frequencies, it is difficult to derive a numerical value for the PA for a given oligomer. However, it is

possible to derive the expected difference in PA of two oligomeric chains. We can write out the expression for a 7mer and 13mer:

$$10 = \frac{g_{PMMA_7H^+}}{g_{AAH^+}} \frac{q^{\ddagger}_{vib,PMMA_7H^+}}{q^{\ddagger}_{vib,AAH^+}} e^{\frac{-\Delta PA_{7-AA}}{RT}} \tag{7.9}$$

$$10 = \frac{g_{PMMA_{13}H^+}}{g_{AAH^+}} \frac{q^{\ddagger}_{vib,PMMA_{13}H^+}}{q^{\ddagger}_{vib,AAH^+}} e^{\frac{-\Delta PA_{13-AA}}{RT}} \tag{7.10}$$

If, as previously discussed, the proton is bound by two adjacent side chains in a PMMA oligomer, then $g_{PMMA_7H^+} = 6$ while $g_{PMMA_{13}H^+} = 12$.

$$10 = 6 \frac{q^{\ddagger}_{vib,PMMA_7H^+}}{q^{\ddagger}_{vib,AAH^+}} e^{\frac{-\Delta PA_{7-AA}}{RT}} \tag{7.11}$$

$$10 = 12 \frac{q^{\ddagger}_{vib,PMMA_{13}H^+}}{q^{\ddagger}_{vib,AAH^+}} e^{\frac{-\Delta PA_{13-AA}}{RT}} \tag{7.12}$$

Dividing eqn. 7.11 by 7.12 gives:

$$2 = \frac{q^{\ddagger}_{vib,PMMA_7H^+}}{q^{\ddagger}_{vib,AAH^+,7mer}} \frac{q^{\ddagger}_{vib,AAH^+,13mer}}{q^{\ddagger}_{vib,PMMA_{13}H^+}} e^{\frac{-\Delta PA_{7-13}}{RT}} \tag{7.13}$$

The vibrational partition functions for the 13mer channels will be the same as those for the 7mer channels, but with additional vibrational frequencies in the products. These additional vibrational frequencies come from the extra oligomer chain not involved in the transition state bonding region, and so will be the same for the two channels. Since they appear in the partition function as a product, they will cancel out, which means that:

$$\frac{q^{\ddagger}_{vib,PMMA_7H^+}}{q^{\ddagger}_{vib,AAH^+,7mer}} = \frac{q^{\ddagger}_{vib,PMMA_{13}H^+}}{q^{\ddagger}_{vib,AAH^+,13mer}}$$

And eqn. 7.13 simplifies to:

$$2 = e^{\frac{-\Delta PA_{7-13}}{RT}} \tag{7.14}$$

Yielding

$$\Delta PA_{7-13} = -RT \ln 2 \tag{7.15}$$

Assuming an ion temperature of 300K results in an expected ΔPA between $PMMA_7$ and $PMMA_{13}$ of only 2 kJ mol^{-1}. Experimentally we observe a difference of 40 ± 30 kJ mol^{-1}, which can only be achieved if the effective ion temperature is 1735 – 12146 K, clearly not reasonable given that in each case dissociation occurs at centre-of-mass collision energies of only a few tenths of an eV. If any two side chains can bind the proton, the reaction degeneracies for the 7mer and 13mer become 21 and 78, respectively and eqn. 15 becomes:

$$\Delta PA_{7-13} = -RT \ln 3.7 \tag{7.16}$$

At 300 K, ΔPA is now 3.3 kJ mol^{-1}, again far too low compared to the experimental results.

The above argument suggests there is a change in the proton-binding motif as chain length increases. If the proton becomes bound by three side chains once the oligomer becomes long enough to accommodate that configuration, this would result in a significant increase in PA. We therefore have the case that PA(monomer) = 845 kJ mol^{-1},

PA(bidentate) = 910 ± 10 kJ mol^{-1} and PA(tridentate) = 950 ± 20 kJ mol^{-1}. It may be surprising that tridentate binding of the proton only adds 40 kJ mol^{-1} to the PA of the oligomeric chain (above that for bidentate binding). However, the trend is consistent with what is known for the binding enthalpies of proton-bound clusters. Kebarle[109] measured the successive binding enthalpies for proton-bound dimers and trimers of water, dimethyl ether, dimethyl sulfoxide, acetonitrile and acetone (the last of which is most closely related to the present situation). The binding enthalpy of the dimers are all ca 125 kJ mol^{-1}. The binding enthalpies for the addition of another molecule are all significantly lower, ranging from the highest value of 83 kJ mol^{-1} for DMSO to the lowest of 39 kJ mol^{-1} for acetonitrile. Unfortunately, the binding enthalpy for the acetone trimer has never been reported, but can be derived from the van't Hoff plot in Kebarle's paper to be 56 kJ mol^{-1}, i.e., less than half of the binding enthalpy of the dimer. And so it is apparent from the measured change in PA for the longer oligomers that the binding of the proton changes from bidentate to tridentate.

8

Conclusions

ESI-MS and MALDI-MS can be used to determine the different distributions, end groups and the overall monomer ratios of PBA/PVAc, PMMA/PVAc and PBA/PMMA copolymers. The former appear to agree fairly well with proton NMR results and with the predictions of a polymerization simulator modelling program. The advantage of ESI-MS is for end-group analysis, which in the present case was impossible by NMR, and for the molecular-level information on copolymer composition. ESI-MS and MALDI-MS produced different monomer and copolymer end group ratios for PBA/PMMA due to inherent ionization efficiency difference in MALDI-MS. It was found that conformation has an effect on the dissociation of ionized polymers. The results are consistent with an increase in internal energy deposition with increasing molecular size. In addition, compact polymer ion conformations appeared to undergo less efficient energy transfer than extended structures.

Protonated PMMA and PBA oligomers can be generated in the gas phase from the dissociation of proton-bound complexes of the oligomers with simple protonated amino acids and peptides. Compared to their metal ion adduct analogues, these protonated oligomers undergo a unique fragmentation chemistry upon collisional activation. These fragmentations are totally different from their metal ion adduct

analogues. Protonted polymer oligomers fragment primarily by eliminating neutral molecules from the monomer side chains until all that is left is the backbone hydrocarbon. It may be possible to obtain complementary information about polymer structure and sequence with this method. For example, it would be interesting to explore the effect of chain branching on the MS/MS of protonated polymers.

Claims to Original Research

1- ESI-MS and MALDI-MS were used to determine the composition (monomer ratios) and structure (end group analysis) relative to ^{1}H NMR spectroscopy and theoretical predictions for three different copolymers: poly(butyl acrylate/vinyl acetate) (PBA/PVAc), poly(methyl methacrylate/vinyl acetate) (PMMA/PVAc) and poly(butyl acrylate/methyl methacrylate) (PBA/PMMA).

Alhazmi, A. M.; Giguère, M.-S.; Dubé, M. A.; Mayer, P. M. A composition of electrospray ionization and matrix-assisted laser desorption/ionization mass spectrometry with nuclear magnatic resonance spectroscopy for the characterization of synthetic co-polymers. Eur. J. Mass Spectrom 2006, 12, 301.

2- I studied the matrix effects on PBA/PMMA copolymer quantitation by MALDI mass spectrometry. The matrix concentration in MALDI sample preparation for synthetic copolymers was found to have an influence on the observed ratio of the different copolymer reaction products. It is therefore useful to estimate the ratio of copolymers terminated by different end groups with complementary techniques such as NMR or ESI-MS, since MALDI alone may lead to erroneous results.

Alhazmi, A. M.; Mayer, P. M. Matrix effects on copolymer quantitation by matrix-assisted laser desorption/ionization mass spectrometry. Rapid Commun. Mass Spectrom. 2007, 21, 3392-3394.

3- The effects of molecular conformation on CID mass spectra of polymers was directly investigated for the first time.

Casey, J.; Alhazmi, A.; Mayer, P. M. Conformtion effects on the dissociation of ionized polymers. Eur. J. Mass Spectrom 2005, 11, 557-563.

4- A new way to generate protonated polymer oligomers in the gas phase was developed by first forming proton-bound adducts with small peptides or amino acids. This approach has also been used to explore oligomer thermochemistry.

Alhazmi, A. M.; Mayer, P. M. Protonating Polymer Oligomers in the Gas Phase to Change Fragmentation Pathways. in preparation, to be submitted to JASMS.

Alhazmi, A. M.; Mayer, P. M. The proton affinity of a polymer: What does that mean? Will be submitted after adding a computational work.. In preparation.

References

(1) Hiemenz, P. *Polymer chemistry*; 2nd ed.; CRC press: Boca Raton, 2007.

(2) Billmeyer, F. W. *Textbook of the polymer science*; 3rd ed.; John Wiley & Sons: New York, 1984.

(3) Bahadur, P.; Sastry, N. V. *Principles of polymer science*; 1st ed.; CRC Press Narosa, Puplishing House: Boca Raton, New Delhi, 2002.

(4) Rudin, A. *The elements of polymer science and engineering*; 2nd ed.; Acamemic press: San Diego, 1999.

(5) Chanda, M. *Introduction to polymer science and chemistry*; CRC press: Boca Raton, 2006.

(6) Carraher, C. E. *Introduction to polymer chemistry*; CRC press: Boca Raton, 2007.

(7) Badeen, C.; Dubé, M. A. *Polym. Chem. Eng.* **2003**, *11*, 53-77.

(8) Alhazmi, A. M.; Giguère, M.-S.; Dubé, M. A.; Mayer, P. M. *Eur. J. Mass Spectrom* **2006**, *12*, 301.

(9) Montaudo, G.; Lattimer, R. P. *Mass spectrometry of polymer*; 1st ed.; CRC Press: Boca Raton, 2002.

(10) Pramanik, B. N.; Ganguly, A. K.; Gross, M. L. *Applied electrospray mass spectrometry*; Marcel Dekker: New York, 2002.

(11) Yamashita, M.; Fenn, J. B. *J. Phys. Chem.* **1984**, *88*, 4451-4459.

(12) Fenn, J. B.; mann, M.; Meng, C. K.; Wong, S. F.; Whitehouse, C. M. *Science* **1989**, *246*, 64-71.

(13) Tanaka, K.; Waki, H.; Ido, Y.; Akita, S.; Yoshida, Y. *Rapid Commun. Mass Spectrom.* **1988**, *2*, 151-153.

(14) Karas, M.; Bachmann, D.; Bahr, U.; Hillenkamp, F. *Int. J. Mass Spectrom* **1987**, *78*, 53.

(15) Karas, M.; Hillenkamp, F. *Anal. Chem.* **1988**, *60*, 2299-2301.

(16) Hunt, S. M.; Sheil, M. M.; Belov, M.; Derrick, P. J. *Anal. Chem.* **1998**, *70*, 1812-1822.

(17) Montaudo, G.; Montaudo, M. S.; Puglisi, C.; Samperi, F. *Rapid Commun. Mass Spectrom.* **1995**, *9*, 453-460.

(18) Barton, Z.; Kemp, T. J.; Buzy, A.; Jennings, K. R. *Polymer* **1995**, *36*, 4927-4933.

(19) Montaudo, G.; Samperi, F.; Montaudo, M. S. *Prog. Polym. Sci* **2006**, *31*, 277-357.

(20) Hanton, S. D. *Chem. Rev.* **2001**, *101*, 527-569.

(21) Montaudo, M. S. *Mass Spectrom. Rev.* **2002**, *21*, 108-144.

(22) Scrivens, J. H.; Jackson, A. T. *Int. J. Mass Spectrom* **2000**, *200*, 261-276.

(23) Montaudo, G.; Garozzo, D.; Montaudo, M. S.; Puglisi, C.; Samperi, F. *Macromolecules* **1995**, *28*, 7983-7989.

(24) Montaudo, G.; Montaudo, M. S.; Puglisi, C.; Samperi, F. *Rapid Commun. Mass Spectrom.* **1995**, *9*, 1158-1163.

(25) Montaudo, G.; Montaudo, M. S.; Puglisi, C.; Samperi, F. *J. Polym. Sci. A: Polym. Chem.* **1996**, *34*, 439-447.

(26) Weidner, S.; Kuhn, G. *Rapid Commun. Mass Spectrom.* **1996**, *10*, 942-946.

(27) Barner-Kowollik, C.; Vana, P.; Davis, T. P. *J. Polym. Sci. A: Polym. Chem.* **2002**, *40*, 675-681.

(28) Maziarz, E. P.; Baker, G. A.; Wood, T. D. *Macromolecules* **1999**, *32*, 4411-4418.

(29) Buback, M.; Frauendorf, H.; Vana, P. *J. Polym. Sci. A: Polym. Chem.* **2004**, *42*, 4266-4275.

(30) Feichtinger, D.; Plattner, D. a.; Chen, P. *J. Am. Chem. Soc* **1998**, *120*, 7125-7126.

(31) Hinderling, C.; Chen, P. *Angew. Chem. Int. Ed.* **1999**, *38*, 2253-2256.

(32) Adlhart, C.; Chen, P. *Helv. Chim. Acta* **2000**, *83*, 2192-2196.

(33) Hinderling, C.; Chen, P. *Int. J. Mass Spectrom* **2000**, *195/196*, 377-383.

(34) Wehrli, D.; Chen, P. *Chimia* **2003**, *57*, 354-357.

(35) Lena, F. d.; Quintanilla, E.; Chen, P. *Chem. Commun* **2005**, 5757-5759.

(36) Chen, P. *Angew. Chem. Int. Ed.* **2003**, *42*, 2832-2847.

(37) Jackson, A. T.; Yates, H. T.; Scrivens, J. H.; Bateman, R. H. *Rapid Commun. Mass Spectrom.* **1996**, *10*, 1668-1674.

(38) Jackson, A. T.; Slade, S. E.; Scrivens, J. H. *Int. J. Mass Spectrom.* **2004**, *238*, 265-277.

(39) Jackson, A. T.; Williams, J. P.; Scrivens, J. H. *Rapid Commun. Mass Spectrom.* **2006**, *20*, 2717-2727.

(40) Jackson, A. T.; Jennings, K. R.; Scrivens, J. H. *J Am Soc Mass Spectrom* **1997**, *8*, 76-85.

(41) Scrivens, J. H.; Jackson, A. T.; Yates, H. T.; Bateman, R. H.; Gidden, J. *Int. J. Mass Spectrom. Ion Processes* **1997**, *165/166*, 363-375.

(42) Gidden, J.; Jackson, A. T.; Scrivens, J. H.; Bowers, M. T. *Int. J. Mass Spectrom.* **1999**, *188*, 121-130.

(43) Jackson, A. T.; Yates, H. T.; Scrivens, J. H. *J Am Soc Mass Spectrom* **1997**, *8*, 1206-1213.

(44) Polce, M. J.; Ocampo, M.; Quirk, R. P.; Wesdemiotis, C. *Anal. Chem.* **2008**, *80*, 347-354.

(45) Jedlinski, Z.; Adamus, G.; Kowalczuk, M.; Schubert, R.; Szewczuk, Z.; Stefanowicz, P. *Rapid Commun. Mass Spectrom.* **1998**, *12*, 357-360.

(46) Chen, R.; Tseng, A. M.; Uhing, M.; Li, L. *J Am Soc Mass Spectrom* **2001**, *12*, 55-60.

(47) Selby, T. L.; Wesdemiotis, C.; lattimer, R. P. **1994**, *5*, 1081-1092.

(48) Jackson, A. T.; Yates, H. T.; Scrivens, J. H. *J. Am. Soc. Mass. Spectrom* **1998**, *9*, 269-274.

(49) Gidden, J.; Bowers, M. T.; Jackson, A. T.; Scrivens, J. H. *J Am Soc Mass Spectrom* **2002**, *13*, 499-505.

(50) Gidden, J.; Wyttenbach, T.; Jackson, A. T.; Scrivens, J. H.; Bowers, M. T. *J. Am. Chem. Soc* **2000**, *122*.

(51) Yamashita, M.; Fenn, J. B. *J. Phys. Chem.* **1984**, *88*, 4671-4675.

(52) Whitehouse, C. M.; Dreyer, R. N.; Yamashita, M.; Fenn, J. B. *Anal. Chem.* **1985**, *57*, 675-679.

(53) Loo, J. A.; Udseth, H. R.; Smith, R. D. *Anal. Biochem.* **1989**, *179*, 404-412.

(54) Saf, R.; Mirtl, C.; Hummel, K. *Acta. polymer.* **1997**, *48*, 513-526.

(55) Taylor, G. *Proc. Roy. Soc. Lond. A* **1964**, *280*, 383-397.

(56) Siu, K. W. M.; Guevremont, R.; Berman, S. S. *Org. Mass Spectrom.* **1993**, *28*, 579-584.

(57) Hoffmann, E. D.; Charette, J.; Stroobant, V. *Mass spectrometry: principle and application*; John wiley and sons: Chichester, 1996.

(58) Smith, R. M.; Busch, K. L. *Understanding mass specta-a basic approch*; John wiley and sons: New York, 1999.

(59) Wolfgang., P.; S., S. H. *Naturforsch* **1953**, *8a*, 448-450.

(60) March, R. E.; Hughes, R. J. *Quadrupole stroge mass spectrometry*; John wiley and sons: New York, 1989.

(61) Herbert, C. G.; Johnstone, R. A. W. *Mass spectrometry basic*; CRC press: Boca Raton, 2003.

(62) Pasch, H.; Schrepp, W. *MALDI-TOF mass spectrometry of synthetic polymers*; Springer: Berlin, 2003.

(63) Yalcin, T.; Dai, Y.; Li, L. *J. Am. Soc. Mass. Spectrom* **1998**, *9*, 1303-1310.

(64) Vertes, A.; Irinyi, G.; Gijbels, R. *Anal. Chem.* **1993**, *65*, 2389-2393.

(65) Johnson, R. E. *Int. J. Mass Spectrom. Ion Processes* **1994**, *139*, 25-38.

(66) Chen, R.; Zhang, N.; Tseng, A. M.; Li, L. *Rapid Commun. Mass Spectrom.* **2000**, *14*, 2175.

(67) Hoteling, A. J.; Erb, W. J.; Tyson, R. J.; Owens, K. G. *Anal. Chem.* **2004**, *76*, 5157.

(68) Somogyi, A.; Bojkova, N.; Padias, A. B.; Hall, H. K. *Macromolecules* **2005**, *38*, 4067.

(69) Allicata, R.; Montaudo, G.; Puglisi, C.; Samperi, F. *Rapid Commun. Mass Spectrom.* **2002**, *16*, 248-260.

(70) Puglisi, C.; Samperi, F.; Alicata, R.; Montaudo, G. *Macromolecules* **2002**, *35*, 3000-3007.

(71) Cox, F. J.; Johnston, M. V.; Qian, K.; Peiffer, D. G. *J. Am. Soc. Mass. Spectrom* **2004**, *15*, 681-688.

(72) Cox, F. J.; Johnston, M. V.; Dasgupta, A. *J. Am. Soc. Mass. Spectrom* **2003**, *14*, 648-657.

(73) Hanton, S. D.; Clark, P. A. C.; Owens, K. G. *J. Am. Soc. Mass. Spectrom* **1999**, *10*, 104.

(74) Schriemer, D. C.; Li, L. *Anal. Chem.* **1997**, *69*, 4169-4175.

(75) Wallace, W. E.; Guttman, C. M.; Hanton, S. D. *J. Res. Natl. Inst. Stand. Technol.* **2003**, *108*, 79.

(76) Schriemer, D. C.; Li, L. *Anal. Chem.* **1996**, *68*, 2721-2725.

(77) Karas, M.; Bahr, U. *Trends Anal. Chem.* **1990**, *9*, 321-325.

(78) Vestal, M. L.; Juhasz, P.; Martin, S. A. *Rapid Commun. Mass Spectrom.* **1995**, *9*, 1044-1050.

(79) Leach, A. R. *Molecular modelling, principle and applications*; 2nd ed.; Prentice Hall: London, 2001.

(80) Young, D. *Computational chemistry* New York, 2001.

(81) Giguère, M.-S. In *Chemistry*; University of Ottawa: Ottawa, 2003.

(82) Dubé, M. A.; Penlidis, A. *Polymer* **1995**, *36*, 587-598.

(83) Jovanovic, R.; Dubé, M. A. *J. Appl. Polym. Sci.* **2001**, *82*, 2958-2977.

(84) Molecular Simulation, Inc, Cerius2 Modeling Environment; Release 4.0 ed.; Molecular Simulations, Inc.: San Diego, USA, 1999.

(85) Hehre, W. J.; Radom, L.; Schleyer, P. v. R.; Pepole, J. A. *Ab initio molecular orbital theory*; John Wiley: New York, USA, 1986.

(86) Frisch, M. J.; Trucks, G. W.; Schlegel, H. B.; Scuseria, G. E.; Robb, M. A.; Cheeseman, J. R.; Zakrzewski, V. G.; Montgomery, J. A.; Stratmann, R. E.; Burant, J. C.; Dapprich, S.; Millam, J. M.; Daniels, A. D.; Kudin, K. N.; Strain, M. C.; Farkas, O.; J. Tomasi; Barone, V.; Cossi, M.; Cammi, R.; Mennucci, B.; Pomelli, C.; Adamo, C.; Clifford, S.; Ochterski, J.; Petersson, G. A.; Ayala, P. Y.; Cui, Q.; Morokuma, K.; Malick, D. K.; Rabuck, A. D.; Raghavachari, K.; Foresman, J. B.; Cioslowski, J.; Ortiz, J. V.; Stefanov, B. B.; Liu, G.; Liashenko,

A.; Piskorz, P.; Komaromi, I.; Gomperts, R.; Martin, R. L.; Fox, D. J.; Keith, T.; Al-Laham, M. A.; Peng, C. Y.; Nanayakkara, A.; Gonzalez, C.; Challacombe, M.; Gill, P. M. W.; Johnson, B.; Chen, W.; Wong, M. W.; Andres, J. L.; Gonzalez, C.; Head-Gordon, M.; Replogle, E. S.; Pople, J. A.; Gaussian Inc.: Pittsburgh PA, 1998.

(87) Baer, T.; hase, W. L. *Unimolecular reaction dynamics, theory and experiments*; Oxford university press: New York, 1996.

(88) Beyer, T.; Swinehart, D. R. *ACM Commum* **1973**, *16*, 379.

(89) Rossignoli, P. J.; Duever, T. A. *Polym. React. Eng.* **1995**, *3*, 361-395.

(90) Gao, J.; Penlidis, A. *J.M.S.-rev. Macromol. Chem, Phys.* **1998**, *C38*, 651-780.

(91) Alhazmi, A. M.; Mayer, P. M. *Rapid Commun. Mass Spectrom.* **2007**, *21*, 3392-3394.

(92) Barry, J. P.; carton, W. J.; Pesci, K. M.; Evans, J. V. *Rapid Commun. Mass Spectrom.* **1997**, *11*, 437-442.

(93) Nielen, M. W. F. *Mass Spectrom. Rev.* **1999**, *18*, 309-344.

(94) Scorah, M. J.; Hua, H.; Dubé, M. A. *J. Appl. Polym. Sci.* **2001**, *82*, 1238-1255.

(95) Marzluff, E. M.; Campbell, S.; Rodgers, M. T.; Beauchamp, J. L. *J. Am. Chem. Soc* **1994**, *116*, 7787-7796.

(96) Meroueh, O.; Hase, W. L. *J. Phys. Chem. A.* **1999**, *103*, 3981-3990.

(97) Meroueh, O.; Hase, W. L. *Int. J. Mass Spectrom.* **2000**, *201*, 233-244.

(98) Laskin, J.; Futrell, J. H. *J. Chem. Phys.* **2002**, *116*, 4302-4310.

(99) Laskin, J.; Bailey, T. H.; Futrell, J. H. *J. Am. Chem. Soc* **2003**, *125*, 1625-1632.

(100) Casey, J.; Alhazmi, A.; Mayer, P. M. *Eur. J. Mass Spectrom* **2005**, *11*, 557-563.

(101) Chaicharoen, K.; Polce, M. J.; Singh, A.; Pugh, C.; Wesdemiotis, C. *Anal. Bioanal. Chem., in press, published online 30 March 2008, DOI 10.1007/s00216-008-1969-0.*

(102) Yalcin, T.; Khouw, C.; Csizmadia, I. G.; Peterson, M. R.; Harrison, A. G. *J Am Soc Mass Spectrom* **1995**, *6*, 1164-1174.

(103) PBA Certificate of Analysis; Polymer Source Inc.

(104) Fayt, R.; Forte, R.; Jacobs, C.; Jerome, R.; Ouhadi, T.; Teyssie, P.; Varshney, S. K. *Macromolecules* **1987**, *20*, 1442-1444.

(105) Bertini, F.; Audisio, G.; Zuev, V. V. *Polym. Degrad. Stab.* **2005**, *89*, 233-239.

(106) Eastmond, G. C.; Ledwith, A.; Russo, S.; Sigwalt, P. *Comperhensive Polymer Science. Polymer Reaction*; Pergamon Press: oxford, 1989; Vol. 6.

(107) Holmes, J. L.; Aubry, C.; Mayer, P. M. *Assigning structures to ions in mass spectrometry*; CRC Press: Boca Raton, FL, 2007.

(108) NIST Chemistry Webbook, NIST standard refernce database. national institute of standards and technology, accessed 13 Sep. 2007.

(109) Lau, Y. K.; Saluja, P. P. S.; Kebarle, P. *J. Am. Chem. Soc* **1980**, *102*, 7429-7433.